Supporting Information

Rec. Nat. Prod. **X:X (202X) XX-XX**

In Vitro and *In Silico* Evaluation of Compounds from *Washingtonia filifera* as Acetylcholinesterase Inhibitors

Aalaa Salem [1], Fatma M. Abdel Bar [2, 3 *], El-Sayed M. Marwan [1], Amal F. Soliman [1, 4], Saleh H. El-Sharkawy [1, 5] and Amira Mira [1, 6]

[1] *Department of Pharmacognosy, Faculty of Pharmacy, Mansoura University Mansoura 35516, Egypt*
[2] *Department of Pharmacognosy, College of Pharmacy, Prince Sattam Bin Abdulaziz University, Al-Kharj 11942, Saudi Arabia*
[3] *Faculty of Pharmacy, Mansoura University Mansoura 35516, Egypt*
[4] *Pharmacognosy Department, Faculty of Pharmacy, Mansoura National University, Gamasa 7731168, Egypt*
[5] *Department of Basic Sciences, Faculty of Physical Therapy, Rashid University, Rashid 5965022, Egypt*
[6] *Department of Pharmacognosy & Pharmaceutical Chemistry, College of Dentistry & Pharmacy Buraydah Private Colleges, Buraydah 51418, Saudi Arabia*

Table of Contents **Page**

Data S1: Identification of compound **1** (*β*-sitosteryl oleate) 3
Data S2: Identification of compound **2** (oleic acid) 3
Data S3: Identification of compound **3** (β-sitosterol) 3
Data S4: Identification of compound **4** (9-hydroxy-7-methoxy-8-[4'-hydroxy-3'-methoxyphenyl]-4-hydroxy-3-methoxyphenylpropane) 3
Data S5: Identification of compound **5** (syringaresinol) 4
Data S6: Identification of compound **6** (diosmetin) 4
Data S7: Identification of compound **7** (tricin) 4
Data S8: Identification of compound **8** (β-sitosterol-3-*O*-β-D-glucoside) 5
Data S9: Identification of compound **9** (luteolin 7-*O*-*β*-D-glucoside) 5
Table S1: ^{1}H-NMR and APT spectral data of compound **1** compared to the reported data of *β*-sitosteryl oleate 6
Table S2: ^{1}H-NMR and APT spectral data of compound **2** compared to the reported data of oleic acid 8
Table S3: ^{1}H-NMR and APT spectral data of compound **4** compared to to the reported data of 9-hydroxy-7-methoxy-8-[4'-hydroxy-3'-methoxyphenyl]-4-hydroxy-3-methoxyphenylpropane 9
Table S4: ^{1}H-NMR and APT spectral data of compound **5** compared to the reported data of syringaresinol 10
Table S5: ^{1}H-NMR and and APT spectral data of compound **6** compared to the reported data of diosmetin 11
Table S6: ^{1}H-NMR and APT spectral data of compound **7** compared to the reported data of tricin 12
Table S7: ^{1}H-NMR and APT spectral data of compound **9** compared to the reported data of luteolin 7-*O*-*β*-D-glucoside 13
Table S8: Predicted ADME properties by the SwissADME online tool 59
Figure S1: Photograph of *W. filifera* fruitless bunches 14

Figure S2: ^{1}H-NMR spectrum ($CDCl_3$, 400 MHz) of compound **1** (*β*-sitosteryl oleate) 15
Figure S3: APT spectrum ($CDCl_3$, 100 MHz) of compound **1** (*β*-sitosteryl oleate) 16
Figure S4: a) HMBC spectrum; and b) EI-MS spectrum of compound **1** (*β*-sitosteryl oleate) 17
Figure S5: ^{1}H-NMR spectrum ($CDCl_3$, 400 MHz) of compound **2** (oleic acid) 18
Figure S6: ^{1}H-NMR spectrum ($CDCl_3$, 400 MHz) of compound **2** (oleic acid) 19
Figure S7: EI-MS spectrum of compound **2** (oleic acid) 20
Figure S8: IR (KBr, υ_{max}) spectrum of compound **3** (β-sitosterol) 21
Figure S9: a) Full ^{1}H-NMR spectrum (CD_3OD, 400 MHz); and **b)** Expansion from 6.33 to 6.56 ppm of compound **4** (*threo*-2,3-*bis*-(4-hydroxy-3-methoxyphenyl)-3-methoxypropanol) 22
Figure S10: APT spectrum (CD_3OD, 100 MHz) of compound **4** (9-hydroxy-7-methoxy-8-[4'-hydroxy-3'-methoxyphenyl]-4-hydroxy-3-methoxyphenylpropane) 23
Figure S11: HSQC spectrum (CD_3OD, 400 MHz) of compound **4** (9-hydroxy-7-methoxy-8-[4'-hydroxy-3'-methoxyphenyl]-4-hydroxy-3-methoxyphenylpropane) 24
Figure S12: HMBC spectrum (CD_3OD, 400 MHz) of compound **4** (9-hydroxy-7-methoxy-8-[4'-hydroxy-3'-methoxyphenyl]-4-hydroxy-3-methoxyphenylpropane) 25
Figure S13: ESI-LC/MS spectrum of compound **4** (9-hydroxy-7-methoxy-8-[4'-hydroxy-3'-methoxyphenyl]-4-hydroxy-3-methoxyphenylpropane) 26
Figure S14: ^{1}H-NMR spectrum (CD_3OD, 400 MHz) of compound **5** (syringaresinol) 27
Figure S15: APT spectrum (CD_3OD, 100 MHz) of compound **5** (syringaresinol) 28
Figure S16: HSQC spectrum (CD_3OD, 400 MHz) of compound **5** (syringaresinol) 29
Figure S17: ESI-LC/MS spectrum of compound **5** (syringaresinol) in CD_3OD 30
Figure S18: ^{1}H-NMR spectrum (CD_3OD, 400 MHz) of compound **6** (diosmetin) 31
Figure S19: ^{1}H-NMR spectral expansion (CD_3OD, 400 MHz) from 6.1 to 7.5 ppm of compound **6** (diosmetin) 32
Figure S20: APT spectrum (CD_3OD, 100 MHz) of compound **6** (diosmetin) 33
Figure S21: HSQC spectrum (CD_3OD, 400 MHz) of compound **6** (diosmetin) 34
Figure S22: HMBC spectrum (CD_3OD, 400 MHz) of compound **6** (diosmetin) 35
Figure S23: HMBC spectral expansion **(**CD_3OD, 400 MHz) from 5.7 to 8.3 ppm for ^{1}H and 60-200 ppm for ^{13}C of compound **6** (diosmetin) 36
Figure S24: ^{1}H NMR spectrum (CD_3OD, 400 MHz) of compound **7** (tricin) 37
Figure S25: APT spectrum (CD_3OD, 100 MHz) of compound **7** (tricin) 38
Figure S26: HSQC spectrum (CD_3OD, 400 MHz) of compound **7** (tricin) 39
Figure S27: HMBC spectrum (CD_3OD, 400 MHz) of compound **7** (tricin) 40
Figure S28: IR (KBr, υ_{max}) spectrum of compound **8** (daucosterol) 41
Figure S29: ^{1}H-NMR spectrum (DMSO-d_6, 400 MHz) of compound **9** (luteolin-7-*O*-β-D-glucoside; cynaroside) 42
Figure S30: APT spectrum (DMSO-d_6, 100 MHz) of compound **9** (luteolin-7-*O*-β-D-glucoside; cynaroside) 43
Figure S31: HSQC spectrum (DMSO-d_6, 400 MHz) of compound **9** (luteolin-7-*O*-β-D-glucoside; cynaroside) 44
Figure S32: HMBC spectrum (DMSO-d_6, 400 MHz) of compound **9** (luteolin-7-*O*-β-D-glucoside; cynaroside) 45
Figure S33: a) Two-dimensional; and b) Three-dimensional interactions of docked structure of β-sitosterol oleate (**1**) (cyan) within the active site of AChE (PDB: 4EY7) 46
Figure S34: a) Two-dimensional; and b) Three-dimensional interactions of docked structure of oleic acid (**2**) (pink) within the active site of AChE (PDB: 4EY7) 47
Figure S35: a) Two-dimensional; and b) Three-dimensional interactions of docked structure of β-sitosterol (**3**) (cyan) within the active site of AChE (PDB: 4EY7) 48
Figure S36: a) Two-dimensional; and b) Three-dimensional interactions of docked structure of 9-hydroxy-7-methoxy-8-[4'-hydroxy-3'-methoxyphenyl]-4-hydroxy-3-methoxyphenylpropane (**4**) (cyan) within the active site of AChE (PDB: 4EY7) 49
Figure S37: a) Two-dimensional; and b) Three-dimensional interactions of docked structure of syringaresinol (**5**) (cyan) within the active site of AChE (PDB: 4EY7) 50
Figure S38: a) Two-dimensional; and b) Three-dimensional interactions of docked structure of 51

diosmetin (**6**) (orange) within the active site of AChE (PDB: 4EY7)
Figure S39: a) Two-dimensional; and b) Three-dimensional interactions of docked structure of tricin (**7**) (orange) within the active site of AChE (PDB: 4EY7) 52
Figure S40: a) Two-dimensional; and b) Three-dimensional interactions of docked structure of daucosterol (**8**) (cyan) within the active site of AChE (PDB: 4EY7) 53
Figure S41: a) Two-dimensional; and b) Three-dimensional interactions of docked structure of luteolin-7-*O*-β-D-glucoside (**9**) (orange) within the active site of AChE (PDB: 4EY7) 54
Figure S42: Two-dimensional interactions of donepezil structure, a) Docked; b) Co-crystallized ligand, and c) three-dimensional superposition of docked structure (purple) and co-crystallized ligand (green) of donepezil from its complex with AChE (PDB: 4EY7) 55
Figure S43: Three-dimensional superposition of docked structures of a) 9-hydroxy-7-methoxy-8-[4'-hydroxy-3'-methoxyphenyl]-4-hydroxy-3-methoxyphenylpropane (**4**) (yellow), and b) syringaresinol (**5**) (yellow), with donepezil (green), the cocrystallized ligand, within the active site of AChE (PDB: 4EY7) 56
Figure S44: BOILED-Egg plot for compounds isolated from *Washingtonia filifera* illustrating the predictions for; BBB: blood-brain barrier, HIA: penetration, and human gastrointestinal absorption. Blue circles represent compounds predicted as active-efflux substrates of P-glycoprotein (PGP^+), while red circles denote compounds predicted as non-substrates (PGP^-). Two molecules are out of range, including **1**: β-Sitosteryl oleate and **3**: β-Sitosterol 57
Figure S45: Bioavailability radar charts for the isolated compounds (**1**–**9**) isolated from *Washingtonia filifera*. The pink region indicates the ideal range for achieving oral bioavailability, while the red boundary outlines the desirable physicochemical characteristics for optimal oral bioavailability 58
References 60

Data S1. Identification of compound 1

The ^{1}H-NMR spectrum of compound **1** (Figure S1, Table S1) showed a β-sitosterol structure with a downfield H-3 signal at δ_H 4.59 indicating the presence of a substituted oxymethine group. The presence of extra signals of an unsaturated fatty acyl chain was evident from the peaks at δ_H 5.34 (2H; H-9` and 10`), 1.25-1.29 (10H; H-12`-15` and H-17`). APT spectrum of **1** (Figure S2, Table S1) showed 47 carbons, of which 29 carbons for the steroidal nucleus and 18 carbons for a 3-*O*-oleate moiety. The most significant peaks were an olefinic carbon at δ_C 122.6 (C-6), a quaternary olefinic carbon at δ_C 139.7 (C-5), and an oxygenated CH at δ_C 73.7 (C-3). The oleate moiety was evident from the signals at δ_C 173.4 (an ester carbonyl group, C-1`), 14.1 (a terminal methyl, C-18`), and 129.8 and 130.0 (two olefinic carbons, C-9` and 10`, respectively). The linkage of the oleate moiety at C-3 of the β-sitosterol nucleus was confirmed from the HMBC correlation (Figure S3a) of H-3 (δ_H 4.59) with C-1` (δ_C 173.4). The EI-MS spectrum of **1** (Figure S3b) displayed a molecular ion peak at *m/z* 679.19 $[M+H]^+$, which is consistent with the molecular formula $C_{47}H_{82}O_2$. Also, the fragment ion peak at *m/z* 415.64 ($C_{29}H_{50}O$) referring to $[M+H\text{-oleoyl}]^+$, indicated the loss of oleic acid. These findings are consistent with the reported data of *β*-sitosteryl oleate [1]. It is the first report of this compound from the genus *Washingtonia*.

Data S2. Identification of compound 2

The ^{1}H-NMR spectrum of compound **2** (Figure S4, Table S2) showed a typical structure of an unsaturated fatty acid. The multiplet signal at δ_H 5.36 indicated two olefinic protons (H-9 and 10) and the signal at δ_H 0.89 (t, 3H) indicated the presence of a terminal methyl (H-18). A prominent proton signal integrating for 20 protons at δ_H 1.28 was attributed to ten overlapping methylene groups, corresponding to H-4 to H-7 and H-12 to H-17. APT spectrum (Figure S5, Table S2) showed a quaternary carbon at δc 180.3 for a free carboxylic acid carbonyl (C-1), a terminal methyl group at δc 14.1 (C-18), and two olefinic carbons at δc 129.7 and 130.0 (C-9 and 10, respectively). The EI-MS spectrum of **2** (Figure S6) displayed a molecular ion peak at m/z 282.11, which was consistent with a molecular formula of $C_{18}H_{34}O_2$. The previously presented data was consistent with an oleic acid structure [2]. Oleic acid was previously identified in *W. filifera* seed oil [3,4] and *W. robusta* fruit oil [5].

Data S3. Identification of compound 3

IR (υ_{max} cm^{-1}) spectrum of compound **3** (Figure S7) showed absorption bands at 3425 (OH stretching), 2933 (=CH stretching), 2859 (C-H stretching), 1666 (C=C stretching), 1459 (CH_2 bending), 1374 (CH_3 bending), 1044 (C-O stretching) and 959 (=C-H bending) [6]. Co-chromatography with an authentic sample of *β*-sitosterol confirmed the identity of compound **3** as β-sitosterol, which was previously identified in *W. robusta* fruit [5].

Data S4. Identification of compound 4

The structure of compound **4** was elucidated through detailed analysis of its ^{1}H and ^{13}C-NMR data (Table S3 and Figures S8-S12), supported by mass spectrometry (Figures S13). The ^{1}H-NMR spectrum of compound **4** (Figure S8 and Table S3) revealed the presence of six aromatic protons resonating at δ_H 6.49-6.65 (H-2,2`, H-5,5`, H-6,6`) for two trisubstituted phenyl groups, along with two oxygenated methylene protons at δ_H 4.05 (1H, *dd*, *J* = 10.9, 5.8 Hz; H_a-9) and at δ_H 3.89 (1H, *d, J* = 10.7, 6.9 Hz; H_b-9), an oxymethine proton at δ_H 4.32 (1H, *d*, *J* = 8.5 Hz; H-7) and a methine proton at δ_H 3.00 (2H, *m*; H-2). The presence of two aromatic methoxyl groups was evident from the signals at δ_H 3.70 (3H, *s*) and at δ_H 3.71 (3H, *s*), indicating two "guaicyl" groups at a C3 chain of a phenylpropanoid. The APT spectrum (Figure S9 and Table S3) displayed resonances of 18 carbons, of which an oxygenated methylene at δ_C 64.97 (C-9), an oxymethine at δ_C 87.42 (C-7) and a methine at δ_C 55.99 (C-8) were the most significant carbons. In addition, it displayed twelve aromatic carbon signals at δ_C 112.41-148.52, along with two methoxyl groups at δ_C 56.34 and at δ_C 56.30 at (C-3 and 3`, respectively). The HSQC correlations of **4** (Figure S10) showed the presence of a third methoxyl group at δ_H 3.23 and δ_C 56.78, suggested a methoxyl substituent at the propane chain. The HMBC spectrum of **4** (Figure S11) showed several significant correlations, including the cross peaks of the protons at; δ_H 4.32 (H-7) with carbons C-1, C-2, and C-6, similarly, the cross peaks of the proton at δ_H 3.00 (H-8) with C-1`, C-2`, and C-6`, confirming the attachment of the two guiacyl moieties at C-7 and C-8, respectively. The cross peaks

of the proton at δ_H 3.00 (H-8) with C-7, C-9 also confired the 2,3-biguiacyl-propan-1,3-ol structure. Other significant correlations were found between the methoxy signal at δ_H 3.23 with C-7, confirming its attachment to this position, in addition to the cross peaks of the methoxy signals at δ_H 3.70 and 3.71 to C-3`and C-3`` assigned to δ_C 148.52 (C-3`) and 148.34 (C-3), respectively. The ESI-LC/MS (Figure S13) of compound **4** displayed a molecular ion peak at *m*/*z* 334.2683 $[M]^-$ (calculated exact mass, 334.1416), 333.2030 $[M-H]^-$ (calculated exact mass, 333.1344), of a molecular formula of $C_{18}H_{22}O_6$. These data were consistent with the known compound, 9-hydroxy-7-methoxy-8-[4'-hydroxy-3'-methoxyphenyl]-4-hydroxy-3-methoxyphenylpropane [7], also referred to as *threo*-2,3-*bis*-(4-hydroxy-3-methoxyphenyl)-3-methoxypropanol [8]. The assignment was substantiated by a close match in the chemical shift values between compound **4** and the reference compound [7]. The proton signals of the aromatic and aliphatic protons, including the methine and methylene protons at C-7, C-8, and C-9, showed similar coupling patterns and chemical shifts (Table S3). Notably, the ^{13}C chemical shift for C-7 in compound **4** was observed at δ_C 87.42 ppm, which aligns well with the reported value for the *threo* isomer (δ_C 87.4 ppm) and clearly differs from the *erythro* configuration (δ_C 84.9 ppm) [8]. Thus, based on comparative NMR and mass spectral analysis, compound **4** was identified as the *threo* stereoisomer of 2,3-*bis*-(4-hydroxy-3-methoxyphenyl)-3-methoxypropanol. This study represents the first report of this compound from the family Arecaceae, expanding the chemotaxonomic profile of this plant family.

Data S5. Identification of compound 5

The ^1H-NMR spectrum of compound **5** (Figure S14, Table S4) revealed the presence of a pair of oxygenated methylene protons at δ_H 4.26 (2H, *m*, H-4a, 8a) and at δ_H 3.90 (2H, overlapped, H-4b, 8b), two oxymethines at δ_H 4.73 (2H, *s*, H-2, 6) and two methines at δ_H 3.15 (2H, *m*, H-1, 5), and a prominent aromatic signal at δ_H 6.67 integrated for 4H (H-2`, 6`and H-2``, 6``), indicating a 3,7-dioxabicyclo(3.3.0)octane lignan derivative [9]. In addition, it displayed four methoxyl groups at δ_H 3.84 suggesting two 4-hydroxy-3,5-dimethoxyphenyl (i.e., syringol-4-yl) moieties. The APT spectrum (Figure S15 and Table S4) displayed 8 resonances for twenty-two carbons, including a pair of oxygenated methylenes at δ_C 71.4 (C-4, 8), two oxymethines at δ_C 86.3 (C-2, 6) and two methines at δ_C 54.1 (C-1, 5), and twelve aromatic carbon signals at δ_C 103.2-148.0, along with four methoxy groups at δ_C 55.4 (12H, s) assigned to C-3`, 5` and C-3``, 5``, indicating a 2,6-*bis*(4-hydroxy-3,5-dimethoxyphenyl)-3,7-dioxabicyclo(3.3.0)octane or 2,6-*bis*(syringol-4-yl)-3,7-dioxabicyclo(3.3.0)octane. The structure of **5** was confirmed by HSQC correlations (Figure S16) and ESI-LC/MS (Figure S17) peak at m/z 417.2760 $[M-H]^+$ (calculated exact mass, 417.1549), corresponding to a molecular formula $C_{22}H_{26}O_8$ of the known compound, syringaresinol [10]. To the best of our knowledge, this is the first report of this compound from the *Washingtonia* genus.

Data S6. Identification of compound 6

The ^1H-NMR spectrum of compound **6** (Figure S18, S19 and Table S5) indicated a flavonoid derivatives from the singlet signal at δ_H 6.49 (1H, *s*, H-3), the two doublets at δ_H 6.16 (1H, *d*, *J*= 2 Hz, H-6) and 6.38 (1H, *d*, *J*= 2 Hz, H-8) of the γ-benzopyrone moiety, in addition to the signals at δ_H 7.34 (1H, *d*, *J*= 2 Hz, H-2`), 6.87 (1H, *d*, *J*= 8.4 Hz, H-5`), and 7.4 (1H, *dd*, *J*= 2.1, 8.4 Hz, H-6`) of a trisubstitued B-ring. In addition, it displayed singlet signal at $\delta_H$ 3.89 representing one methoxyl group. APT spectrum (Figure S20 and Table S5) displayed six oxygenated aromatic carbon signals, including the signals at $\delta_c$ 161.5 (C-5), 164.7 (C-7), 152.3 (C-3`), 148.1 (C-4`), along with a carbonyl at δ_c 182.6 (C-4), and a signal at δ_c 103.0 (C-3), indicating a flavone skeleton. HSQC correlations were used to assign all protons with their carbons (Figure S21). The HMBC spectrum of **6** (Figures S22 and S23) assigned the methoxyl group to the signal at 148.1 (C-4`). Thus, the structure of **6** as diosmetin (5,7,3`-trihydroxy-4`-methoxy flavone) [11]. Diosmetin is reported herein for the first time from the genus *Washingtonia*.

Data S7. Identification of compound 7

The ^1H-NMR spectrum of **7** (Figure S24 and Table S6) displayed a singlet at δ_H 6.57 (1H, *s*, H-3) of a flavone skeleton, two doublets of two meta-coupled protons of ring A at δ_H 6.26 (1H, *d*, *J*= 2 Hz, H-6) and 6.47 (1H, *d*, *J*= 2 Hz, H-8). Also, it showed a singlet at δ_H 7.16 of two protons integrations (H-2` and H-6`**)** of the B-ring. In addition, it displayed singlet signal at δ_H 3.96 of six protons integration, suggesting two methoxyl groups. The APT spectrum (Figure S25 and Table S6) displayed six oxygenated aromatic carbon

signals, including the signals at δ_c 164.9 (C-2), 162.0 (C-5), 165.1 (C-7), 158.4 (C-9), 140.1 (C-4`), and 148.5 (C-3`, 5`). Moreover, it showed a carbonyl carbon at δ_c 182.9 (C-4) along with a methine signal at δ_c 103.7 (C-3), indicating a flavone skeleton. The HMBC spectrum (Figure S26) showed cross peaks correlating the signal at δ_H 6.6 (H-3) with carbons at δ_C 182.9 (C-4) and the methoxy group at δ_H 3.9 with the carbon signals at δ_C 148.5 (C-3`, 5`). The previously presented data of 7 was consistent with those reported for tricin (5,7,4`-trihydroxy-3`,5`-dimethoxy flavone) [12]. It worth noting that this compound was previously identified in *W. filifera* leaves [13].

Data S8. Identification of compound 8

The IR (υ_{max}) spectrum of compound **8** (Figure S28) showed absorption bands at 3384 cm^{-1} (O-H stretching), 2956 cm-1, 2928 and 2870 cm^{-1} (CH stretching), 1668 cm^{-1} (C=C stretching), 1463 and 1258 cm^{-1} (CH_2 bending), and 1164, 1018 cm^{-1} (C-O stretching). These absorbances were consistent with those reported for *β*-sitosterol-3-*O*-*β*-D-glucoside [6]. The identity of compound **8** was confirmed by co-chromatography against *β*-sitosterol-3-*O*-*β*-D-glucoside authentic sample. It is the first time to be isolated from the *Washingtonia* genus.

Data S9. Identification of compound 9

^{1}H-NMR spectrum of compound **9** (Figure S29 and Table S7) indicated a flavonoid derivative from three singlet proton signals at δ_H 6.69 (1H, *s*, H-3), 6.40 (1H, *s*, H-6) and 6.75 (1H, *s*, H-8) of a γ-benzopyrone moiety. Also, from the signals at δ_H 7.41 (1H, *m*, overlapped, H-6`), 6.87 (1H, *m*, overlapped, H-5`) and 7.38 (1H, *brs*, H-2`) of a trisubstituted B-ring. The proton doublet at δ_H 5.03 with *J* value of 8.0 Hz was assigned to an anomeric sugar proton in the *β*-configuration. Other sugar protons resonated at δ_H 3.69-3.21. The APT spectrum (Figure S30 and Table S7) displayed six oxygenated aromatic carbon signals, including δ_c 165.0 (C-2), 161.6 (C-5), 163.5 (C-7), 157.5 (C-9), 146.3 (C-3`), and 150.4 (C-4`), in addition to a carbonyl carbon at δ_c 182.4 (C-4) along with signal at δ_c 103.7 (C-3), confirming a flavone skeleton. The appearance of a carbon signal at δ_c 100.4 (C-1``), in addition to four methine carbon signals at δ_c 73.6, 77.7, 70.1 and 76.9, and a methylene carbon signal at δ_c 61.1 was assigned for a glucose moiety. The HSQC spectrum of **9** (Figure S31) was used to correlate various protons with their carbons. HMBC spectrum (Figure S32) confirmed the structure of **9** through the cross peaks correlating the proton at δ_H 6.69 (H-3) with the carbon signals at δ_C 182.4 (C-4), 165.0 (C-2) and 121.9 (C-1`). Also, it showed a cross peak between the anomeric proton signal at δ_H 5.03 (H-1``) with the oxygenated carbon at δ_C 163.46 (C-7), confirming glycosylation at C-7. The previously presented data of **9** were consistent with that reported for luteolin 7-*O*-*β*-D-glucoside (Table S7) [14]. It is the first time to be isolated from the *Washingtonia* genus.

Table S1: [1]H-NMR and APT spectral data of compound **1** compared to the reported data of *β*-sitosterol-oleate

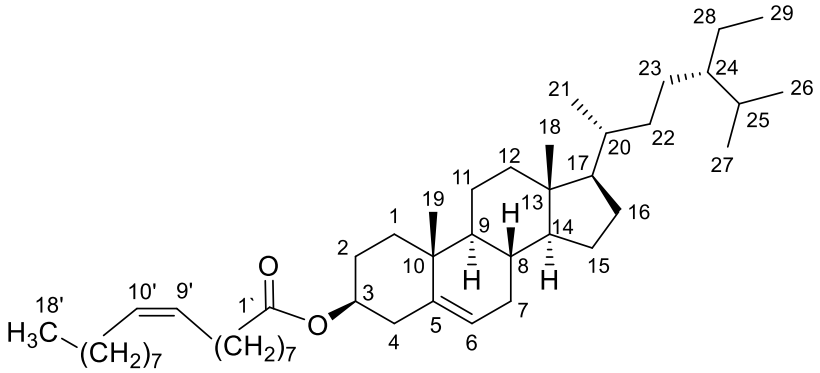

1

H/C no.	Compound **1** ($CDCl_3$)			*β*-Sitosterol-oleate ($CDCl_3$) **[1]**	
	APT*		^{1}H-NMR*	^{13}C-NMR **	^{1}H-NMR**
1	37.0	CH_2	1.86 (2H, *m*)	37.1	1.85 (2H, *m*)
2	32.0	CH_2	1.98 (2H, *m*)	32.1	1.97 (2H, *m*)
3	73.7	CH	4.59 (1H, *m*)	73.7	4.59 (1H, *m*)
4	39.7	CH_2	2.00 (2H, *m*)	39.8	1.99 (2H, *m*)
5	139.7	C		139.8	
6	122.6	CH	5.36 (1H, *m*)	122.7	5.35 (1H, *s*)
7	32.0	CH_2	1.95 (2H, *m*)	32.0	1.93 (2H, *m*)
8	31.9	CH	1.49 (1H, *m*)	31.9	1.49 (1H, *m*)
9	50.0	CH	0.93 (1H, *m*)	50.1	0.93 (1H, *m*)
10	36.6	C		36.7	
11	21.0	CH_2	1.47 (2H, *m*)	21.1	1.47 (2H, *m*)
12	38.2	CH_2	2.29 (2H, *m*)	38.2	2.29 (2H, *m*)
13	42.3	C		42.4	
14	56.7	CH	1.02 (1H, *m*)	56.7	1.00 (1H, *m*)
15	24.3	CH_2	0.96 (2H, *m*)	24.4	0.98 (2H, *m*)
16	28.3	CH_2	1.83 (2H, *m*)	28.3	1.83 (2H, *m*)
17	56.0	CH	1.07 (1H, *m*)	56.1	1.07 (1H, *m*)
18	11.9	CH_3	0.68 (3H, *s*)	11.9	0.65 (3H, *s*)
19	19.3	CH_3	1.02 (3H, *s*)	19.4	1.00 (3H, *s*)
20	36.2	CH	1.30 (1H, *m*)	36.2	1.31 (1H, *m*)
21	18.8	CH_3	0.91 (3H, *d*)	18.9	0.9 (3H, *d*)
22	23.9	CH_2	1.23 (2H, *m*)	33.9	1.23 (2H, *m*)
23	26.1	CH_2	1.14 (2H, *m*)	26.0	1.14 (2H, *m*)
24	45.8	CH	0.91 (1H, *m*)	45.9	0.91 (1H, *m*)
25	29.2	CH	1.29 (2H, *m*)	29.2	1.29 (2H, *m*)
26	19.8	CH_3	0.85 (3H, *d*, *J* = 4.0)	19.9	0.85 (3H, *d*)
27	19.0	CH_3	0.82 (3H, *d*, *J* = 4.0)	19.1	0.81 (3H, *d*)
28	23.1	CH_2	1.25 (2H, *m*)	23.1	1.25 (2H, *m*)
29	12.0	CH_3	0.84 (3H, *overlap*.)	12.1	0.83 (3H, *t*)
1`	173.4	C		173.4	
2`	34.8	CH_2	2.26 (2H, *m*)	34.8	2.25 (2H, *t*)
3`	25.1	CH_2	1.60 (2H, *m*)	25.5	1.59 (2H, *m*)
4`	29.1	CH_2	1.29 (2H, *m*)	29.2	1.29 (2H, *m*)
5`	29.6	CH_2	1.25 (2H, *m*)	29.6	1.23 (2H, *m*)
6`	29.4	CH_2	1.25 (2H, *m*)	29.4	1.23 (2H, *m*)
7`	29.7	CH_2	1.25 (2H, *m*)	29.8	1.23 (2H, *m*)
8`	27.2	CH_2	1.99 (2H, *m*)	27.2	1.98 (2H, *m*)
9`	129.8	CH	5.34 (1H, *m*)	129.9	5.32 (1H, *dd*)
10`	130.0	CH	5.34 (1H, *m*)	130.1	5.32 (1H, *dd*)

11`	27.2	CH_2	1.99 (2H, *m*)	27.3	1.98 (2H, *m*)
12`	29.8	CH_2	1.25 (2H, *m*)	29.9	1.23 (2H, *m*)
13`	29.5	CH_2	1.25 (2H, *m*)	29.5	1.23 (2H, *m*)
14`	29.7	CH_2	1.25 (2H, *m*)	29.7	1.23 (2H, *m*)
15`	29.3	CH_2	1.29 (2H, *m*)	29.3	1.29 (2H, *m*)
16`	27.8	CH_2	1.85 (2H, *m*)	27.9	1.85 (2H, *m*)
17`	22.7	CH_2	1.26 (2H, *m*)	22.8	1.26 (2H, *m*)
18`	14.1	CH_3	0.88 (3H, *overlap*.)	14.3	0.86 (3H, *t*)

* The chemical shifts (δ) are expressed in ppm, APT and ^{1}H-NMR are measured in $CDCl_3$ at 100 MHz and 400 MHz, respectively. *Overlap*.: Ovelapping signals.

** Published data [1], ^{13}C and ^{1}H-NMR are measured in $CDCl_3$ at 150 MHz and 600 MHz, respectively.

Table S2: ^{1}H-NMR and APT spectral data of compound **2** compared to the reported data of oleic acid

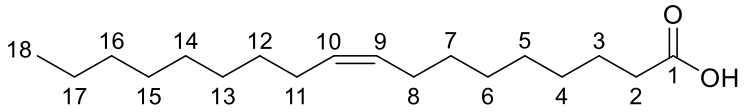

2

H/C no.	Compound 2 ($CDCl_3$) APT *		^{1}H-NMR*	Oleic acid ($CDCl_3$) [2] ^{13}C-NMR **	^{1}H-NMR**
1	180.3	C		180.50	
2	34.1	CH_2	2.36, *t*, *J*= 8.0	33.96	2.36
3	24.7	CH_2	1.64, *m*	24.59	1.64
4-7	29.3	CH_2	1.28, *s*	29-31	1.30
8	27.2	CH_2	2.03, *m*	27.12	2.03
9	129.7	CH	5.36, *m*	130	5.36
10	130.0	CH	5.36, *m*	130	5.36
11	27.2	CH_2	2.03, *m*	27.12	2.03
12-16	29.3	CH_2	1.28, *s*	29-31	1.30
17	22.7	CH_2	1.28, *s*	22.52	1.30
18	14.1	CH_3	0.89, *t*, *J*= 8.0	14.07	0.89

* The chemical shifts (δ) are expressed in ppm, APT and ^{1}H-NMR are measured in $CDCl_3$ at 100 MHz and 400 MHz, respectively.

** Published data [2], ^{13}C-NMR and ^{1}H-NMR are measured in $CDCl_3$ at 100 MHz and 400 MHz, respectively.

Table S3: [1]H-NMR and APT spectral data of compound **4** compared to the reported data of 9-hydroxy-7-methoxy-8-[4'-hydroxy-3'-methoxyphenyl]-4-hydroxy-3-methoxyphenylpropane

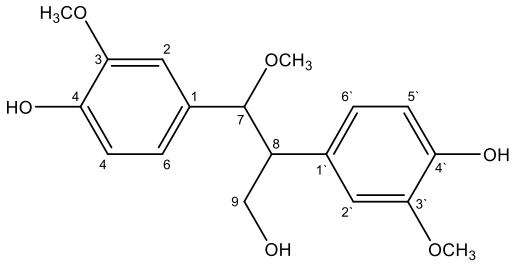

Position (H/C)	**4***		**9-Hydroxy-7-methoxy-8-[4'-hydroxy-3'-methoxyphenyl]-4-hydroxy-3-methoxyphenylpropane [7]****	
	δ_C	**δ_H**	**δ_C**	**δ_H (*J* in Hz)**
1	132.67 (C)		132.53	
2	112.41 (CH)	6.53 (1H, *d*, *J* = 1.4)	112.09	7.00 (1H, *d*, *J* = 1.8)
3	148.52 (C)		148.33	
4	146.83 (C)		147.50	
5	115.49 (CH)	6.61 (1H, *d*, *J* = 8.0)	115.99	7.12 (1H, *d*, *J* = 8.1)
6	122.65 (CH)	6.49 (1H, *dd*, *J* = 8.5, 1.8)	121.54	6.97 (1H, *dd*, *J* = 8.1, 1.8)
7	87.42 (CH)	4.32 (1H, *d*, *J* = 8.5)	86.23	4.82 (1H, *d*, *J* = 7.7)
8	55.99 (CH)	3.00 (1H, *m*)	55.6	3.59 (1H, *m*)
9	64.97 (CH_2)	4.05 (1H, *dd*, *J* = 10.9, 5.8) 3.89 (1H, *d*, *J* = 10.7, 6.9)	64.28	4.54 (1H, *dd*, *J* = 10.6, 5.5) 4.47 (1H, *dd*, *J* = 10.6, 6.6)
1'	132.67 (C)		131.90	
2'	114.37 (CH)	6.49 (1H, *d*, *overlap.*)	114.37	7.01 (1H, *d*, *J* = 1.8)
3'	148.34 (C)		148.05	
4'	146.83 (C)		146.70	
5'	115.71 (CH)	6.65 (1H, *d*, *J* = 8.0)	115.83	7.10 (1H, *d*, *J* = 7.7)
6'	121.56 (CH)	6.56 (1H, *dd*, *J* = 8.1, 1.5)	122.73	6.95 (1H, *dd*, *J* = 7.7, 1.8)
7-OMe	56.78 (CH_3)	3.23 (3H, *s*)	56.57	3.34 (3H, *s*)
3-OMe	56.34 (CH_3)	3.70 (3H, *s*)	55.86	3.67 (3H, *s*)
3'-OMe	56.30 (CH_3)	3.71 (3H, *s*)	55.83	3.65 (3H, *s*)

* The chemical shift values (δ) are expressed in ppm in CD_3OD at 400 MHz for [1]H and 100 MHz for [13]C. HSQC was used to assign protons to their carbon positions.

** Reported NMR data of 9-hydroxy-7-methoxy-8-[4'-hydroxy-3'-methoxyphenyl]-4-hydroxy-3-methoxyphenylpropane in C_5D_5N (400 MHz for [1]H and 100 MHz for [13]C) [7].

Table S4: ^{1}H-NMR and APT spectral data of compound **5** compared to the reported data of syringaresinol

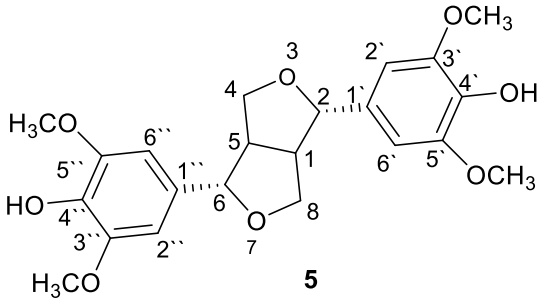

5

H/C no.	Compound 5 (CD_3OD)			Syringaresinol ($CDCl_3$) [10] **	
	APT *		^{1}H-NMR*	^{13}C-NMR**	^{1}H-NMR**
1'/1"	131.8	Q		132.04	
2'/2"	103.2	CH	6.67, *s*	102.69	6.61, *s*
3'/3"	148.0	Q		147.13	
4'/4"	134.9	Q		134.29	
5'/5"	148.0	Q		147.13	
6'/6"	103.2	CH	6.67, *s*	102.69	6.61, *s*
1/5	54.1	CH	3.15, *m*	54.29	3.12, *m*
2/6	86.3	CH	4.73, *s*	86.01	4.76, *d*
4/8	71.4	CH_2	Ha: 4.26, *m* Hb: 3.90, *overlap*.	71.75	4.30, *m* 3.94, *d*
3', 3", 5', 5"-OCH_3	55.4	CH_3	3.84, *s*	56.33	3.92, *s*

* The chemical shifts (δ) are expressed in ppm, APT and ^{1}H-NMR are measured in CD_3OD at 100 MHz and 400 MHz, respectively. *Overlap*.: Ovelapping signals.

** Published data [10], APT and ^{1}H-NMR are measured in $CDCl_3$ at 150 MHz and 600 MHz, respectively.

Table S5: [1]H-NMR and APT spectral data of compound **6** compared to the reported data of diosmetin

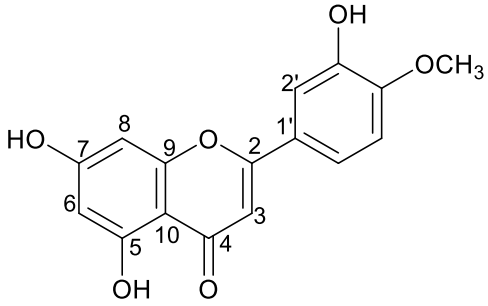

6

H/C no.	**Compound 6 [5,7, 3`-Trihydroxy-4`-methoxy flavone]** (CD_3OD)			**Diosmetin **** (DMSO-d_6) **[11]**	
	^{13}C-NMR*		**^{1}H-NMR***	**^{13}C-NMR****	**^{1}H-NMR****
2	164.7	Q		163.5	
3	103.0	CH	6.49, *s*	103.5	6.73, *s*
4	182.6	Q		181.7	
5	161.5	Q		161.5	
6	99.1	CH	6.16, *d*, *J* = 2.0 Hz	98.9	6.19, *d*, *J* = 2 Hz
7	164.7	Q		164.2	
8	94.0	CH	6.38, *d*, *J* = 2.0 Hz	93.9	6.46, *d*, *J* = 2 Hz
9	157.5	Q		157.3	
10	104.3	Q		103.8	
1'	122.4	Q		123.0	
2'	109.3	CH	7.34, *d*, *J* = 2.0 Hz	113.0	7.41, *d*, *J* = 2.3 Hz
3'	152.3	Q		146.8	
4'	148.1	Q		151.1	
5'	115.5	CH	6.87, *d*, *J* = 8.4 Hz	112.1	7.06, *d*, *J* = 8.6 Hz
6'	120.5	CH	7.4, *dd*, *J* = 2.1, 8.4 Hz	118.1	7.52, *dd*, *J* = 2.3, 8.6 Hz
4`-O-CH_3	55.5	CH_3	3.89, *s*	55.8	3.85, *s*

* The chemical shifts (δ) are expressed in ppm, APT and [1]H-NMR are measured in CD_3OD at 100 MHz and 400 MHz, respectively.

** Published data [11], ^{13}C and [1]H-NMR are measured in DMSO-d_6 at 100 MHz and 400 MHz, respectively.

Table S6: [1]H-NMR and APT spectral data of compound **7** compared to the reported data of tricin

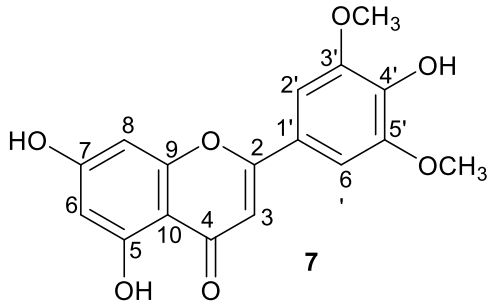

7

H/C no.	Compound 7 [5,7,4`-Trihydroxy-3`,5`-dimethoxy flavone] (CD_3OD)			Tricin** (DMSO-d_6) [12]	
	APT*		^{1}H-NMR*	^{13}C-NMR**	^{1}H-NMR**
2	164.9	Q		163.6	
3	103.7	CH	6.57, *s*	104.4	6.96, *s*
4	182.9	Q		181.7	
5	162.0	Q		161.4	
6	99.4	CH	6.26, *d*, *J* = 2.0 Hz	98.9	6.20, *d*, *J* = 1.9 Hz
7	165.1	Q	-	164.4	
8	94.4	CH	6.47, *d*, *J* = 2.0 Hz	94.2	6.55, *d*, *J* = 1.9 Hz
9	158.4	Q		157.3	
10	104.5	Q		103.5	
1'	121.7	Q		120.4	
2'	104.2	CH	7.16, *s*	103.6	7.31, *s*
3'	148.5	Q		148.2	
4'	140.1	Q		139.9	
5'	148.5	Q		148.2.	
6'	104.2	CH	7.16, *s*	103.6	7.31, *s*
3`,5`-O-CH_3	56.3	CH_3	3.96, *s*	56.3	3.88, *s*

* The chemical shifts (δ) are expressed in ppm, APT and [1]H-NMR are measured in CD_3OD at 100 MHz and 400 MHz, respectively.

** Published data [12], ^{13}C and [1]H-NMR are measured in DMSO-d_6 at 125.8 MHz and 500.1 MHz, respectively.

Table S7: [1]H-NMR and APT spectral data of compound **9** compared to the reported data of luteolin 7-*O*-*β*-D-glucoside

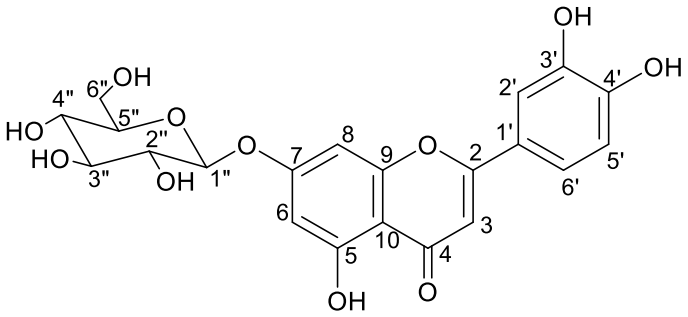

9

H/C no.	Compound 9 [5,4`,5`-Trihydroxy-7-*O*-*β*-D-glucoside flavone] (DMSO-d_6)			Luteolin 7-*O*-*β*-D-glucoside** (DMSO-d_6) [14]	
	APT*		**^{1}H-NMR***	**^{13}C-NMR****	**^{1}H-NMR****
2	165.0	Q		164.9	
3	103.7	CH	6.69, *s*	103.5	6.76, s
4	182.4	Q		182.3	
5	161.6	Q		161.6	
6	100.1	CH	6.40, *s*	99.9	6.45, d, *J* = 1.7 Hz
7	163.5	Q		163.4	
8	95.2	CH	6.75, *s*	95.1	6.79, d, *J* = 1.7 Hz
9	157.5	Q		157.4	
10	105.8	Q		105.8	
1'	121.9	Q		121.6	
2'	114.1	CH	7.38, *brs*	113.9	7.43, *brs*
3'	146.3	Q		146.4	
4'	150.4	Q		150.7	
5'	116.5	CH	6.87, *m*	116.4	6.90, d, *J* = 8.4 Hz
6'	119.7	CH	7.41, *m* (*overlap*.)	119.6	7.45, d, *J* = 8.4 Hz
1"	100.4	CH	5.03, d, *J* = 8.0 Hz	100.3	5.08, d, *J* = 7.3 Hz
2"	73.6	CH	3.29, *m*	73.6	3.26, m
3"	77.7	CH	3.46, *m*	77.6	3.45, m
4"	70.1	CH	3.21, *m*	70.0	3.17, m
5"	76.9	CH	3.32, *m*	76.9	3.30, m
6"	61.1	CH_2	6"a: 3.69, *d*, *J* = 12.0 Hz 6"b: 3.46, *m*	61.1	6"a: 3.72, d, *J* = 9.9 Hz 6"b: 3.48, m

* The chemical shifts (δ) are expressed in ppm, APT and [1]H-NMR are measured in DMSO-d_6 at 100 MHz and 400 MHz, respectively. *Overlap*.: Ovelapping signals.

** Published data [14], [13]C and [1]H-NMR are measured in DMSO-d_6 at 100 MHz and 400 MHz, respectively.

Figure S1: Photograph of *W. filifera* fruitless bunches

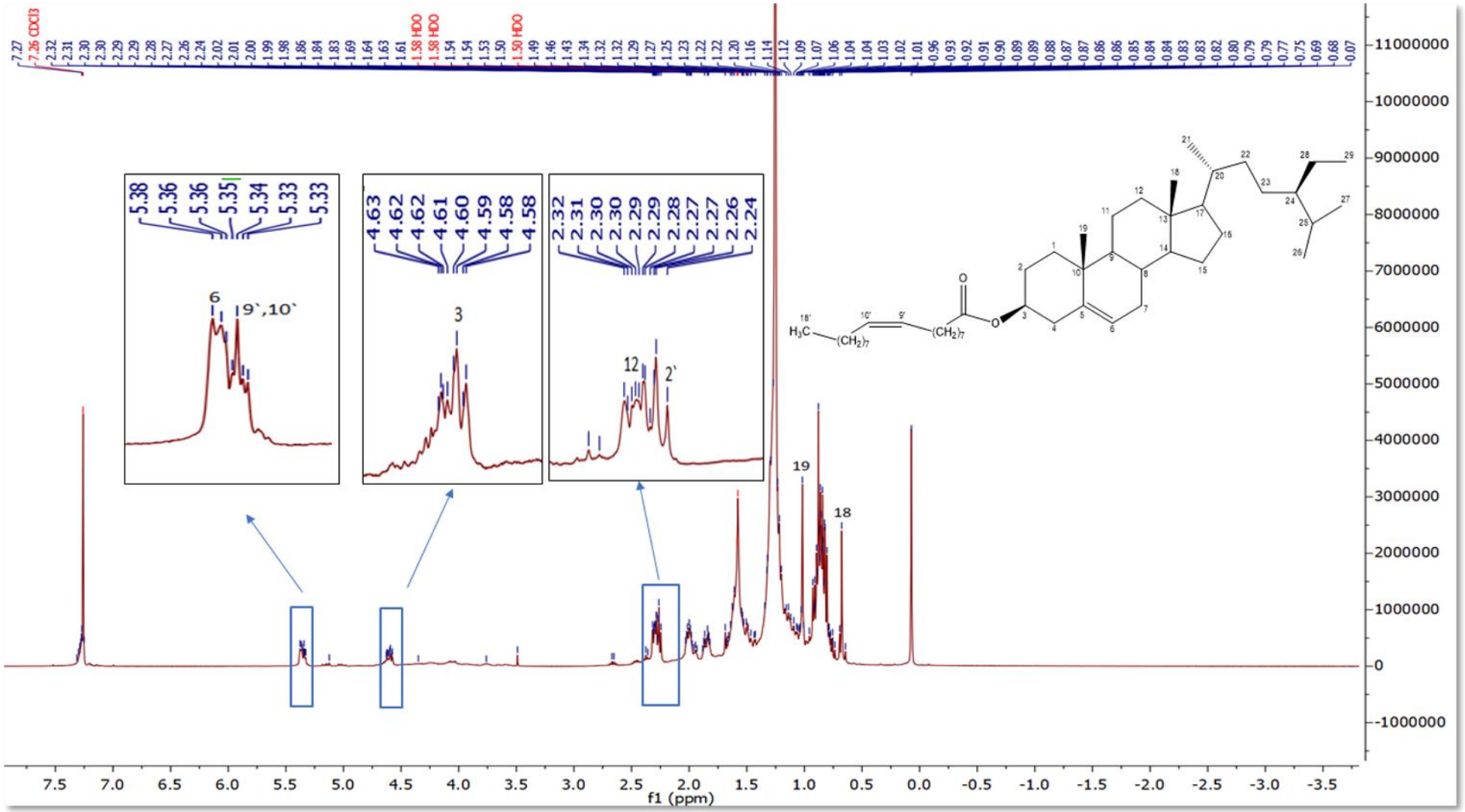

Figure S2: ^{1}H-NMR spectrum ($CDCl_3$, 400 MHz) of compound **1** (β-sitosteryl oleate)

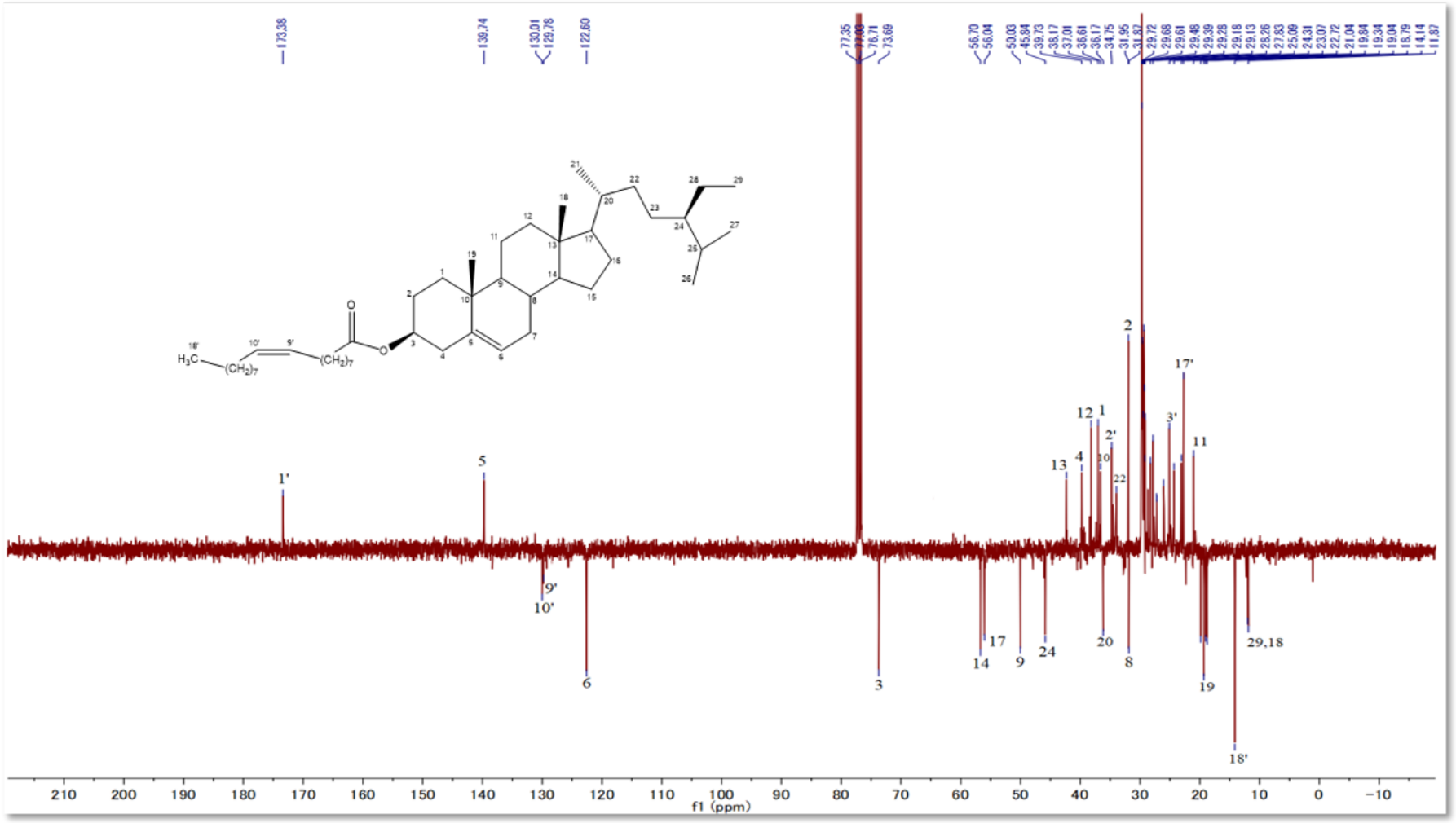

Figure S3: APT spectrum ($CDCl_3$, 100 MHz) of compound **1** (β-sitosteryl oleate)

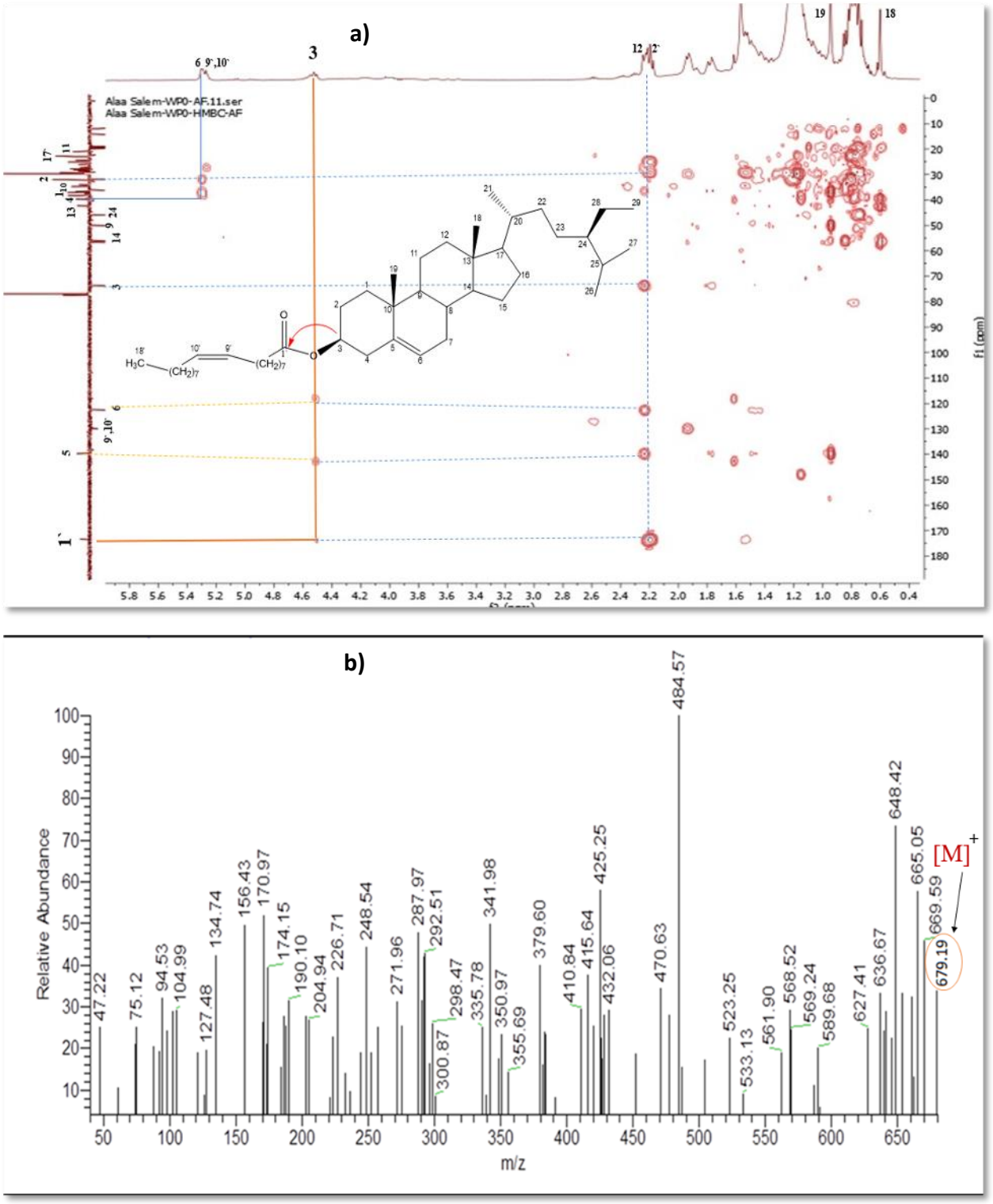

Figure S4: a) HMBC spectrum; and b) EI-MS spectrum of compound **1** (β-sitosteryl oleate)

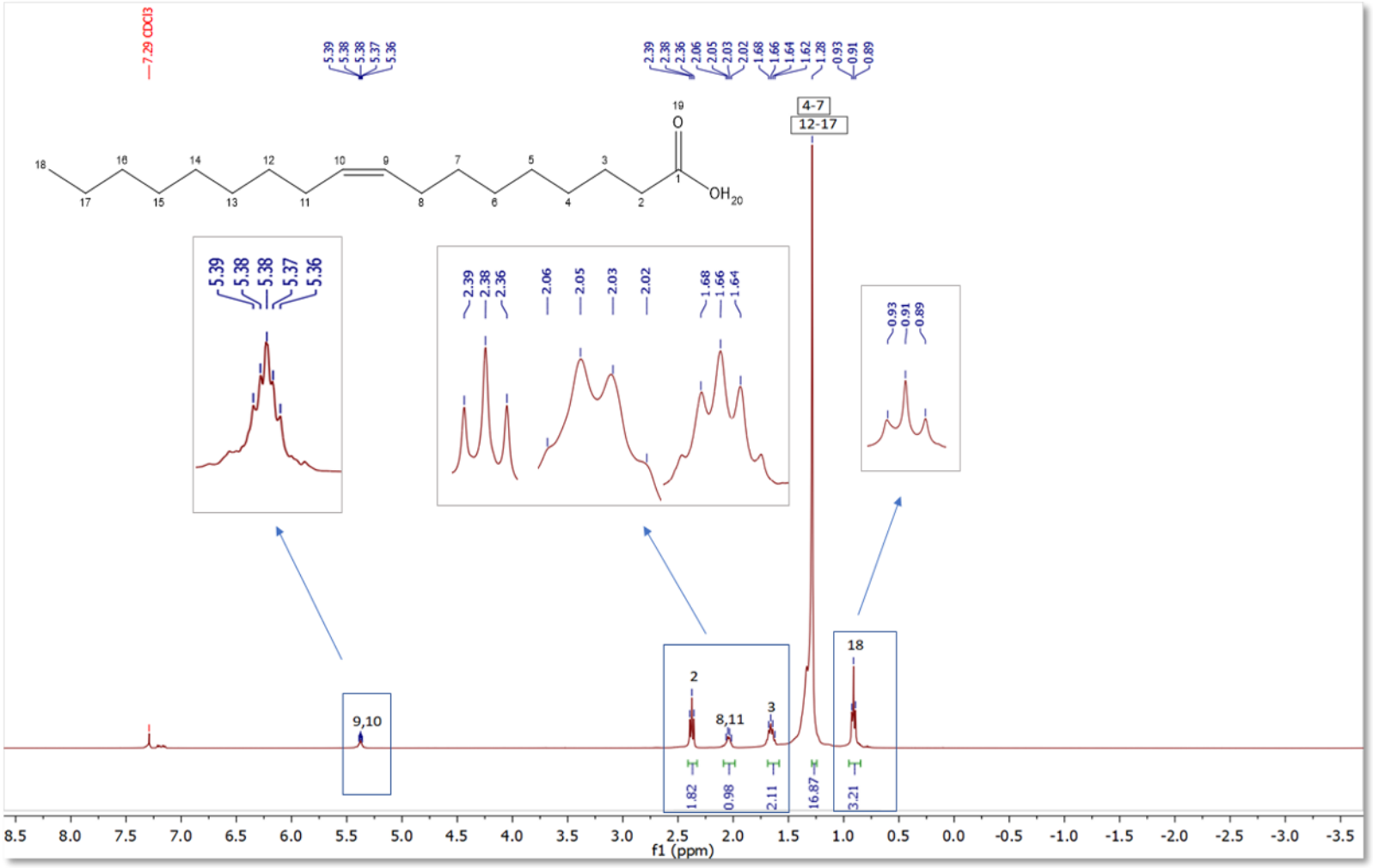

Figure S5: ^{1}H-NMR spectrum ($CDCl_3$, 400 MHz) of compound **2** (oleic acid)

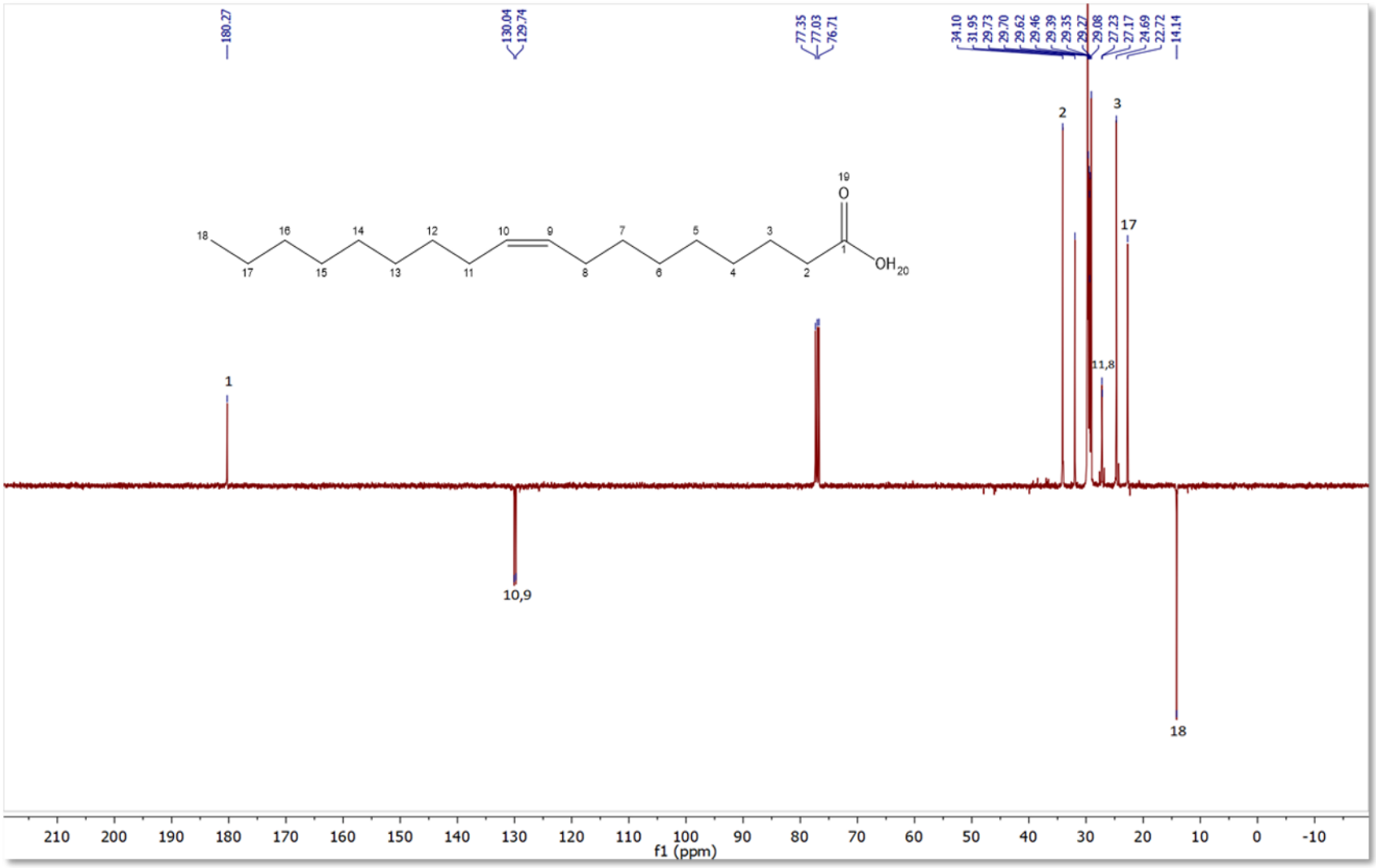

Figure S6: APT spectrum ($CDCl_3$, 100 MHz) of compound **2** (oleic acid)

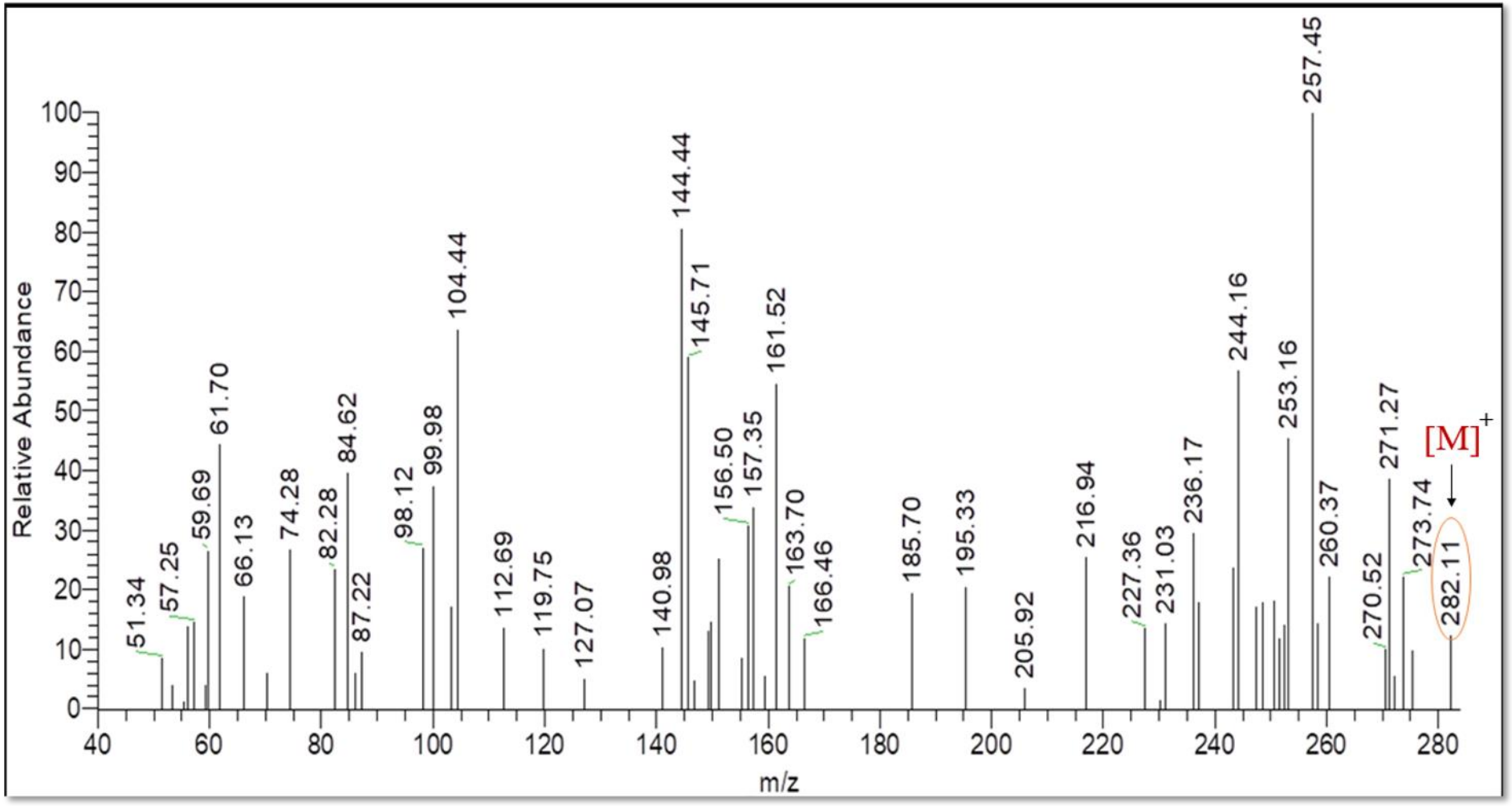

Figure S7: EI-MS spectrum of compound **2** (oleic acid)

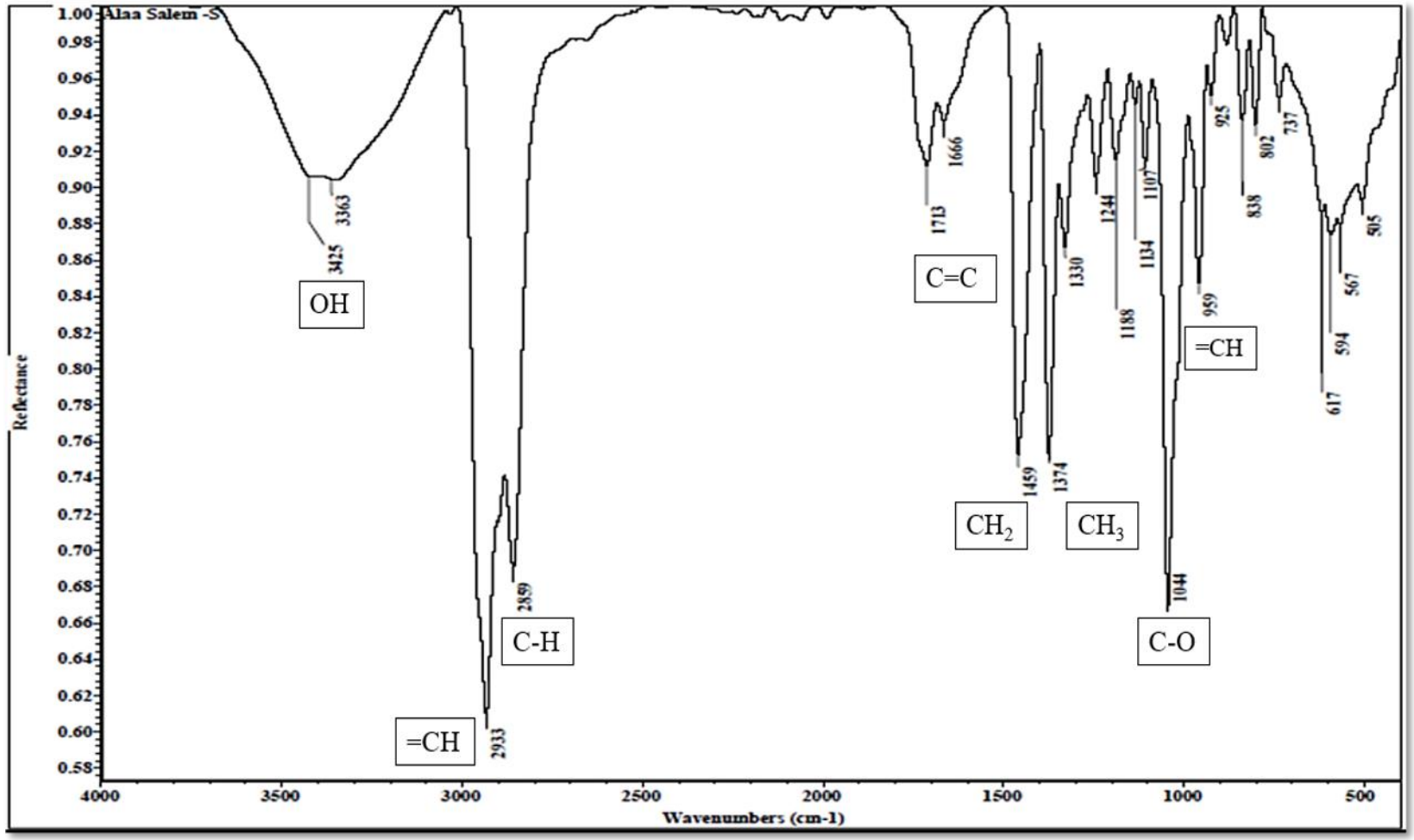

Figure S8: IR (KBr, υ_{max}) spectrum of compound **3** (β-sitosterol)

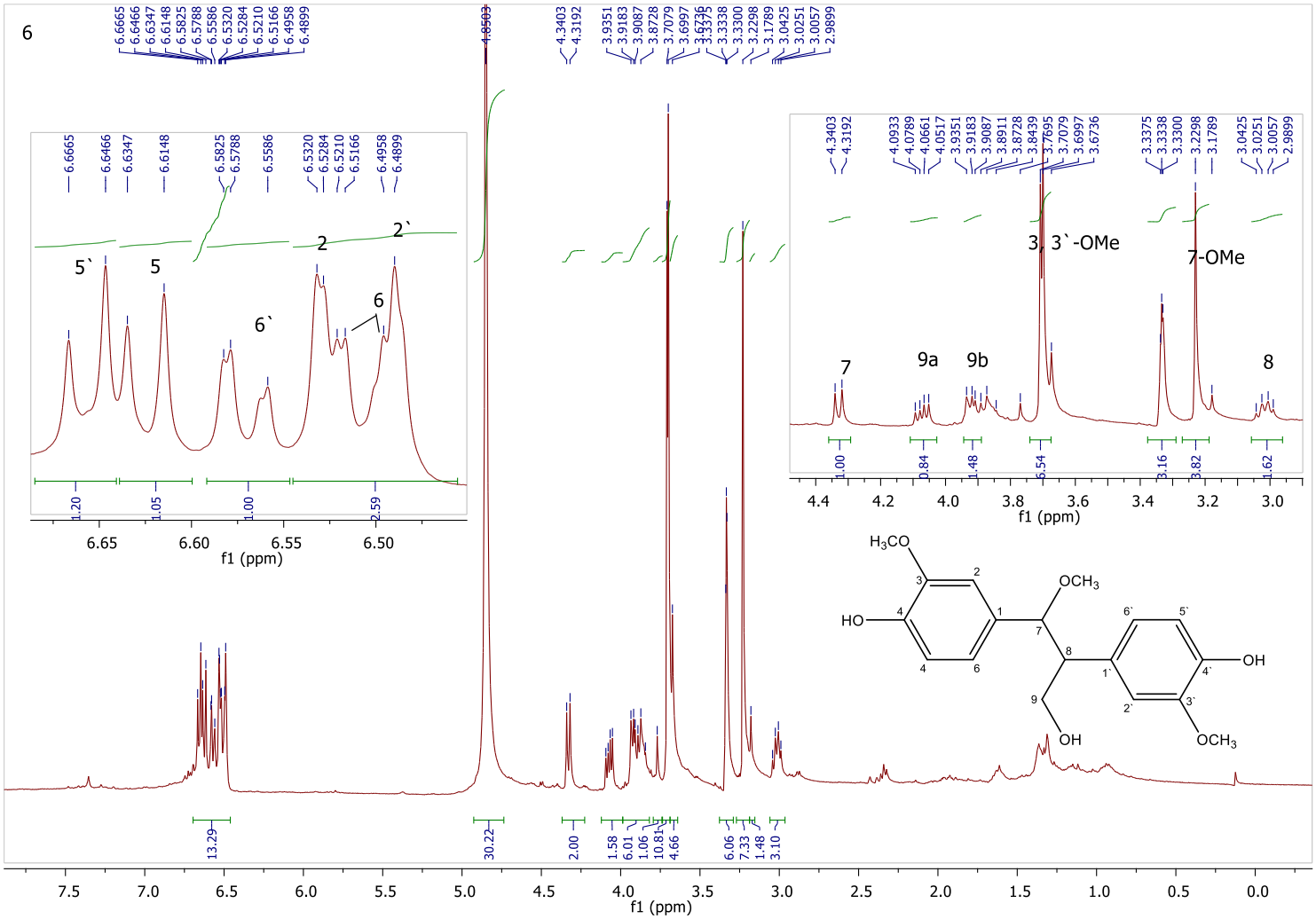

Figure S9: ^{1}H-NMR spectrum (CD_3OD, 400 MHz) of compound **4** (9-hydroxy-7-methoxy-8-[4'-hydroxy-3'-methoxyphenyl]-4-hydroxy-3-methoxyphenylpropane)

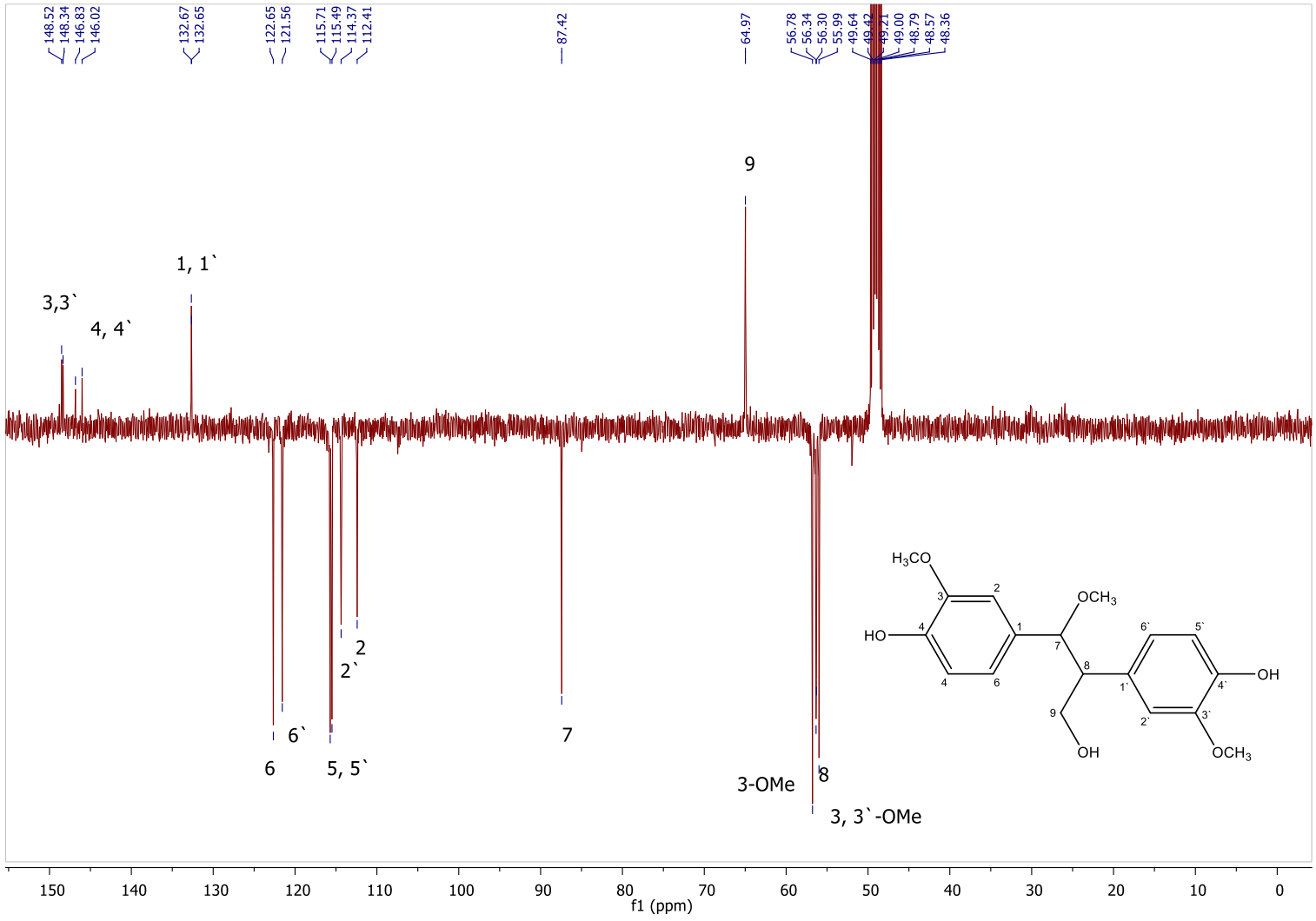

Figure S10: APT spectrum (CD_3OD, 100 MHz) of compound **4** (9-hydroxy-7-methoxy-8-[4'-hydroxy-3'-methoxyphenyl]-4-hydroxy-3-methoxyphenylpropane)

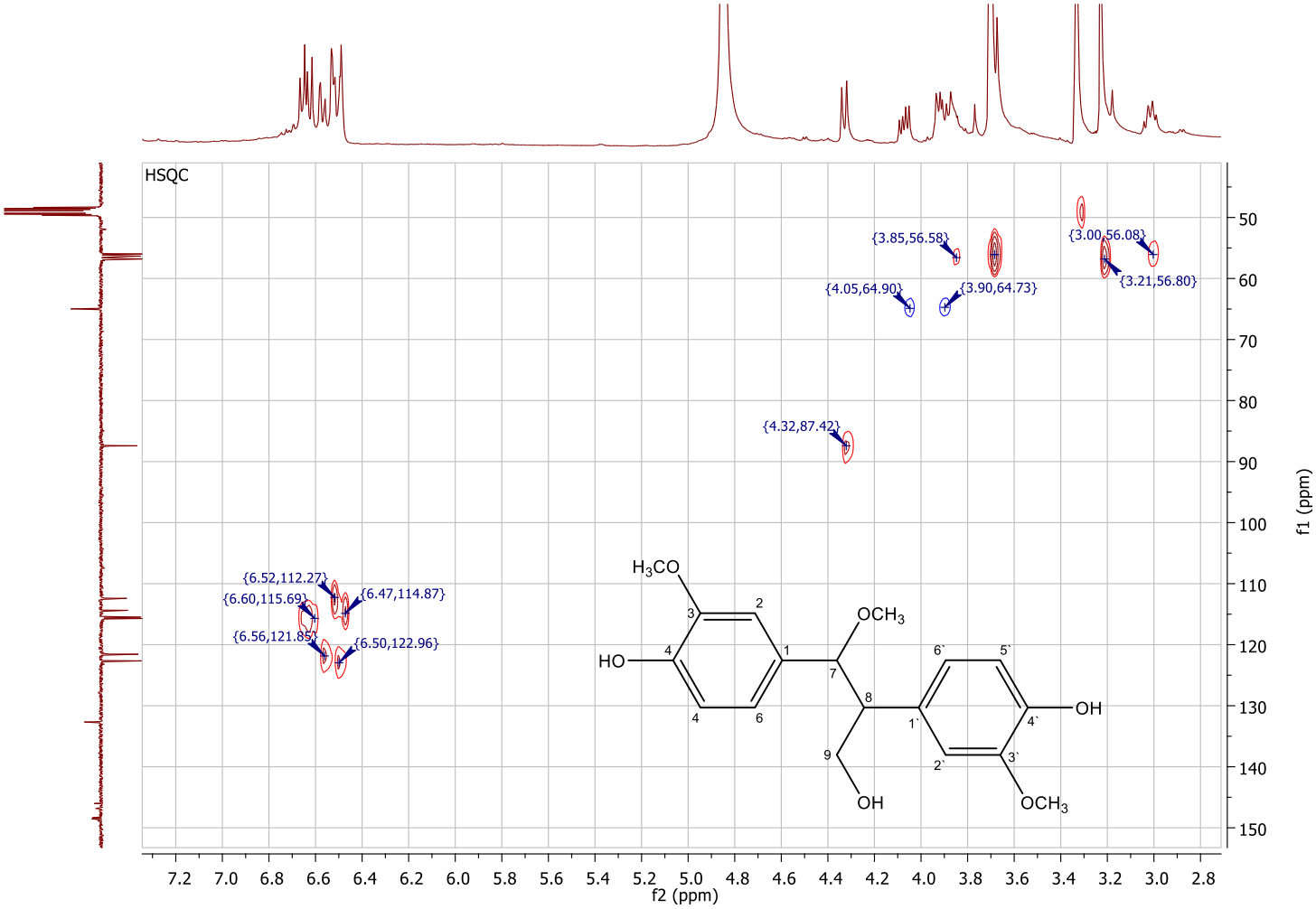

Figure S11: HSQC spectrum (CD_3OD, 400 MHz) of compound **4** (9-hydroxy-7-methoxy-8-[4'-hydroxy-3'-methoxyphenyl]-4-hydroxy-3-methoxyphenylpropane).

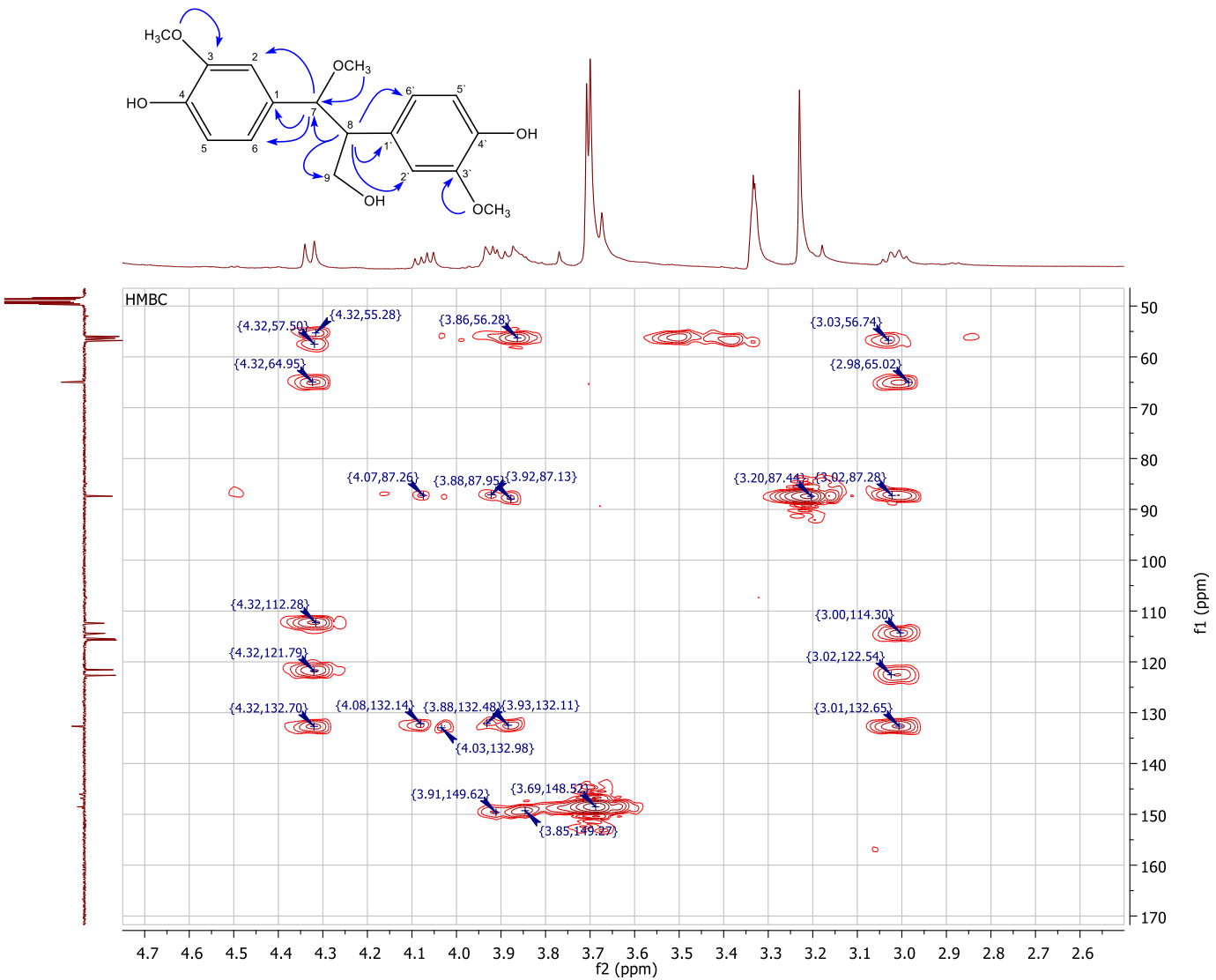

Figure S12: HMBC spectrum (CD_3OD, 400 MHz) of compound **4** (9-hydroxy-7-methoxy-8-[4'-hydroxy-3'-methoxyphenyl]-4-hydroxy-3-methoxyphenylpropane)

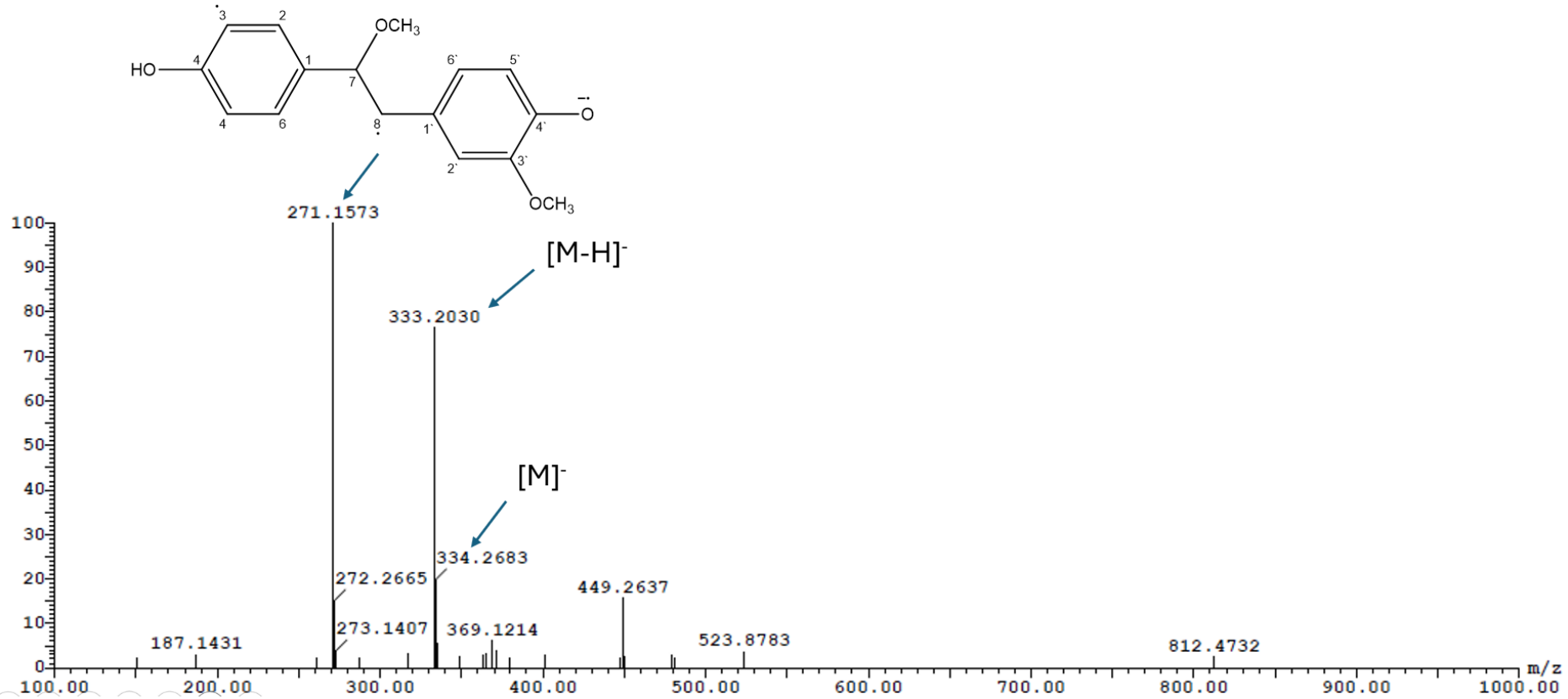

Figure S13: ESI-LC/MS spectrum (negative mode) of compound **4** (9-hydroxy-7-methoxy-8-[4'-hydroxy-3'-methoxyphenyl]-4-hydroxy-3-methoxyphenylpropane).

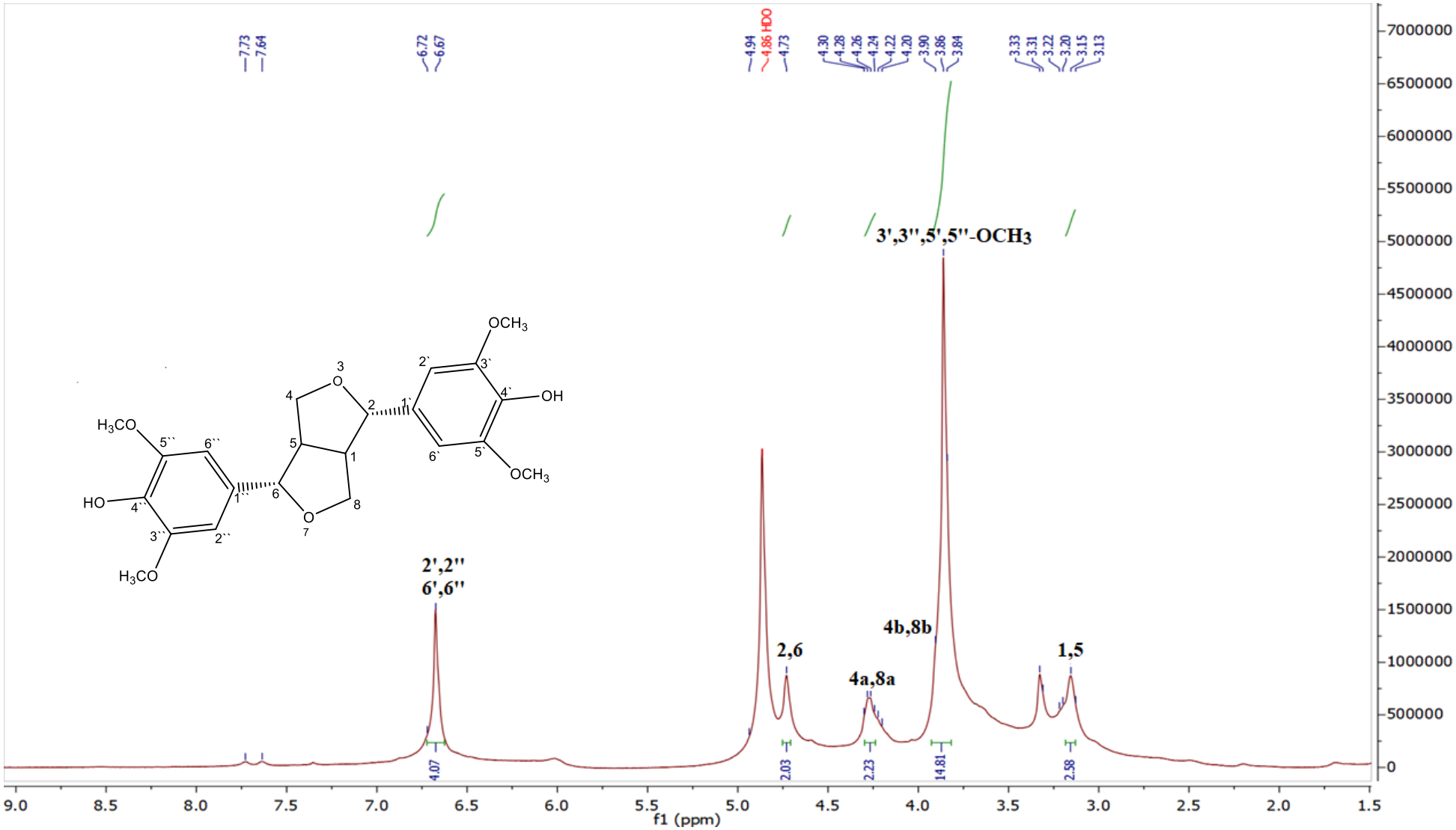

Figure S14: ^{1}H-NMR spectrum (CD_3OD, 400 MHz) of compound **5** (syringaresinol).

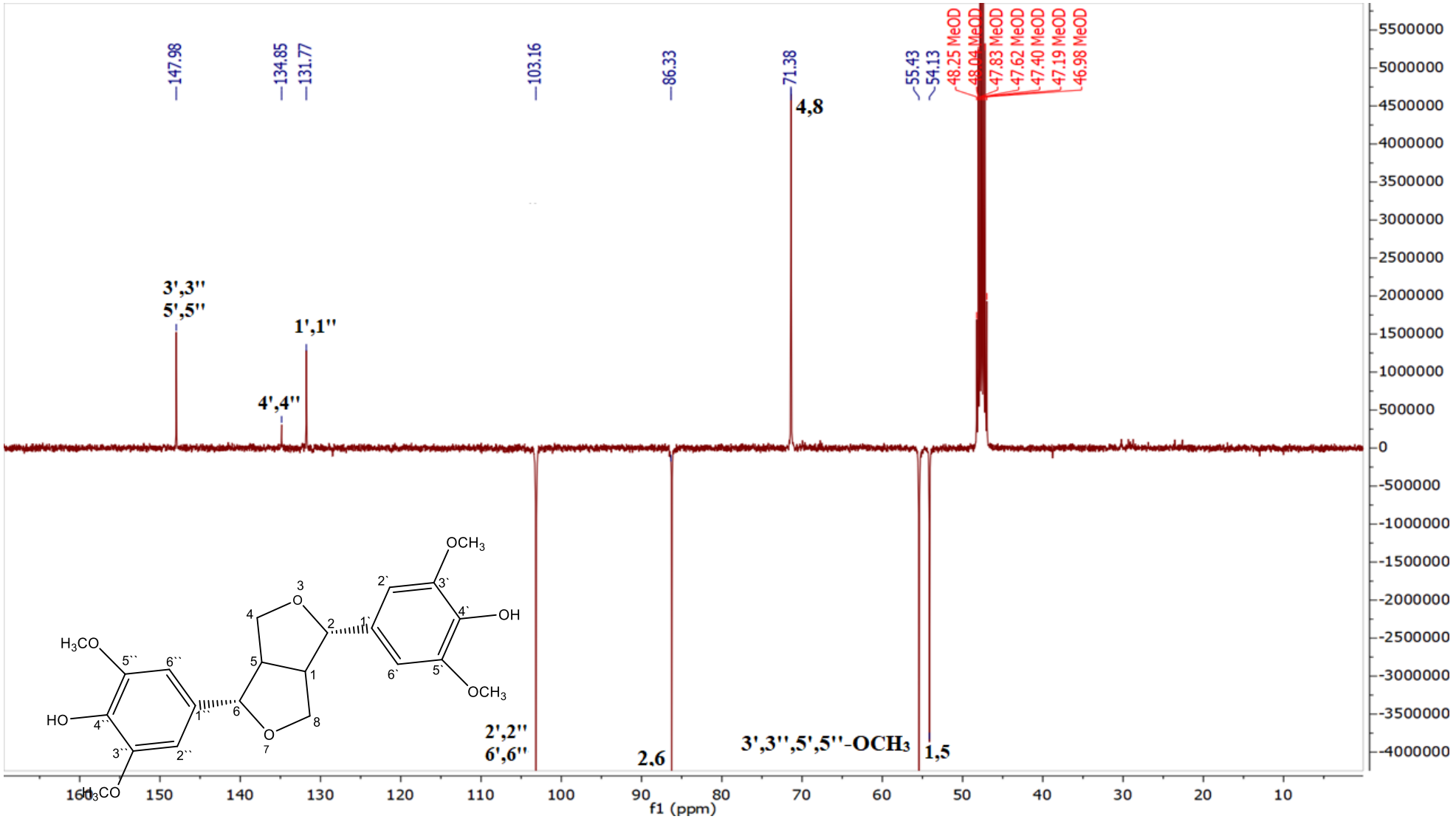

Figure S15: APT spectrum (CD_3OD, 100 MHz) of compound **5** (syringaresinol)

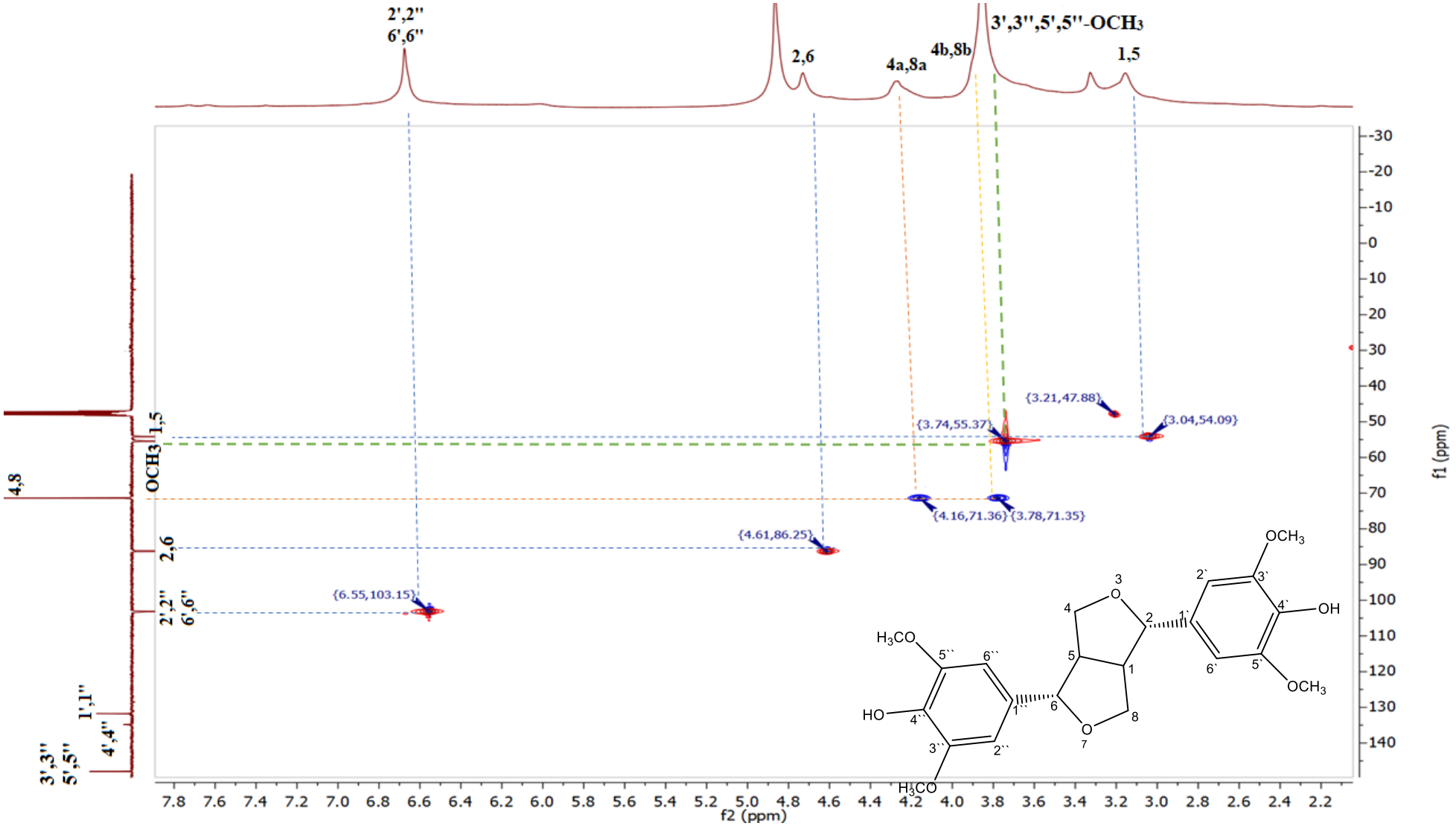

Figure S16: HSQC spectrum (CD_3OD, 400 MHz) of compound **5** (syringaresinol)

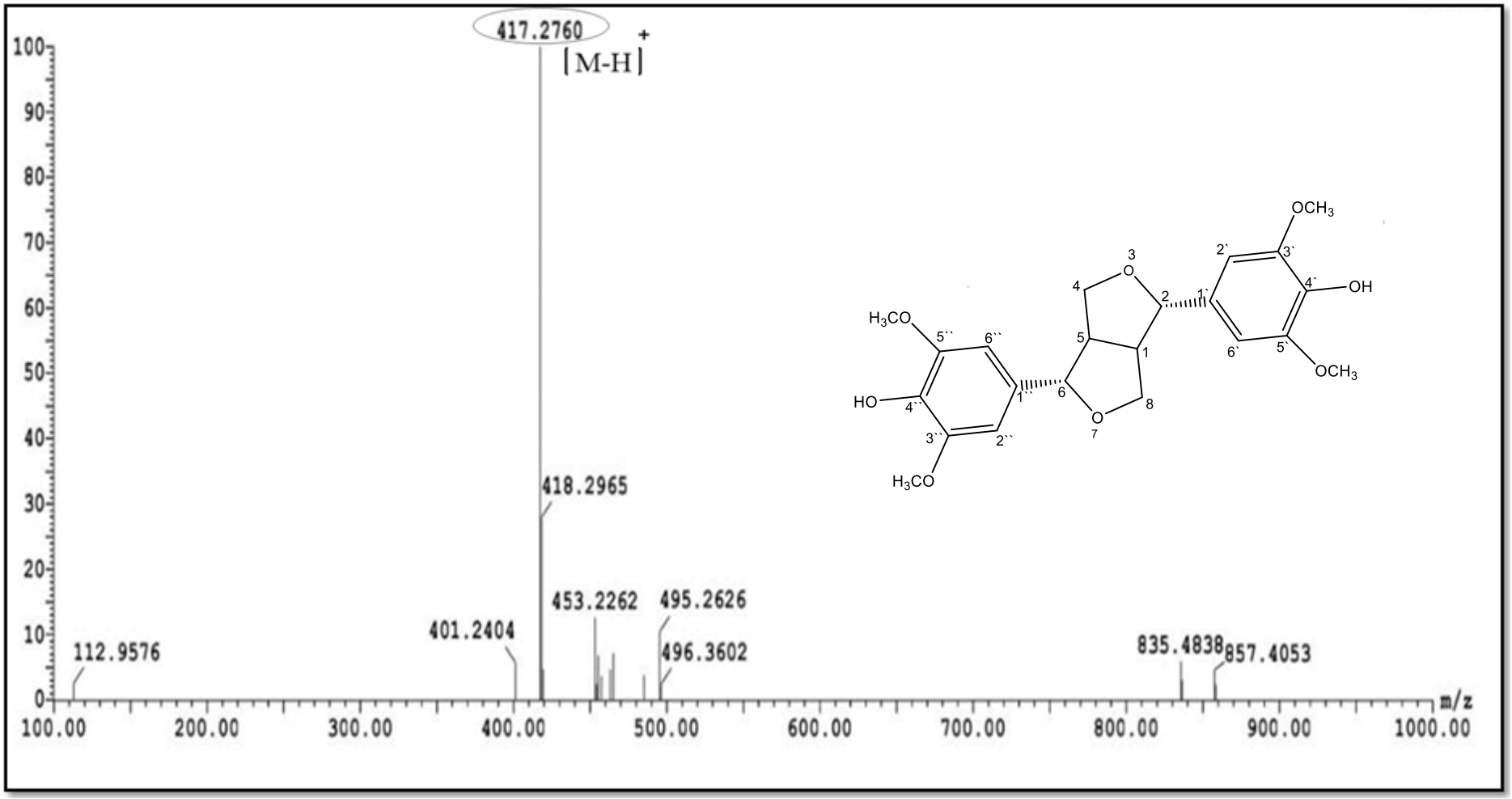

Figure S17: ESI-LC/MS spectrum of compound **5** (syringaresinol) in CD_3OD

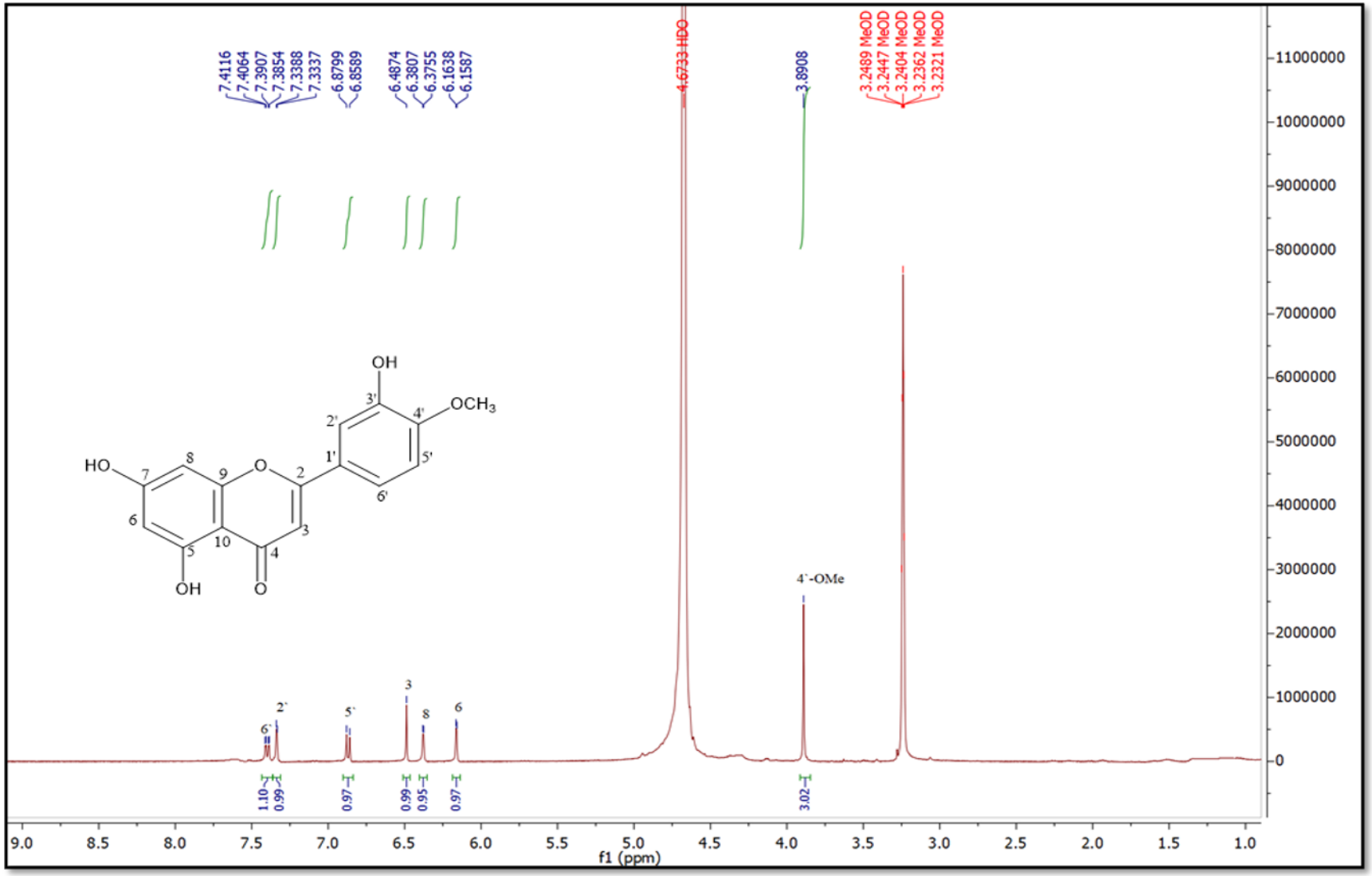

Figure S18: ^{1}H-NMR spectrum (CD_3OD, 400 MHz) of compound **6** (diosmetin)

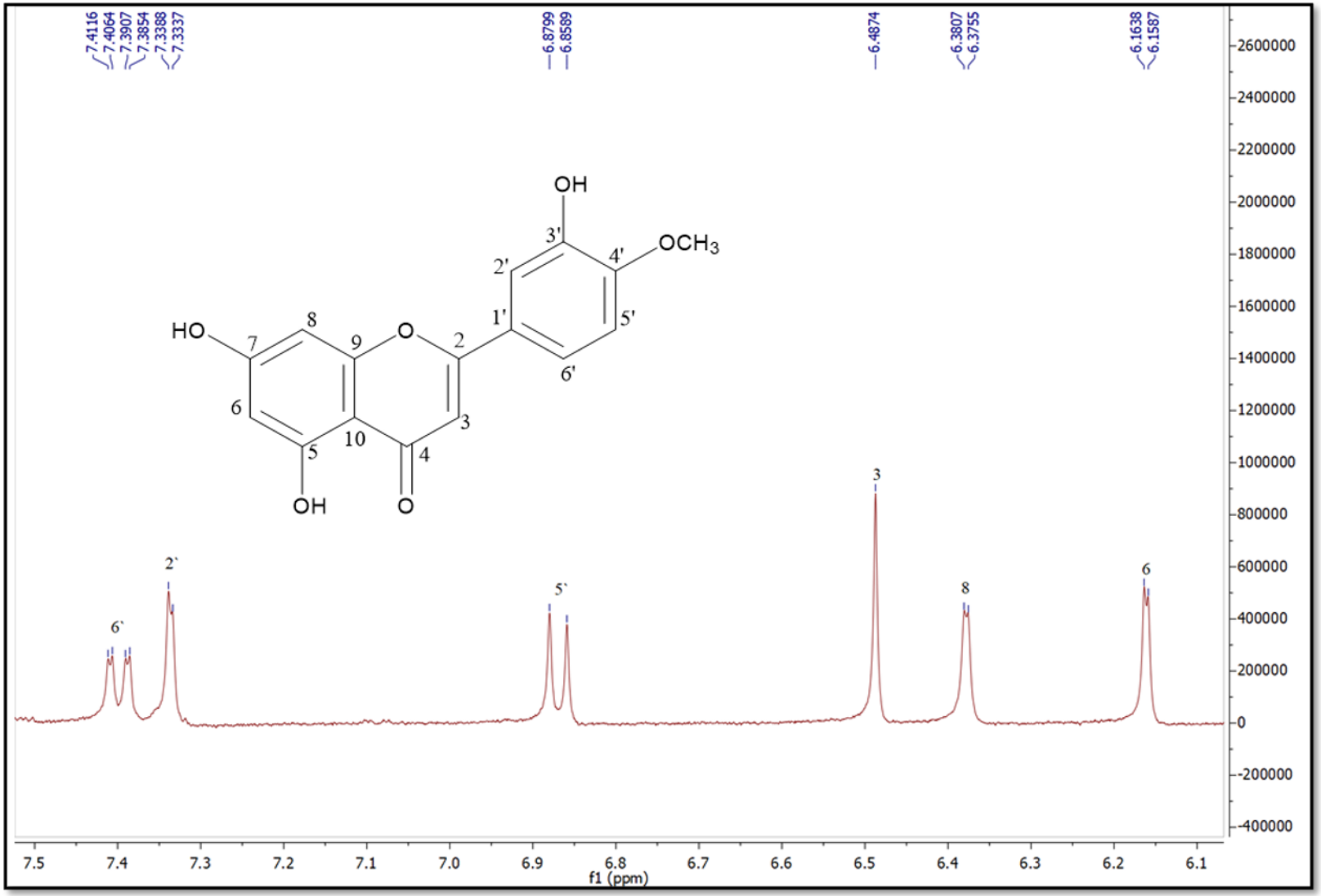

Figure S19: ^{1}H-NMR spectral expansion (CD_3OD, 400 MHz) from 6.1 to 7.5 ppm of compound **6** (diosmetin)

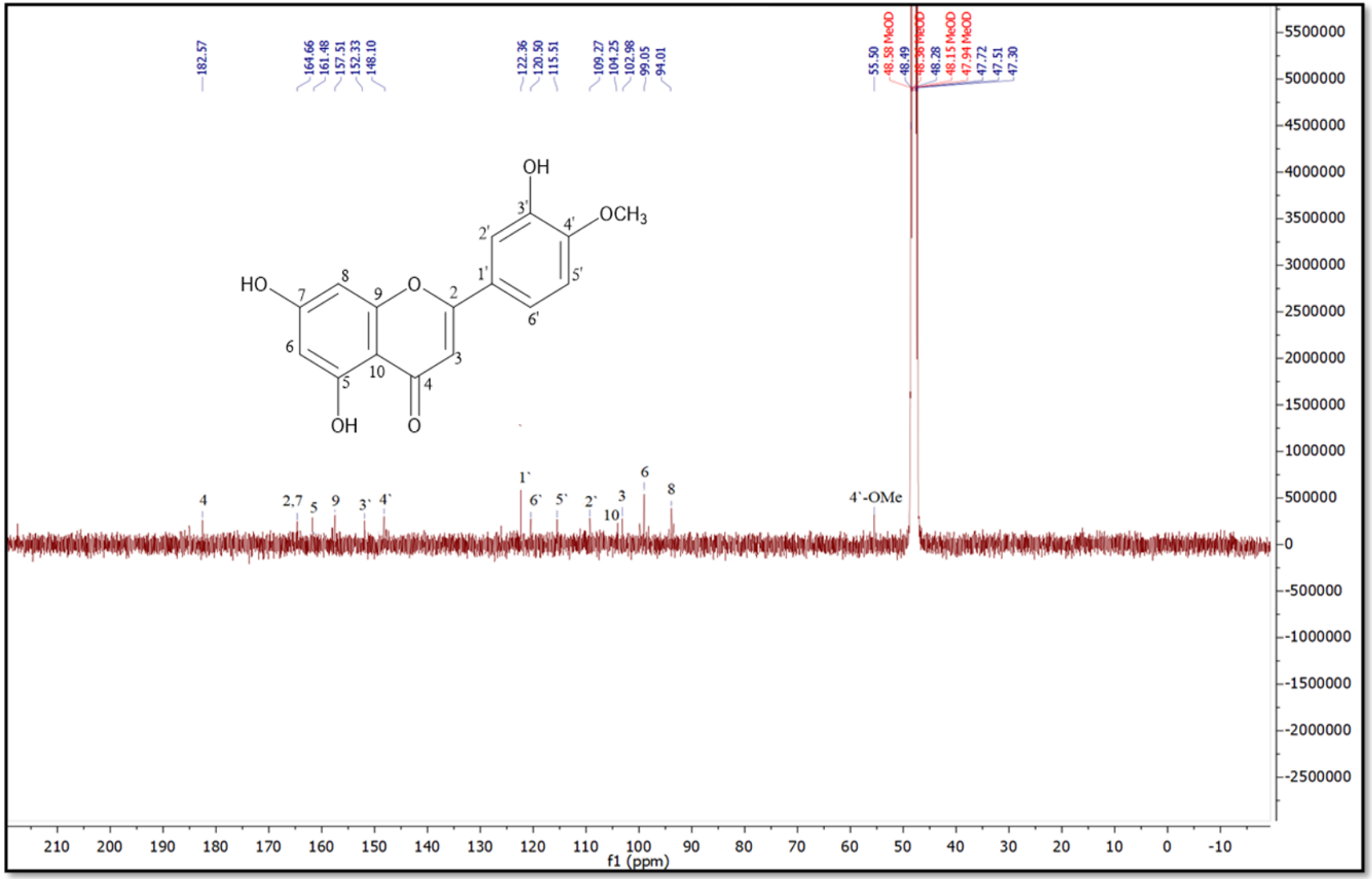

Figure S20: APT spectrum (CD_3OD, 100 MHz) of compound **6** (diosmetin)

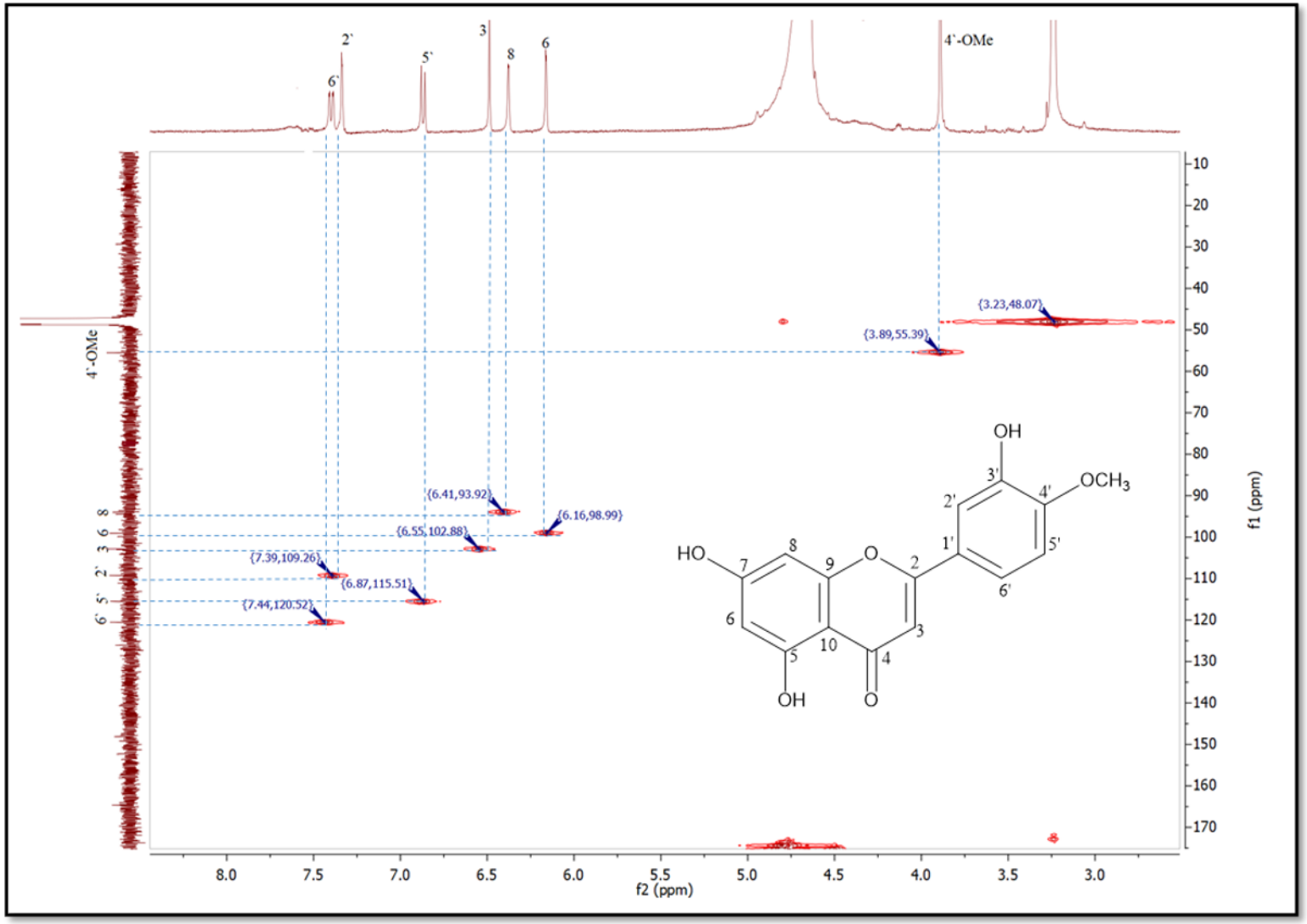

Figure S21: HSQC spectrum (CD_3OD, 400 MHz) of compound **6** (diosmetin)

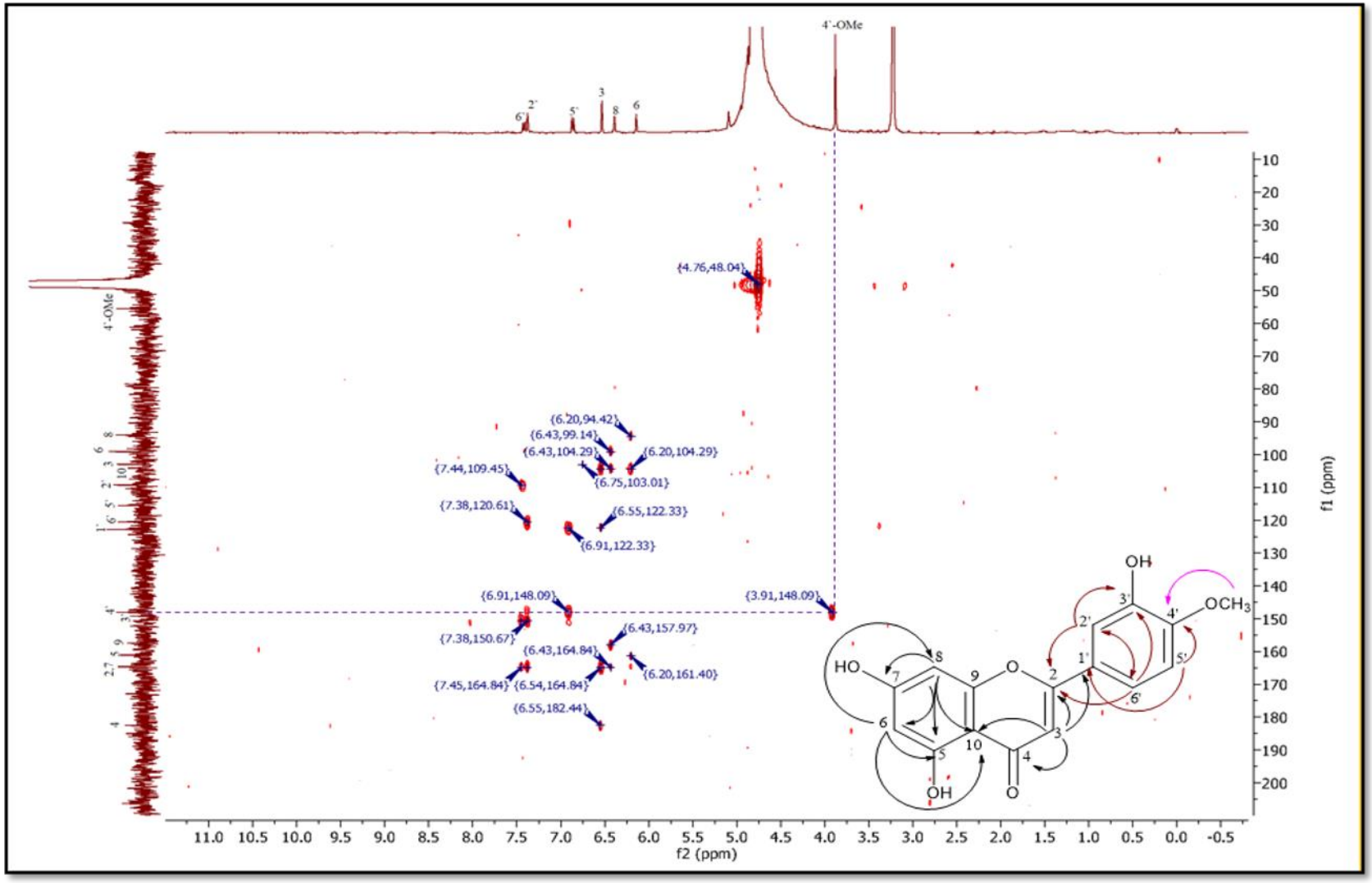

Figure S22: HMBC spectrum (CD_3OD, 400 MHz) of compound **6** (diosmetin)

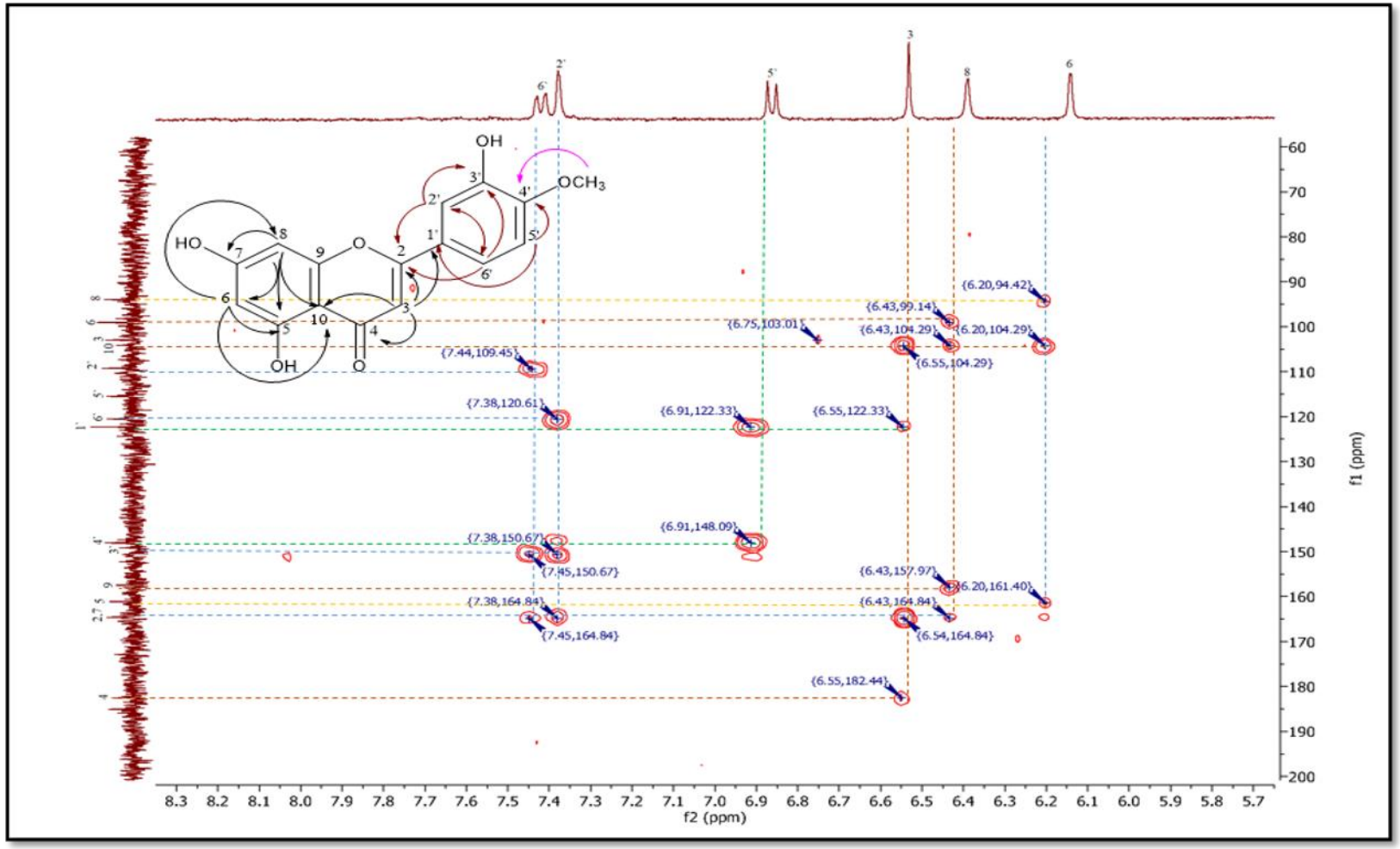

Figure S23: HMBC spectral expansion (CD_3OD, 400 MHz) from 5.7 to 8.3 ppm for ^{1}H and 60-200 ppm for ^{13}C of compound **6** (diosmetin)

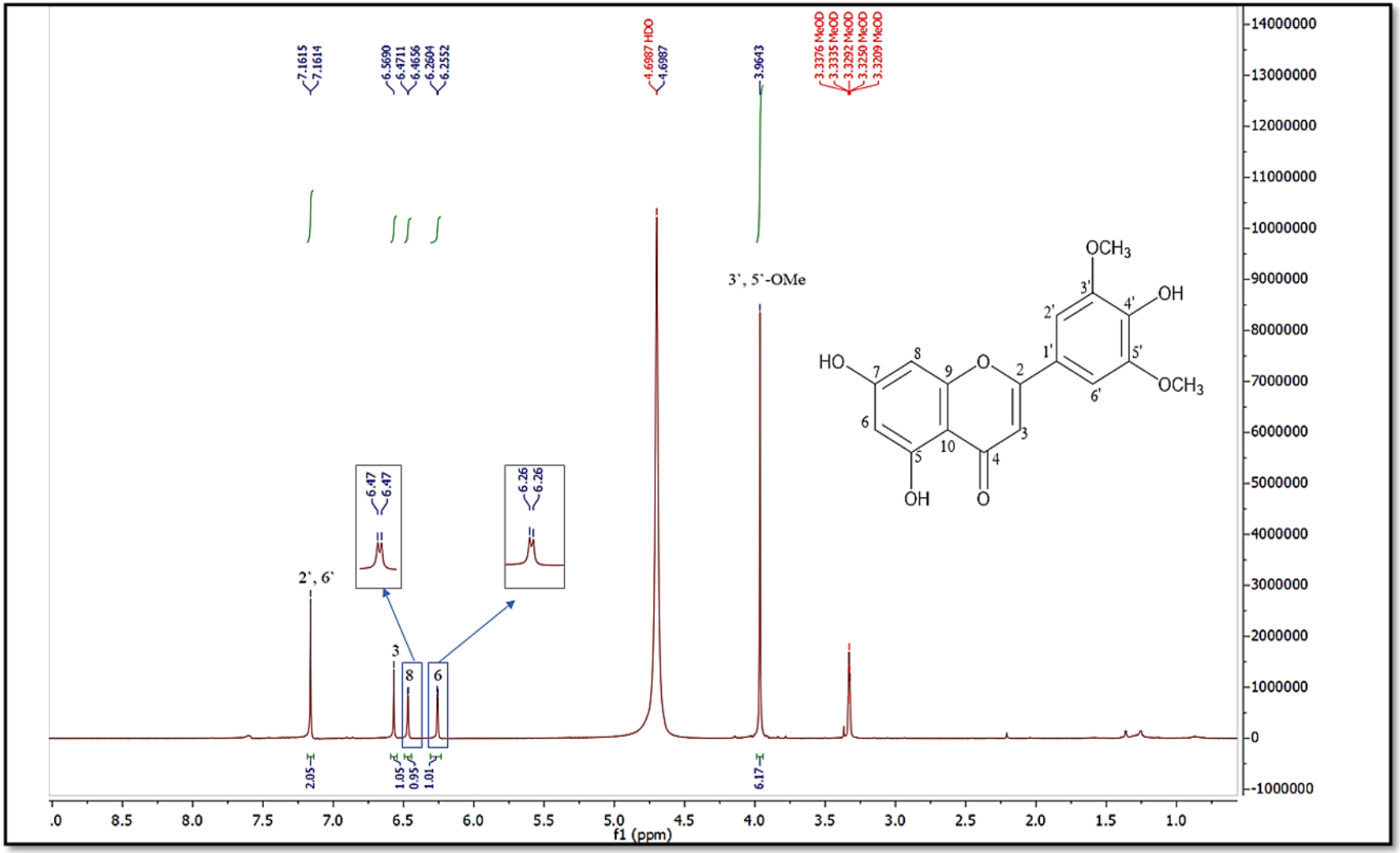

Figure S24: ^{1}H NMR spectrum (CD_3OD, 400 MHz) of compound **7** (tricin)

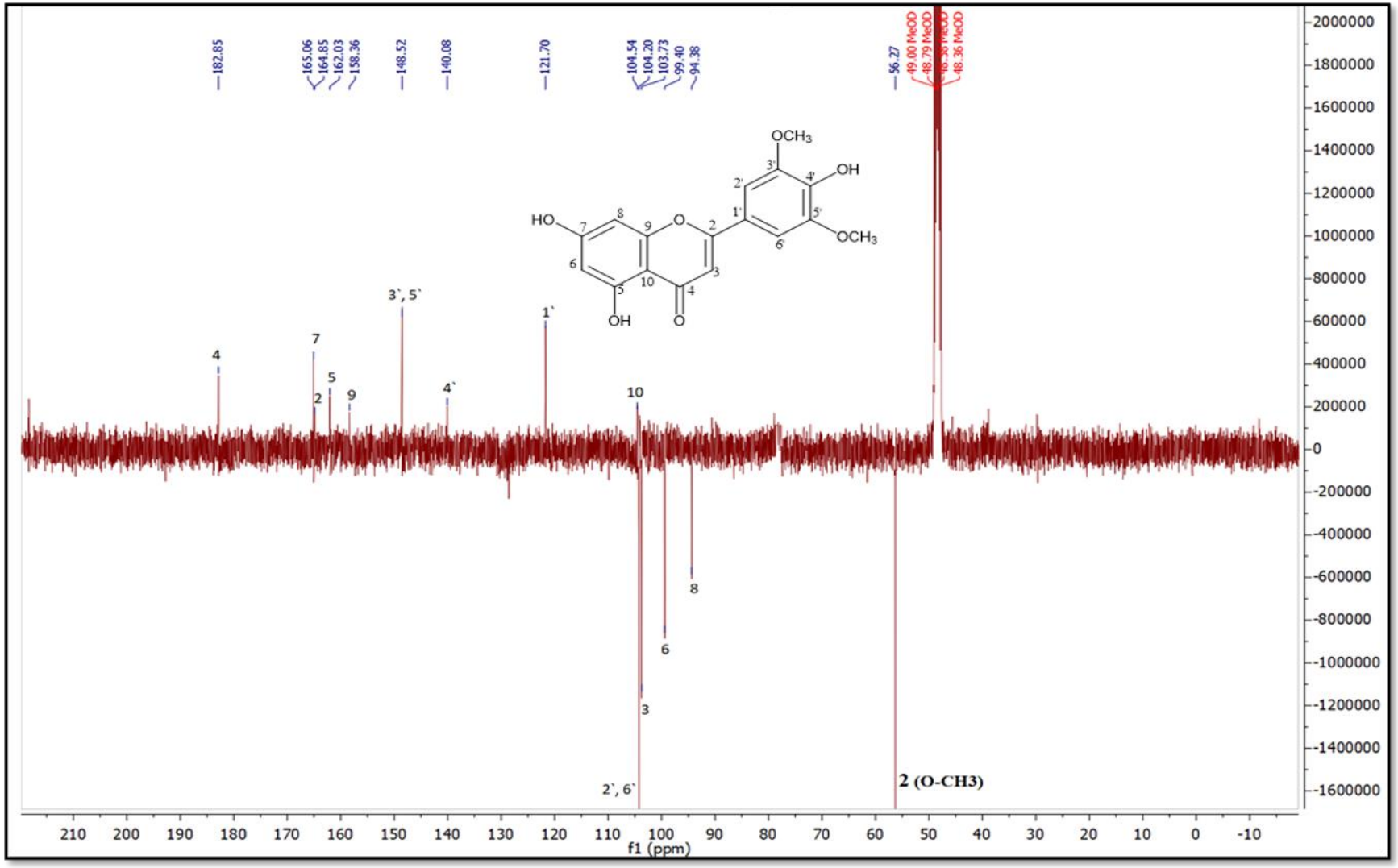

Figure S25: APT spectrum (CD_3OD, 100 MHz) of compound **7** (tricin)

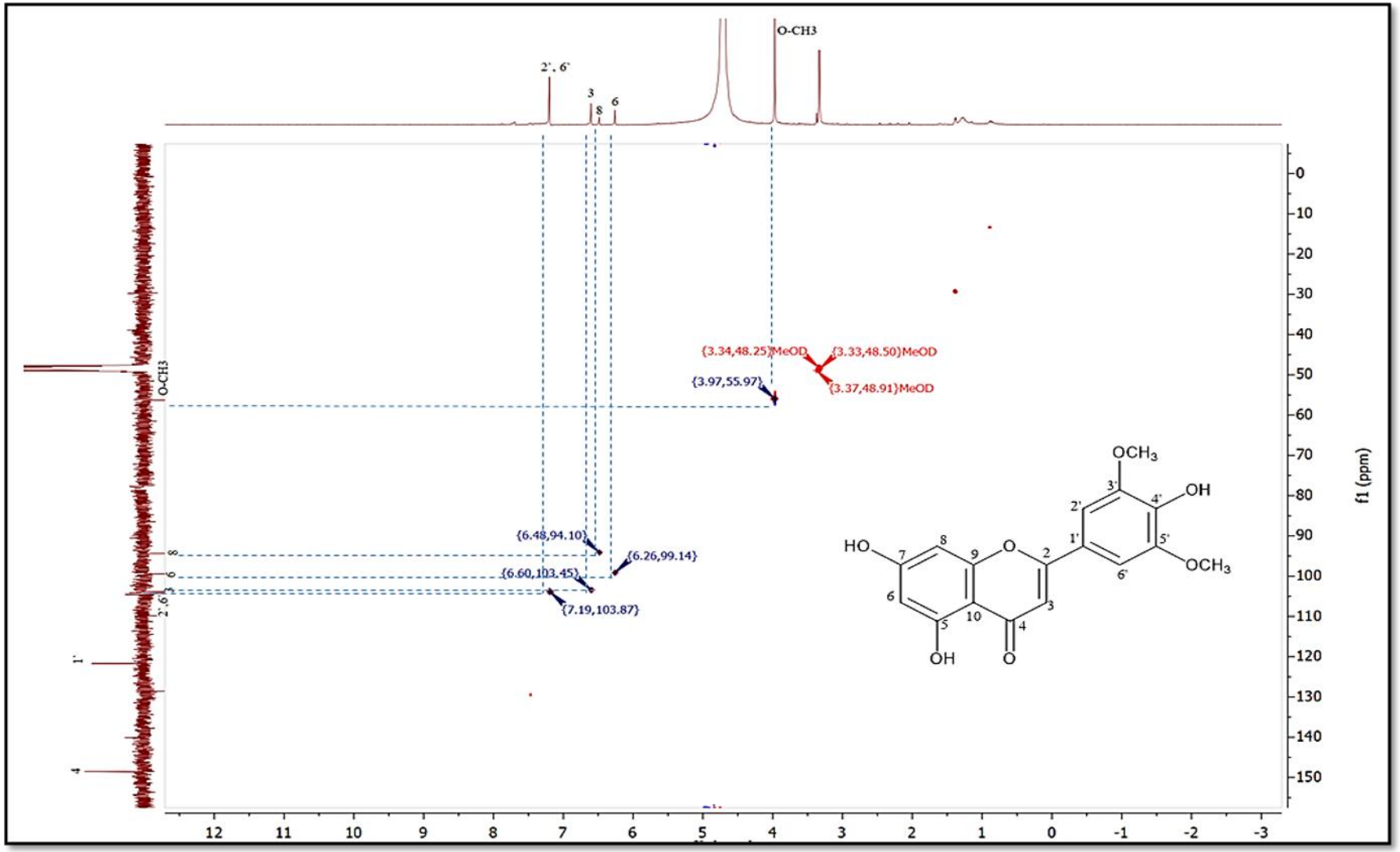

Figure S26: HSQC spectrum (CD_3OD, 400 MHz) of compound **7** (tricin)

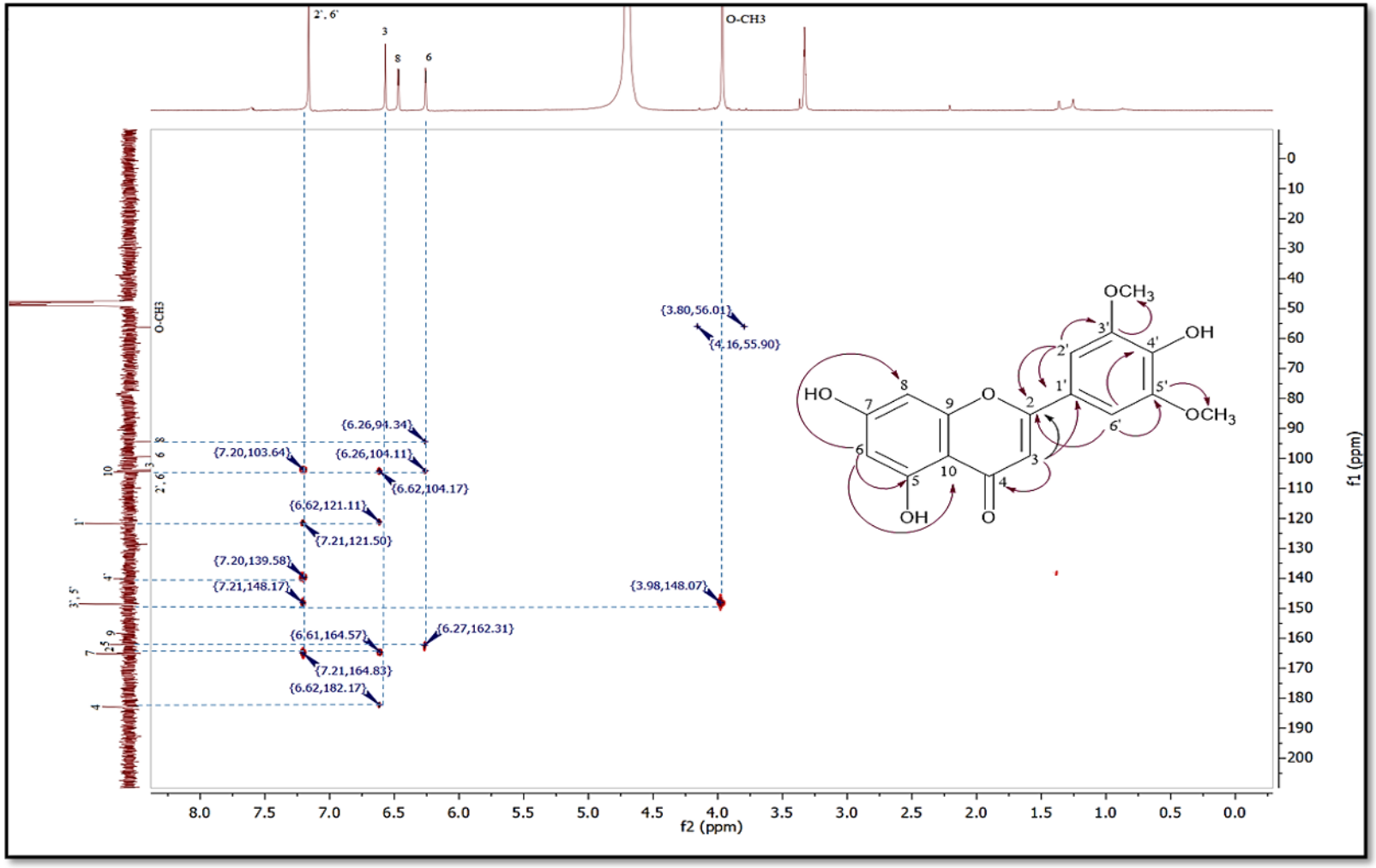

Figure S27: HMBC spectrum (CD_3OD, 400 MHz) of compound **7** (tricin)

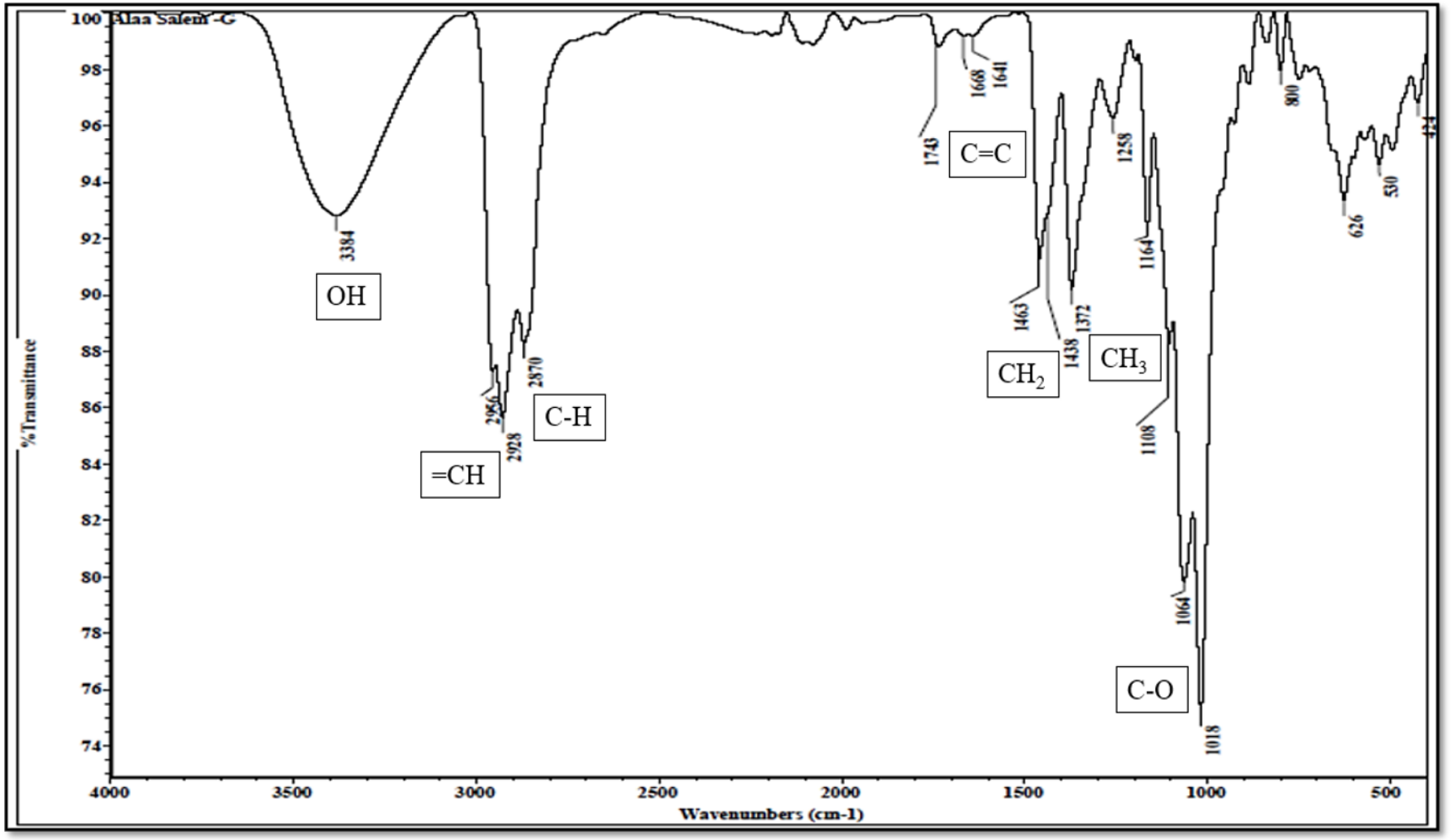

Figure S28: IR (KBr, υ_{max}) spectrum of compound **8** (daucosterol)

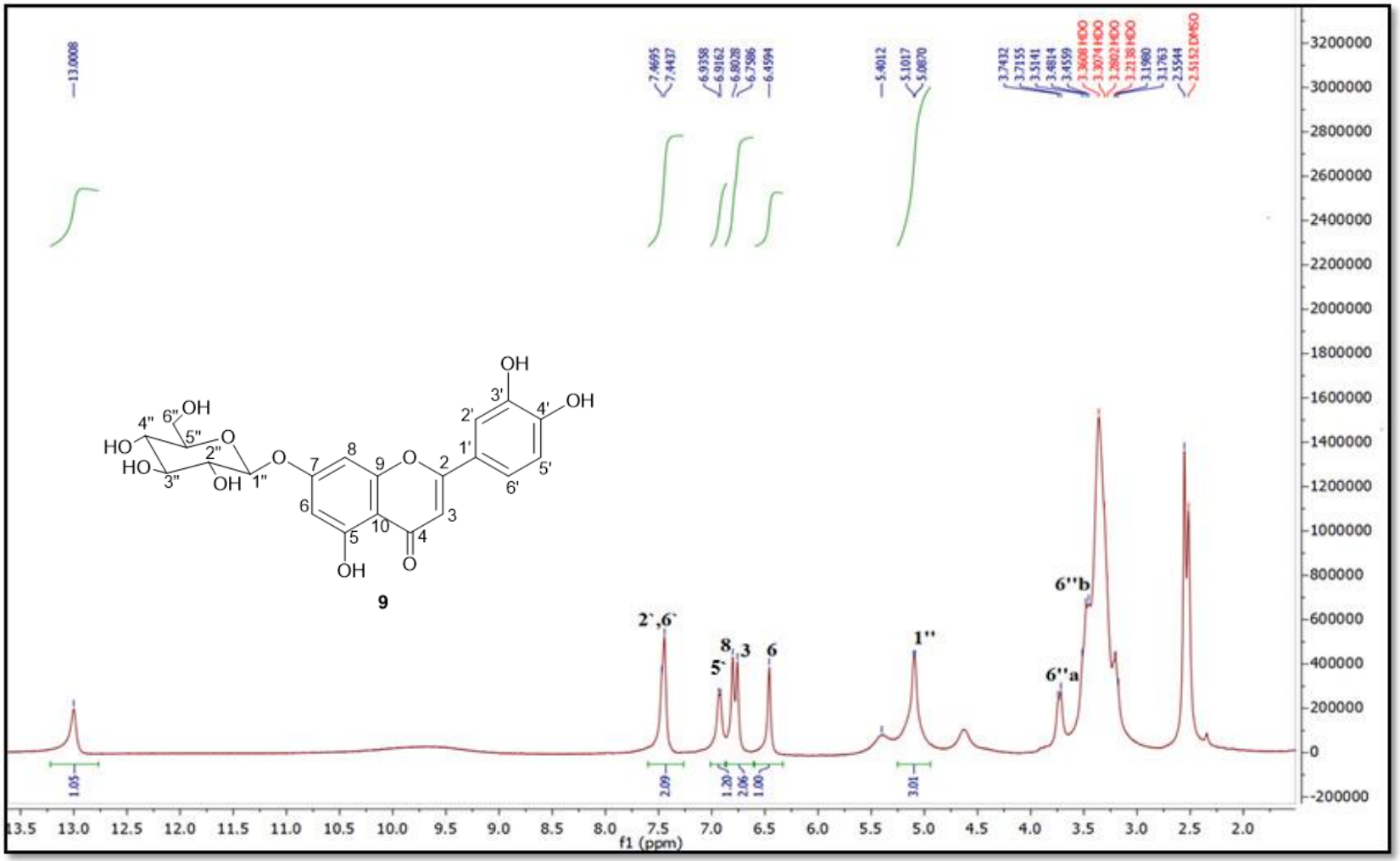

Figure S29: [1]H-NMR spectrum (DMSO-d_6, 400 MHz) of compound **9** (luteolin-7-*O*-β-D-glucoside; cynaroside)

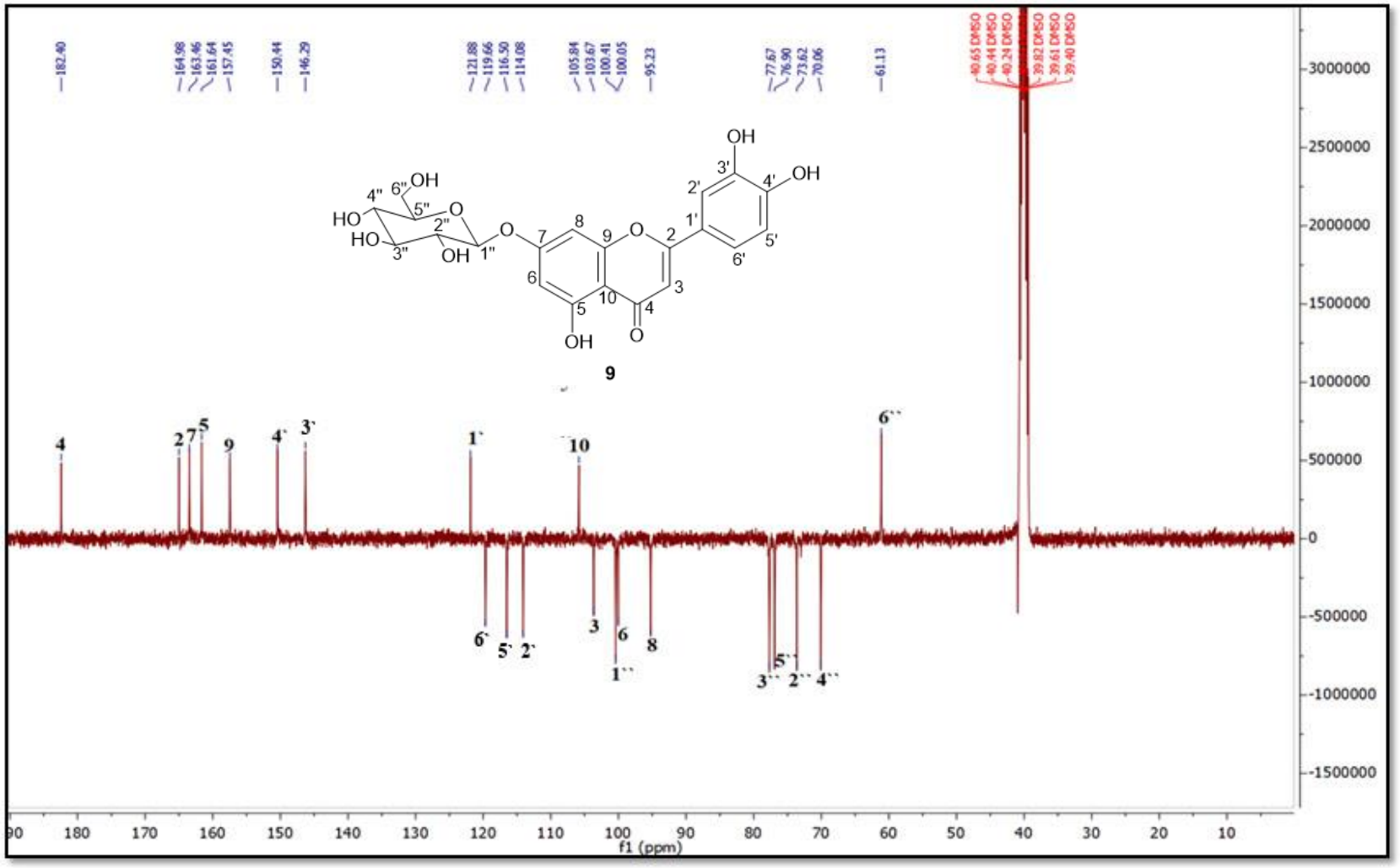

Figure S30: APT spectrum (DMSO-d_6, 100 MHz) of compound **9** (luteolin-7-*O*-β-D-glucoside; cynaroside)

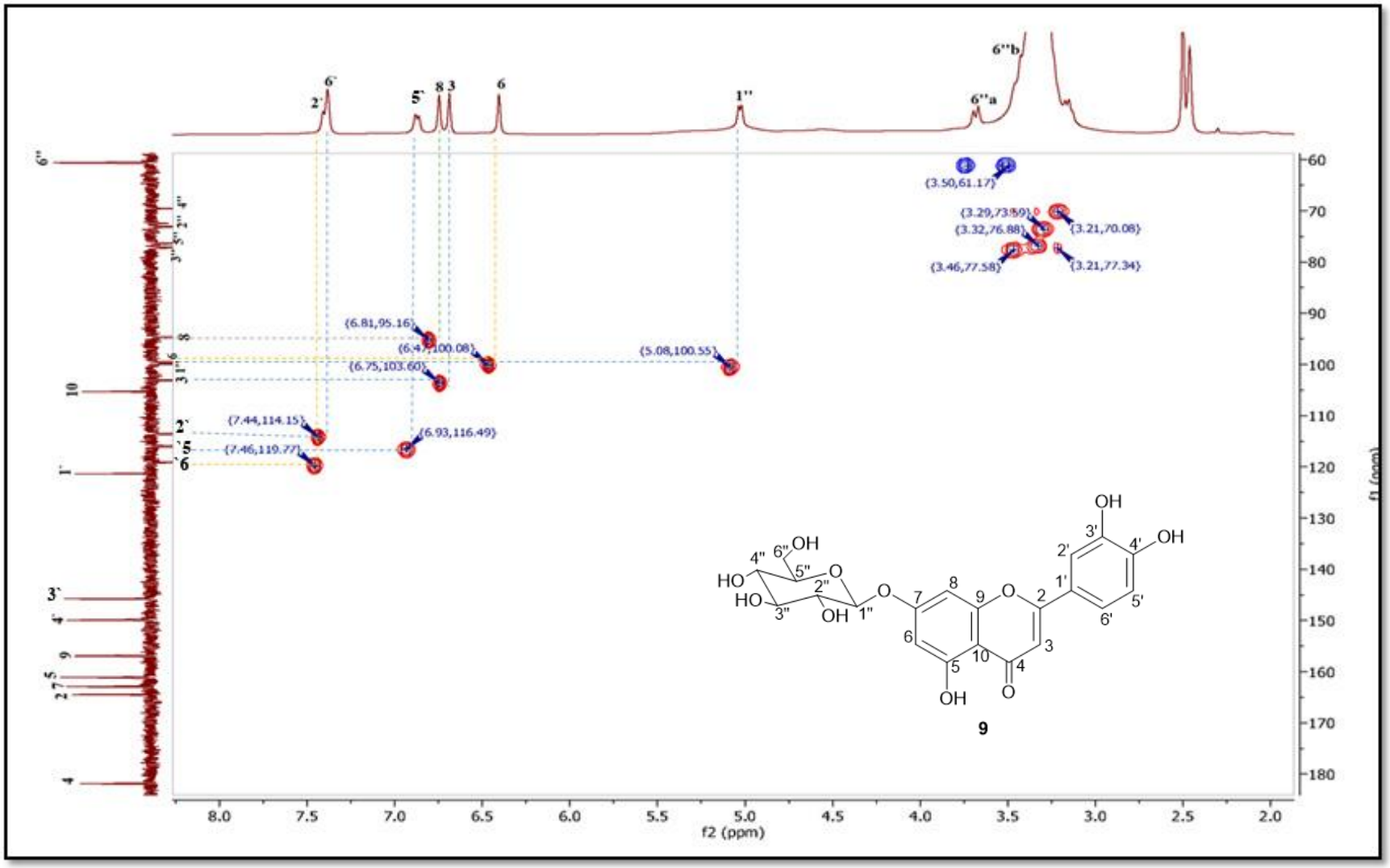

Figure S31: HSQC spectrum (DMSO-d_6, 400 MHz) of compound **9** (luteolin-7-*O*-β-D-glucoside; cynaroside)

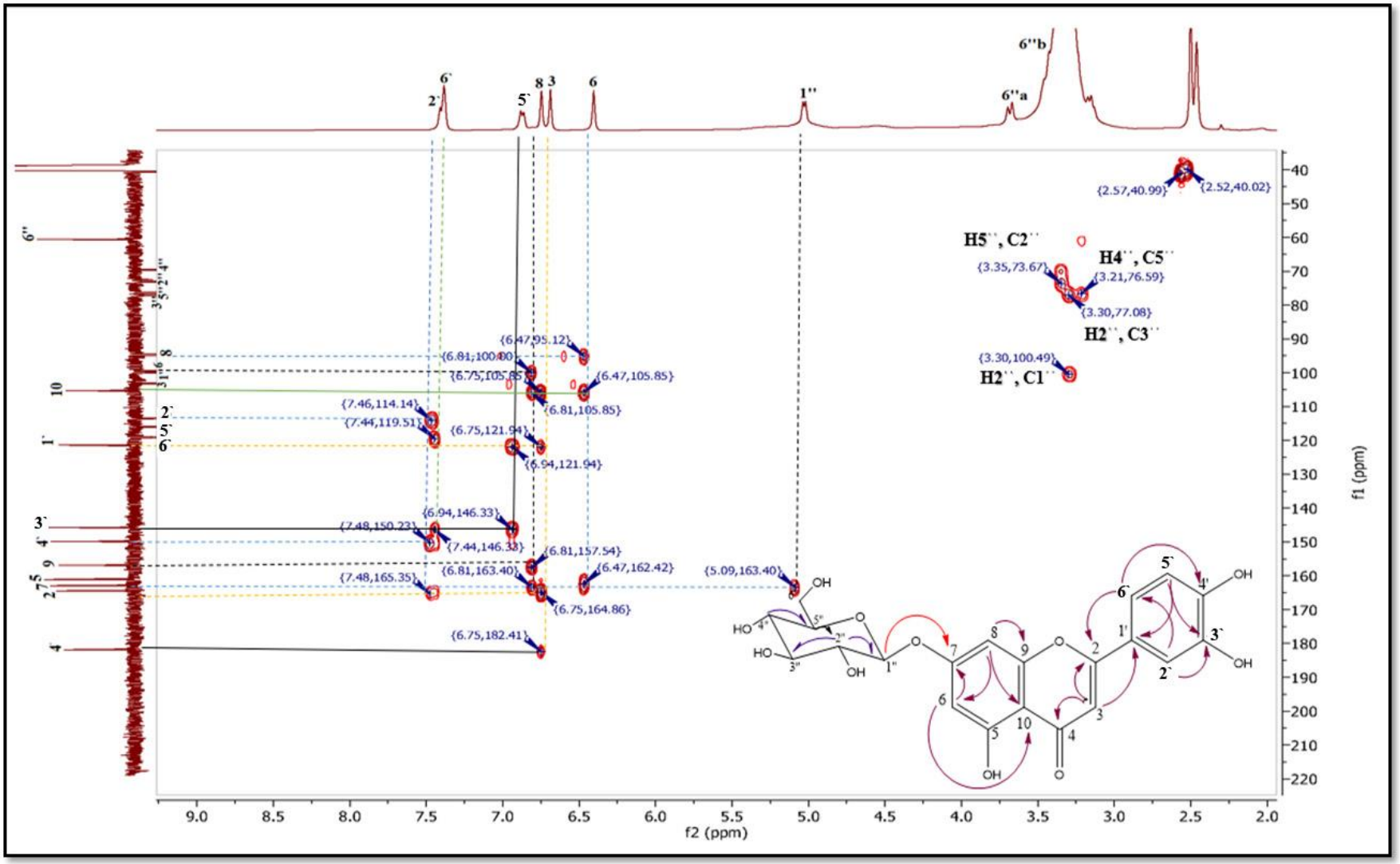

Figure S32: HMBC spectrum (DMSO-d_6, 400 MHz) of compound **9** (luteolin-7-*O*-β-D-glucoside; cynaroside).

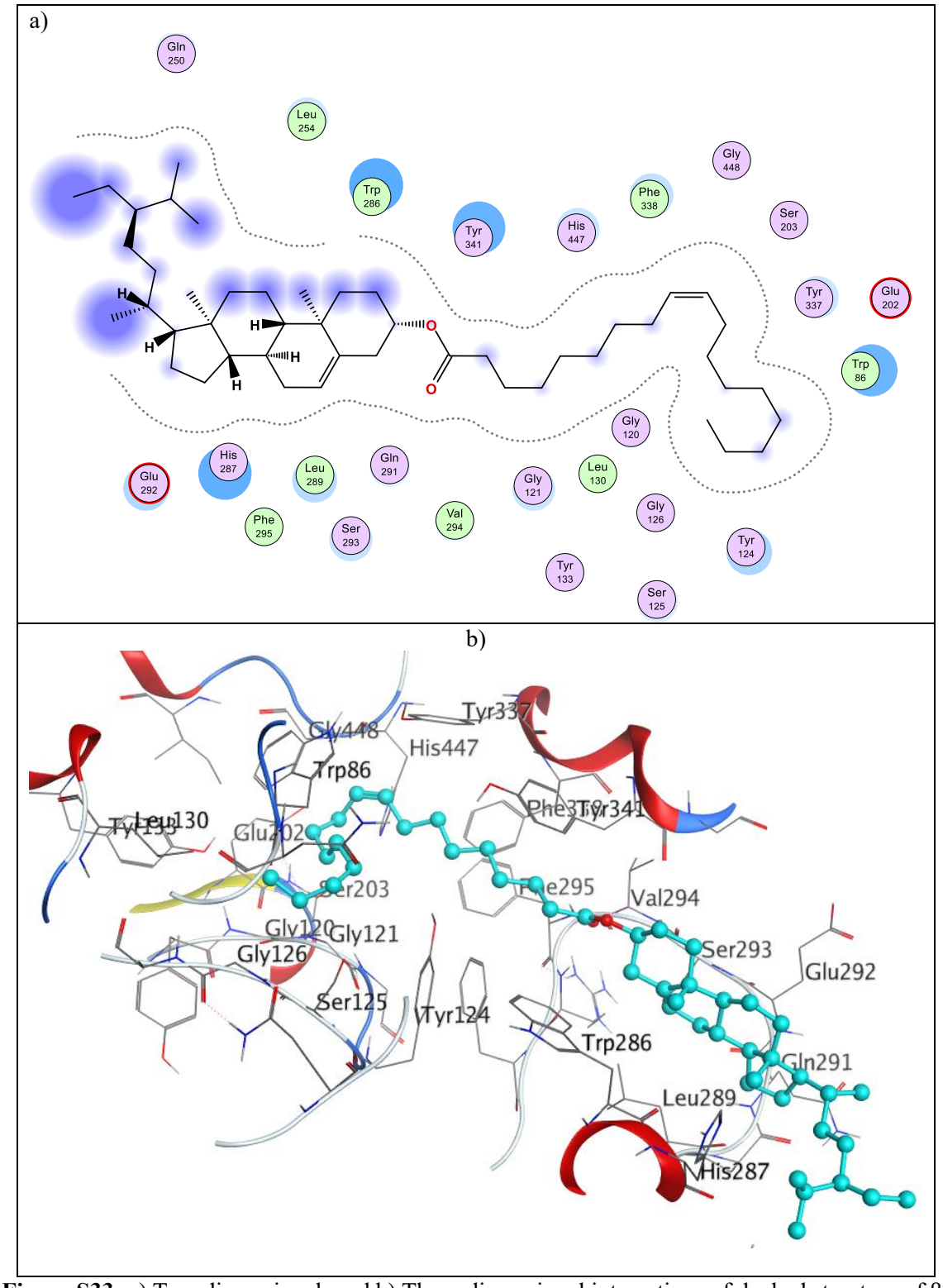

Figure S33: a) Two-dimensional; and b) Three-dimensional interactions of docked structure of β-sitosterol oleate (**1**) (cyan) within the active site of AChE; PDB: 4EY7 [15].

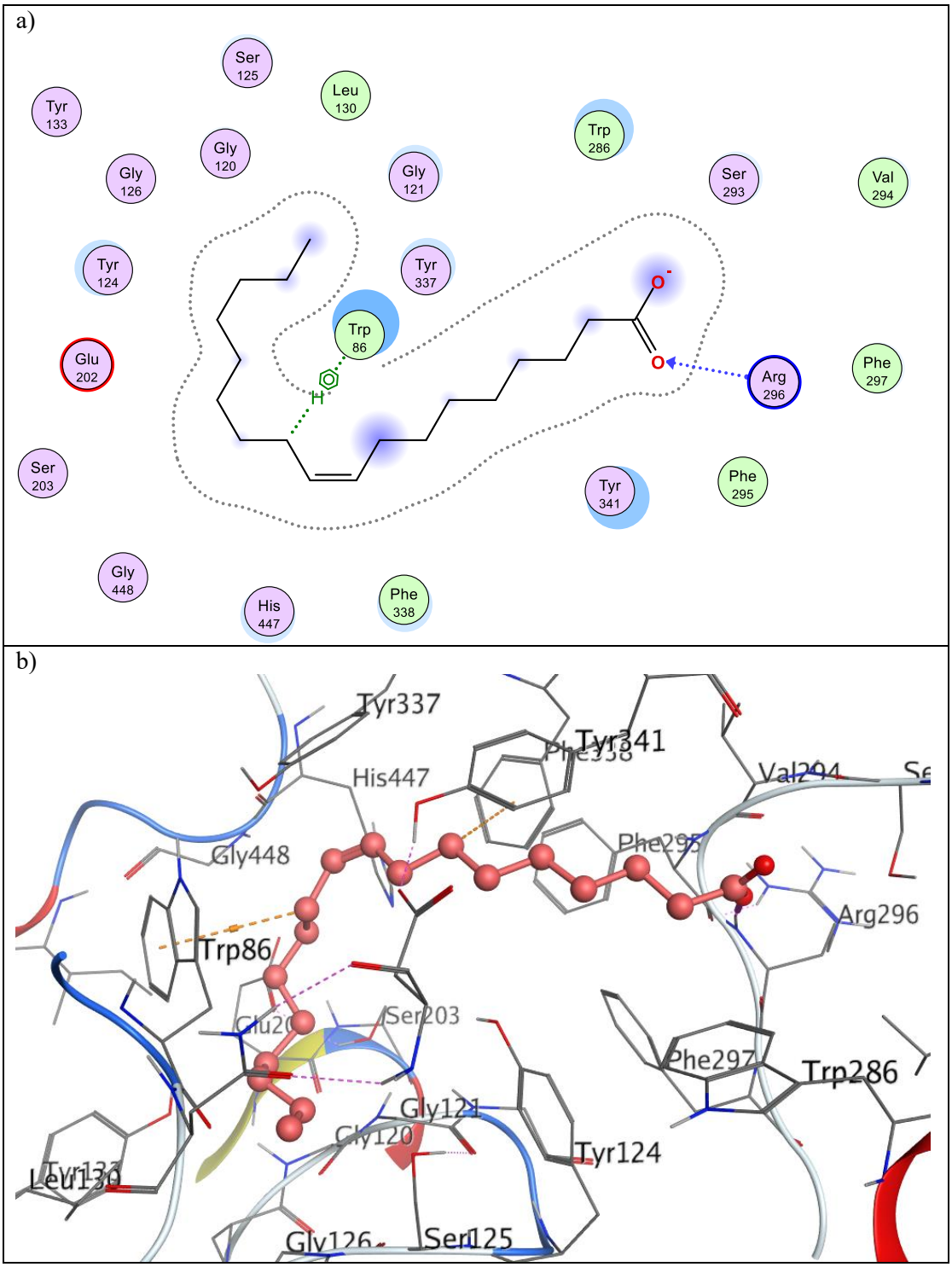

Figure S34: a) Two-dimensional; and b) Three-dimensional interactions of docked structure of oleic acid (**2**) (pink) within the active site of AChE; PDB: 4EY7 [15].

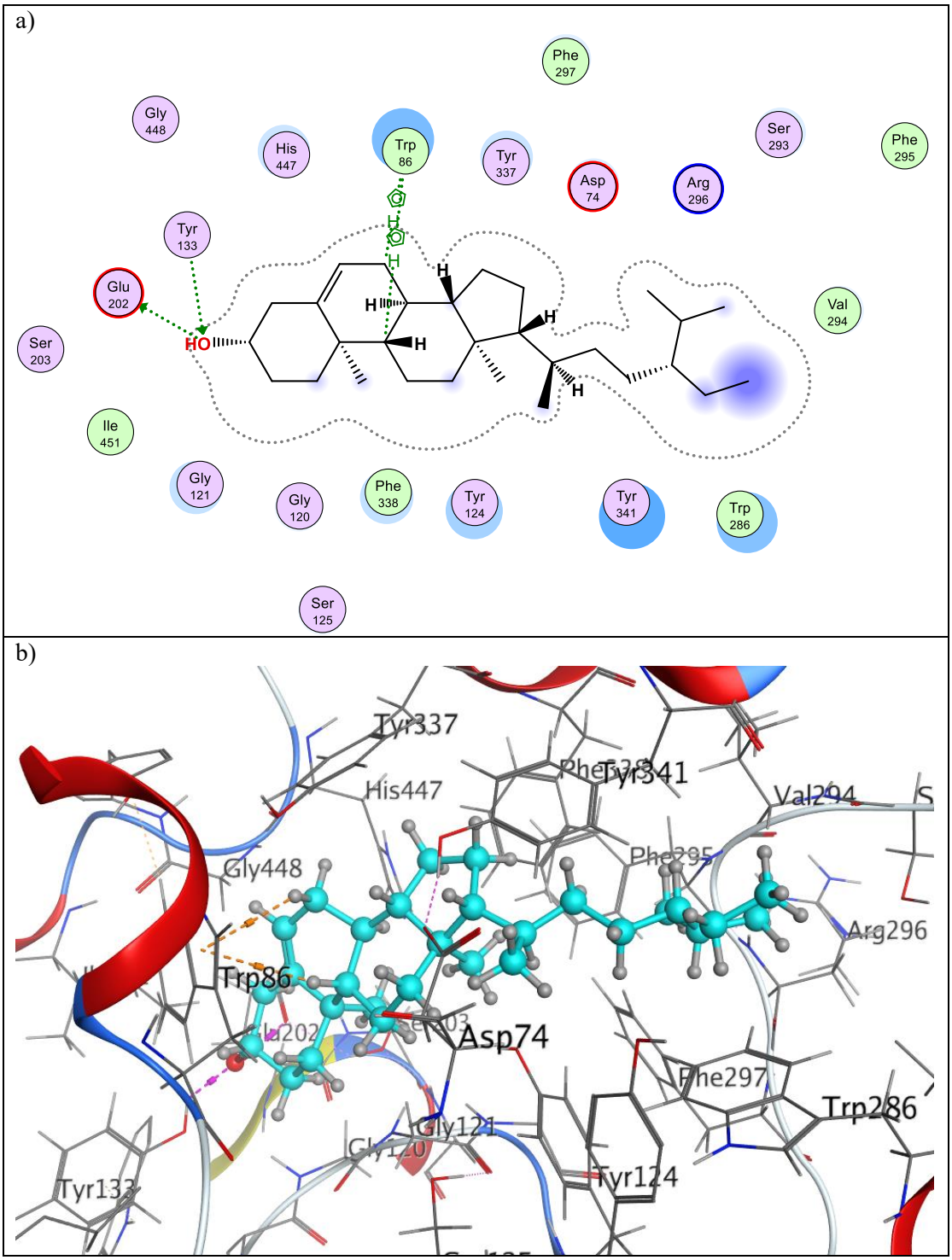

Figure S35: a) Two-dimensional; and b) Three-dimensional interactions of docked structure of β-sitosterol (**3**) (cyan) within the active site of AChE; PDB: 4EY7 [15]

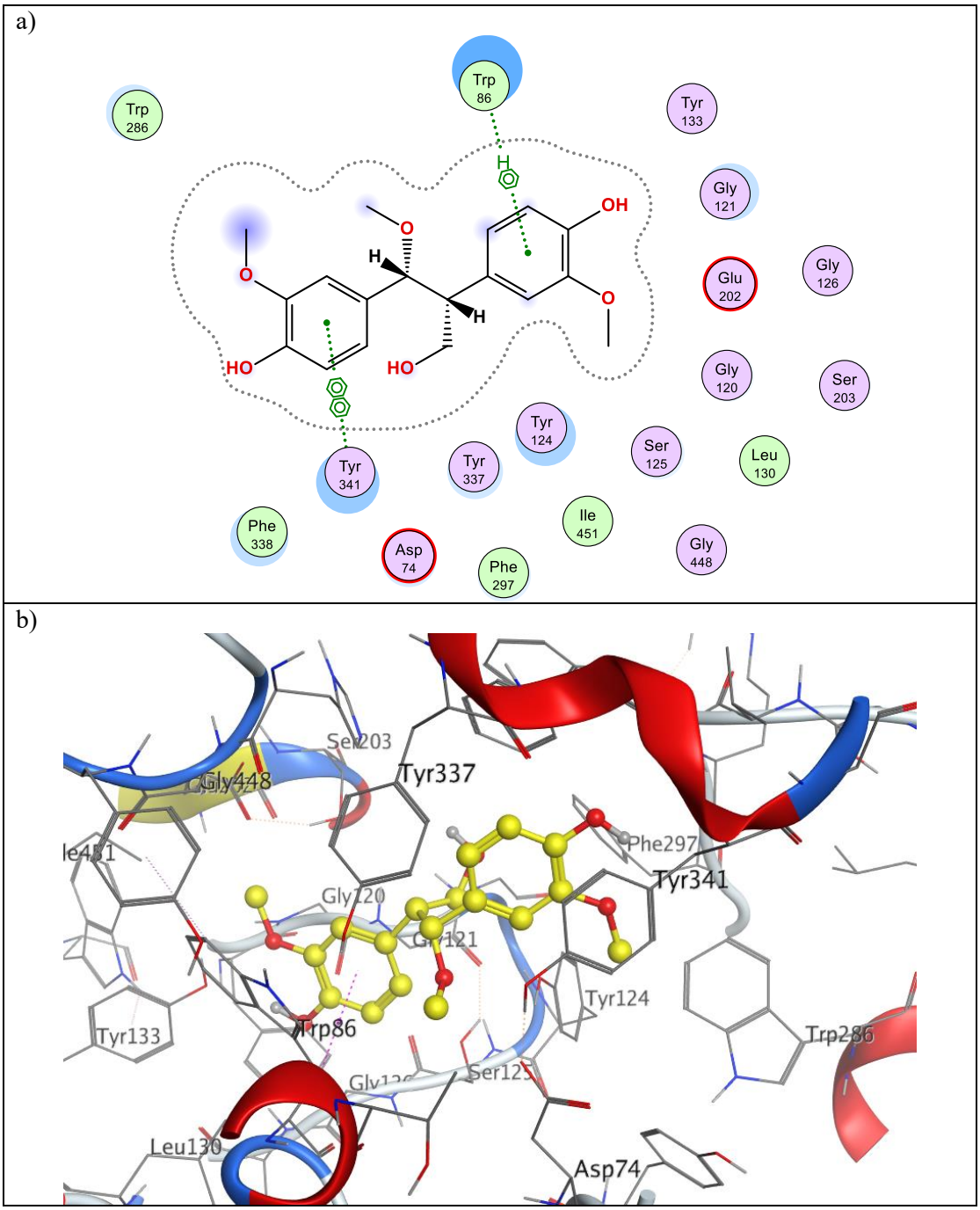

Figure S36: a) Two-dimensional; and b) Three-dimensional interactions of docked structure of *threo*-2,3-*bis*-(4-hydroxy-3-methoxyphenyl)-3-methoxypropanol (**4**) (yellow) within the active site of AChE; PDB: 4EY7 [15]

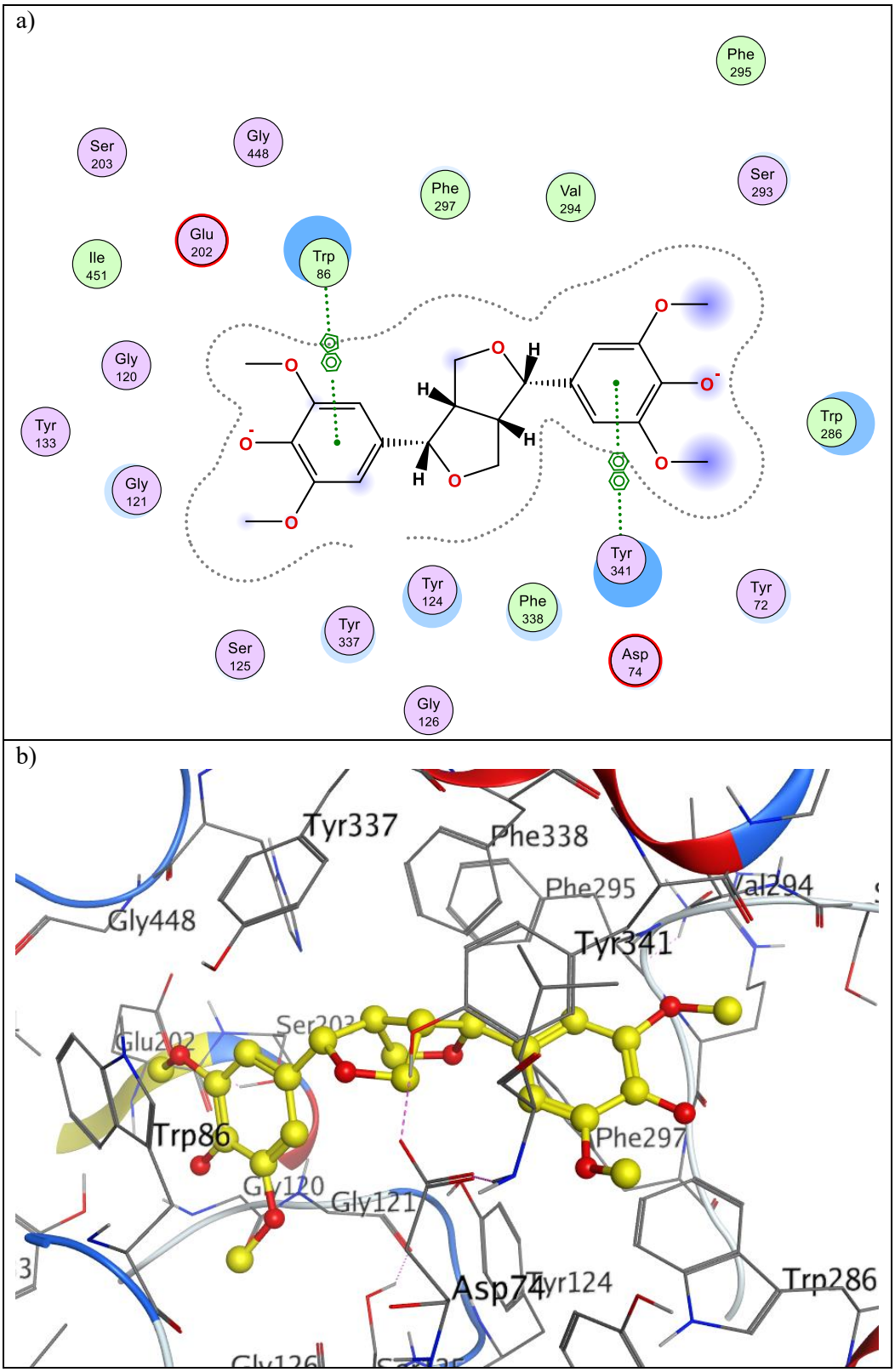

Figure S37: a) Two-dimensional; and b) Three-dimensional interactions of docked structure of syringaresinol (**5**) (cyan) within the active site of AChE; PDB: 4EY7 [15].

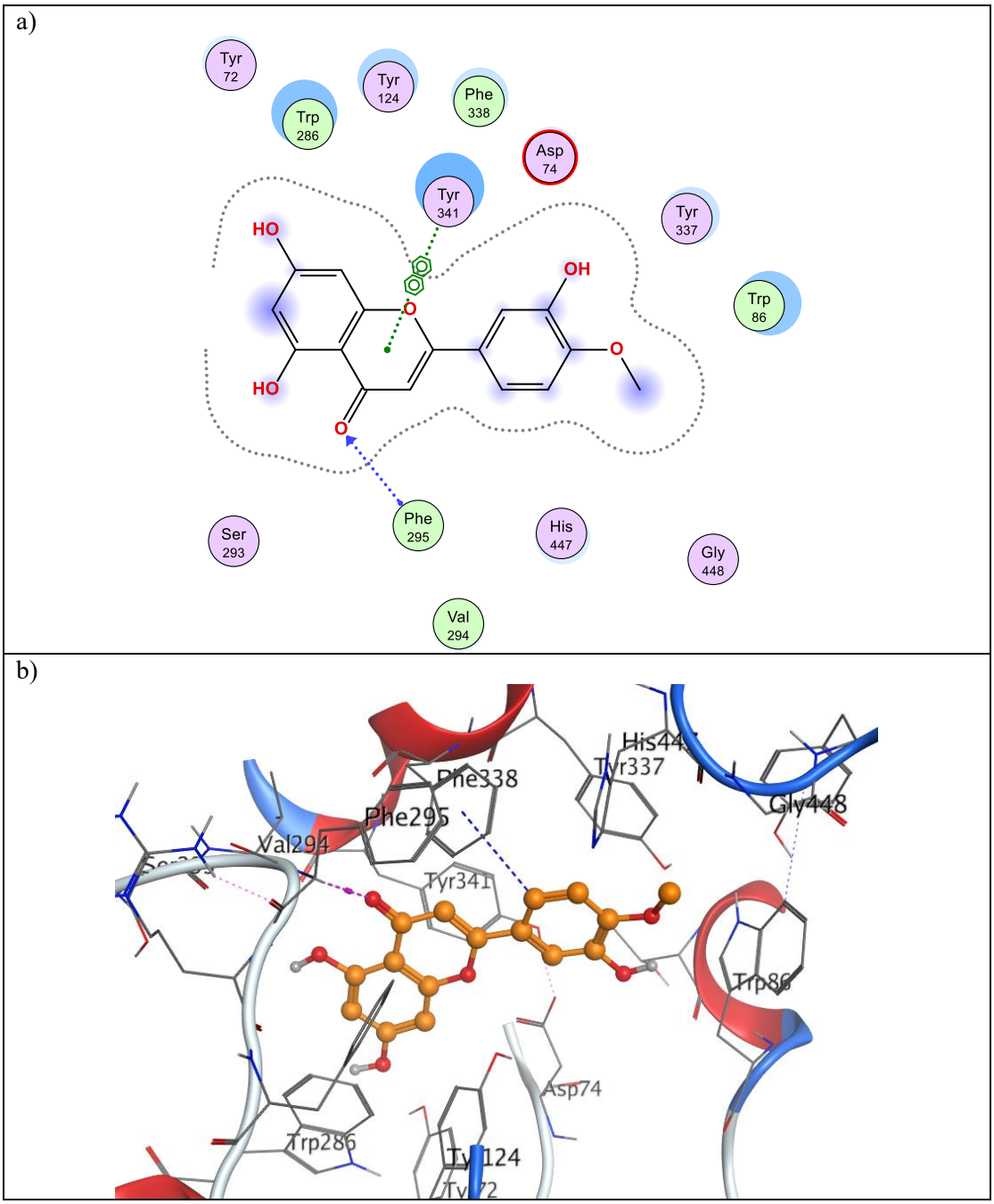

Figure S38: a) Two-dimensional; and b) Three-dimensional interactions of docked structure of diosmetin (**6**) (orange) within the active site of AChE; PDB: 4EY7 [15].

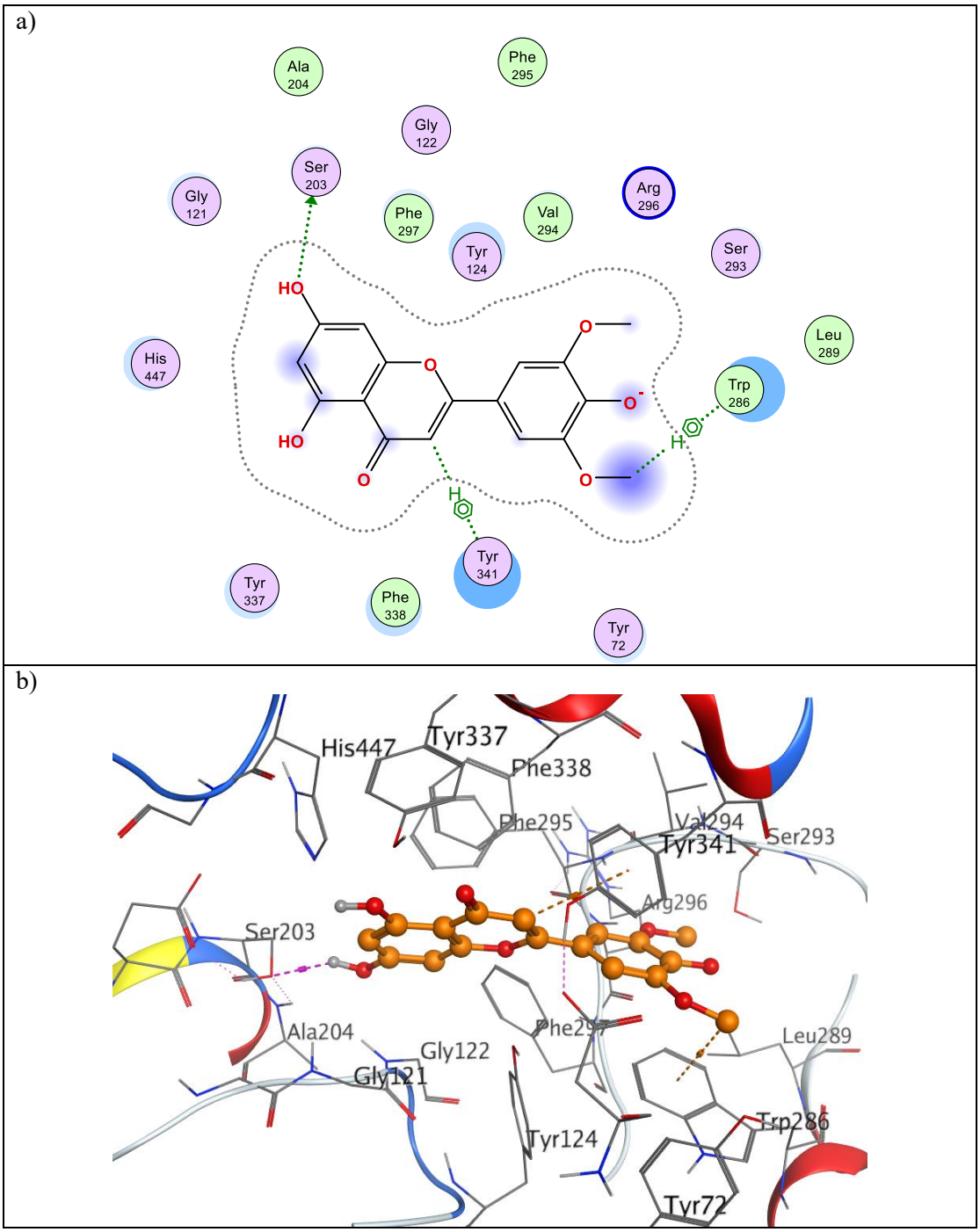

Figure S39: a) Two-dimensional; and b) Three-dimensional interactions of docked structure of tricin (**7**) (orange) within the active site of AChE; PDB: 4EY7 [15].

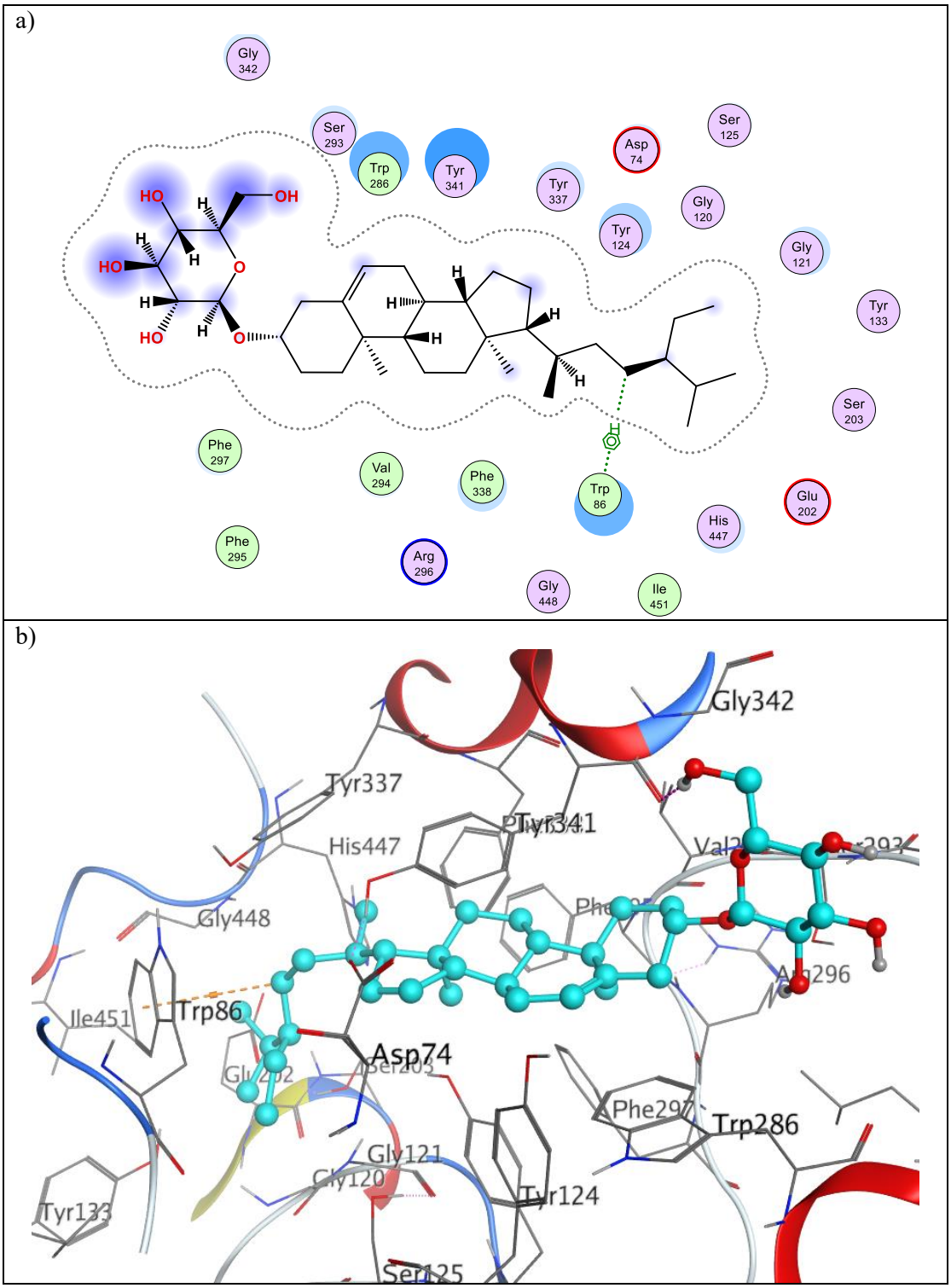

Figure S40: a) Two-dimensional; and b) Three-dimensional interactions of docked structure of daucosterol (**8**) (cyan) within the active site of AChE; PDB: 4EY7 [15].

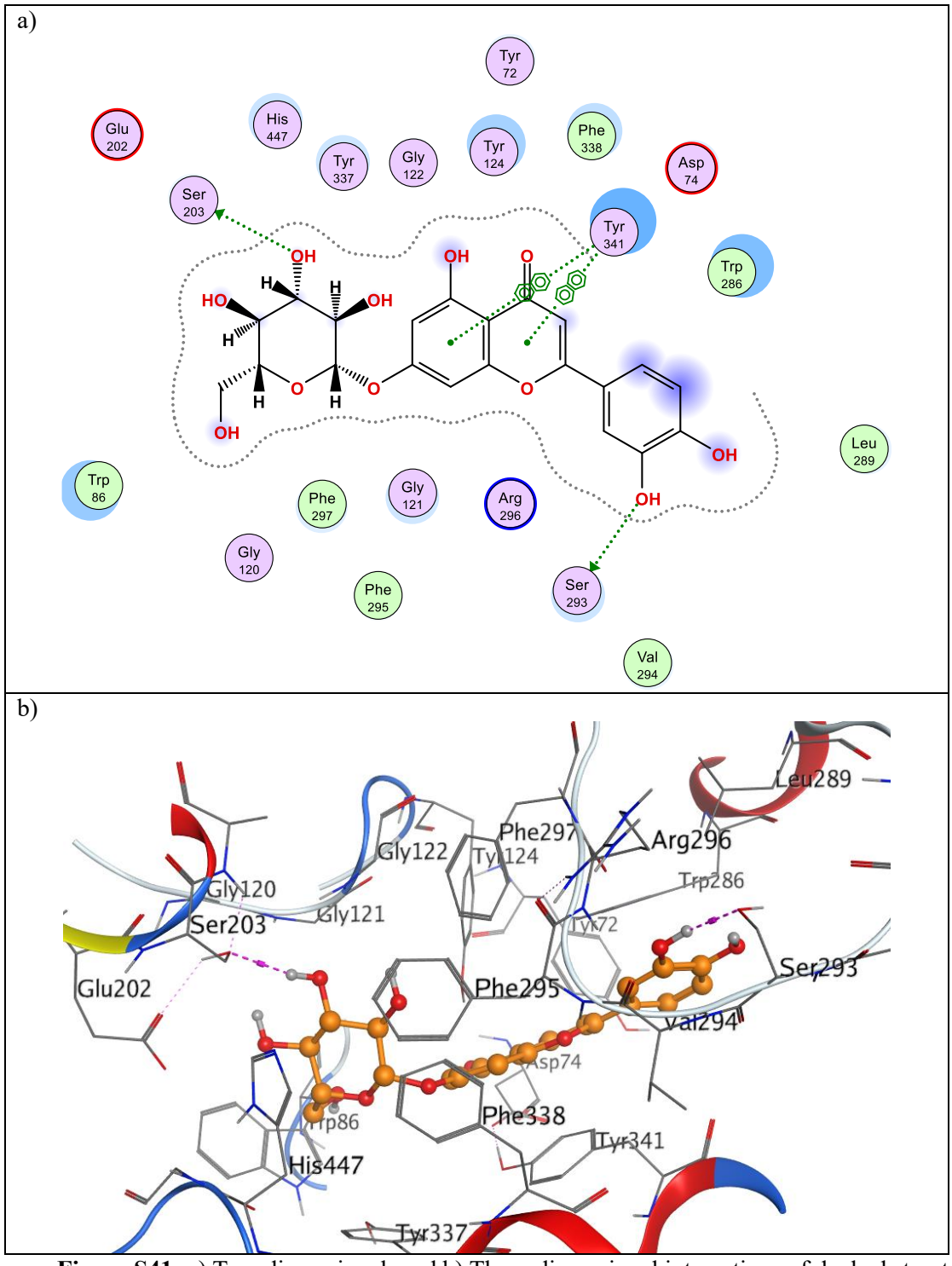

Figure S41: a) Two-dimensional; and b) Three-dimensional interactions of docked structure of luteolin-7-*O*-β-D-glucoside = cynaroside (**9**) (orange) within the active site of AChE; PDB: 4EY7 [15].

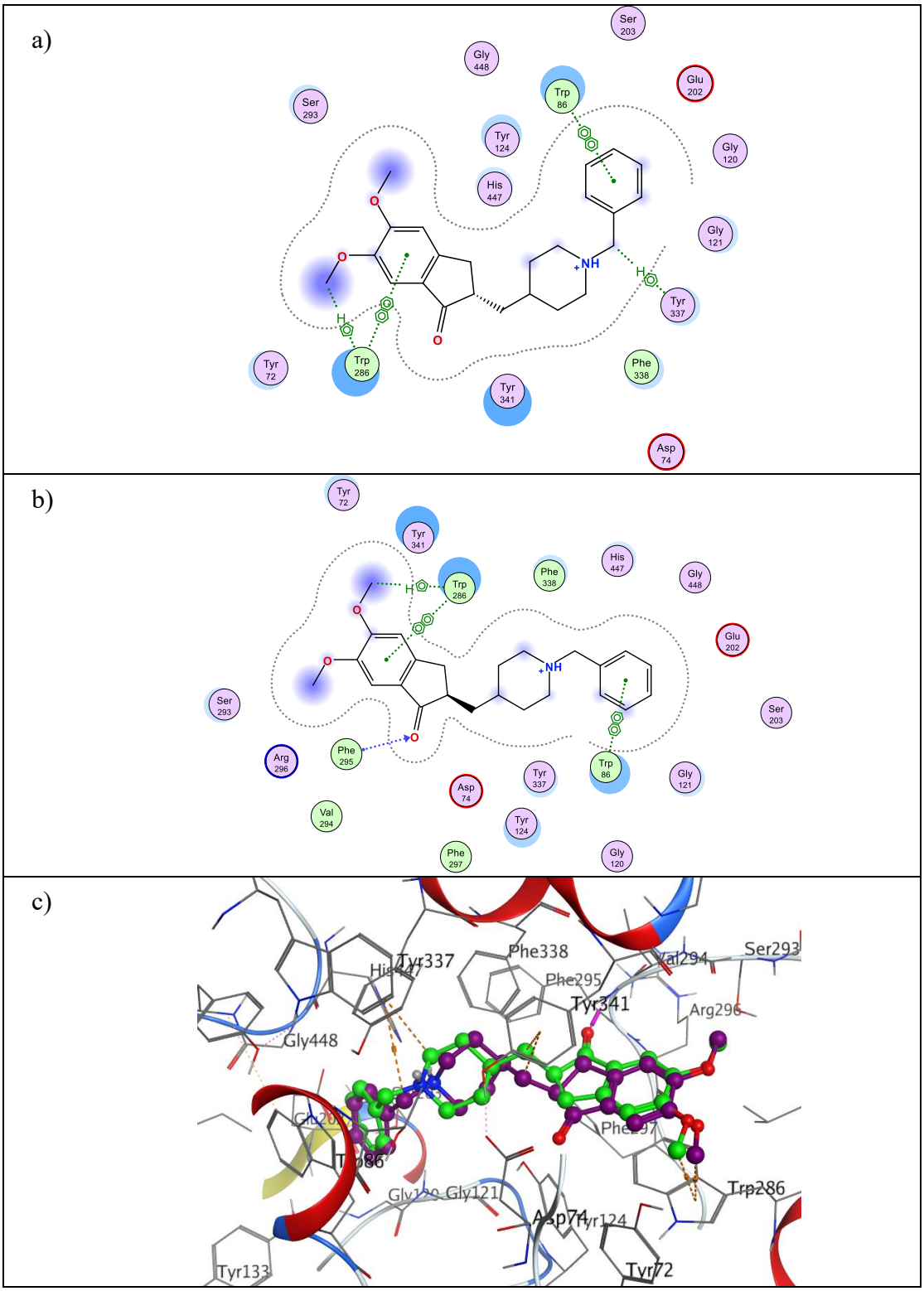

Figure S42: Two-dimensional interactions of donepezil structure, a) Docked; b) Co-crystallized ligand, and c) three-dimensional superposition of docked structure (purple) and co-crystallized ligand (green) of donepezil from its complex with AChE (PDB: 4EY7) [15].

a)

b)

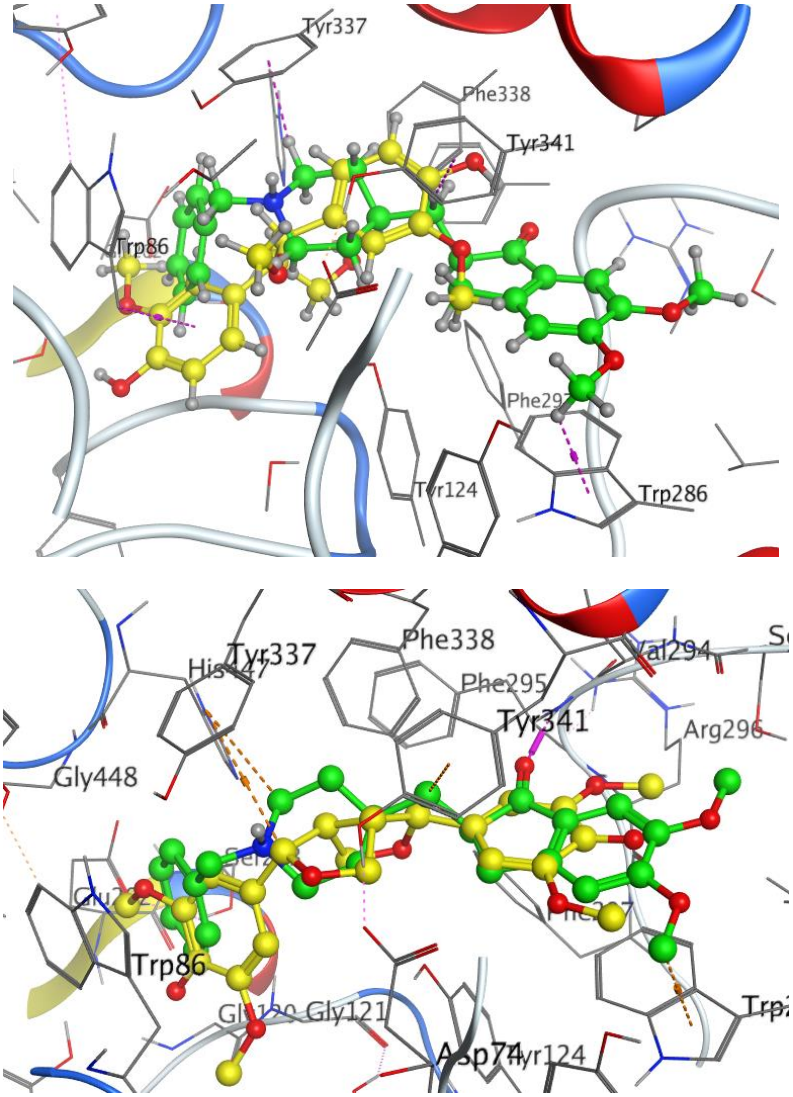

Figure S43. Three-dimensional superposition of docked structures of a) *threo*-2,3-*bis*-(4-hydroxy-3-methoxyphenyl)-3-methoxypropanol (**4**) (yellow), and b) syringaresinol (**5**) (yellow), with donepezil (green), the cocrystallized ligand, within the active site of AChE (PDB: 4EY7)

3.4. Prediction of ADME Properties

The early evaluation of ADME (Absorption, Distribution, Metabolism, and Excretion) properties of a potential drug is crucial to ensure that the drug reaches the target at adequate concentration and reflects its medicinal chemistry compatibility. In this study, the SwissADME web tool [16] was utilized for evaluating the ADME characteristics and drug-likeness properties of the isolated compounds (**1-9**). The results of analysis of ADME and drug-likeness properties of compounds **1-9** (Table S8) revealed significant variability in their pharmacokinetic profiles and drug-likeness potential. Compound **1** (β-sitosteryl oleate) showed the highest lipophilicity (Log*P*= 12.94) and low bioavailability score (0.17) due to its high molecular weight (679.15 g/mol) and multiple Lipinski's rule violations [17]. Conversely, **2** (oleic acid) and several other compounds (e.g., **4**-**7**) demonstrated moderate lipophilicity and higher bioavailability scores (0.55–0.85), aligning better with drug-likeness properties. Concerning GI absorption, most compounds such as **2**, **4**, and **5**, exhibited high gastrointestinal (GI) absorption, suggesting a possibility for oral administration. No compounds were predicted to cross the blood-brain barrier (BBB), which may limit their use in CNS-targeted therapies (Figure S44).

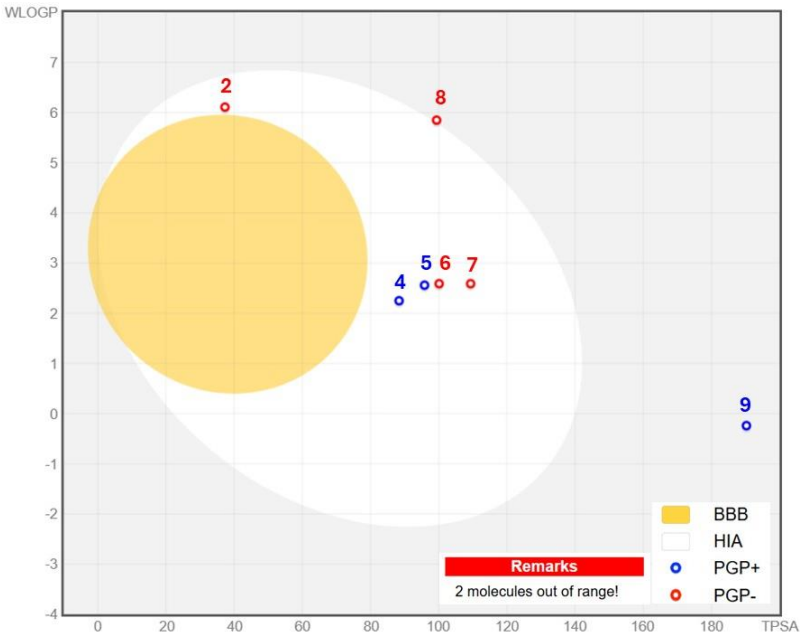

Figure S44: BOILED-Egg plot for compounds isolated from *Washingtonia filifera* illustrating the predictions for; BBB: blood-brain barrier, HIA: penetration, and human gastrointestinal absorption. Blue circles represent compounds predicted as active-efflux substrates of P-glycoprotein (PGP^+), while red circles denote compounds predicted as non-substrates (PGP^-). Two molecules are out of range, including **1**: β-Sitosteryl oleate and **3**: β-Sitosterol.

The solubility of investigated compounds varies significantly, with **9** (cynaroside) being soluble and highly polar (TPSA= 190.28), while **1** and **3** are poorly soluble, reflecting challenges in formulation and bioavailability. According to Lipinski's rule of five, compounds are likely to be poorly absorbed or less permeated when they exceed specific thresholds, including more than 5 hydrogen bond donors, 10 hydrogen bond acceptors, a molecular weight above 500, or a LogP value over 5 [17]. The number of hydrogen bond acceptors and donors varies for the investigated compounds, with **9** having the highest number of H-bond donors (7) and acceptors (11) indicating its poor absorption and bioavailability. Regarding P-gp substrate and CYP inhibition, the majority of compounds are non-substrates for P-glycoprotein (P-gp), which may reduce efflux-related bioavailability issues. However, **4** and **5** inhibit CYP isoforms like CYP2D6 and CYP3A4, indicating potential drug-drug interactions.

All compounds, except **9**, have zero PAINS (pan-assay interference compounds) alerts, suggesting a lower probability of assay interference [18]. Overall, compounds like **4** (*threo*-2,3-*bis*-(4-hydroxy-3-methoxyphenyl)-3-methoxypropanol) and **5** (syringaresinol) exhibited a balanced profile of solubility, bioavailability, and GI absorption, making them promising candidates for further exploration (Figure S45). However, the high molecular weight and lipophilicity of compounds like **1** limit their drug-like potential. Further optimization could focus on improving solubility and reducing CYP interactions of **4** and **5** to enhance their pharmacokinetic profiles.

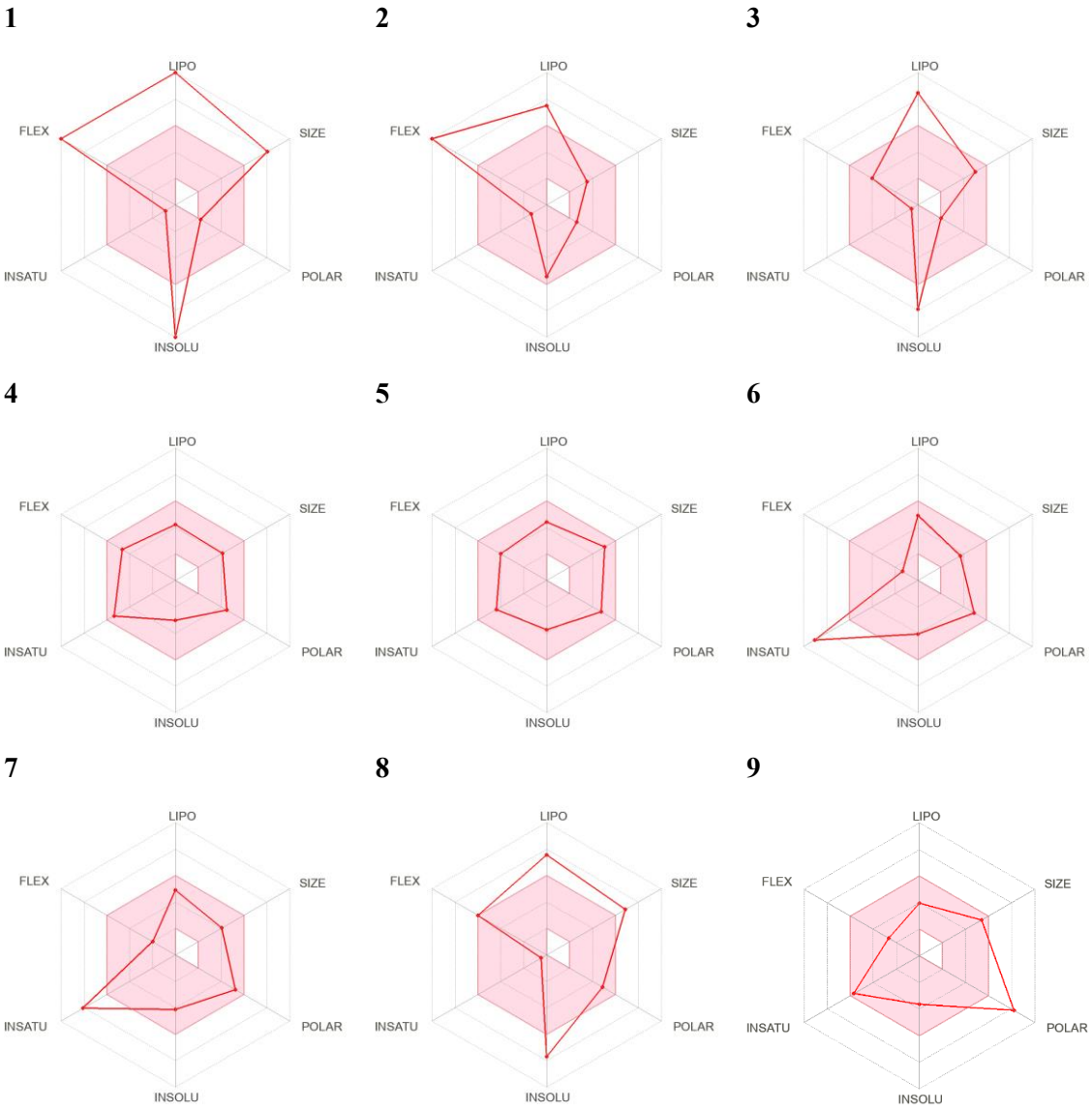

Figure S45: Bioavailability radar charts for the isolated compounds (**1**–**9**) isolated from *Washingtonia filifera*. The pink region indicates the ideal range for achieving oral bioavailability, while the red boundary outlines the desirable physicochemical characteristics for optimal oral bioavailability.

Table S8: Predicted ADME properties by the SwissADME online tool.

Molecules ID	**1**	**2**	**3**	**4**	**5**	**6**	**7**	**8**	**9**
Molecular formula	$C_{47}H_{82}O_2$	$C_{18}H_{34}O_2$	$C_{29}H_{50}O$	$C_{18}H_{22}O_6$	$C_{22}H_{26}O_8$	$C_{16}H_{12}O_6$	$C_{17}H_{14}O_7$	$C_{35}H_{60}O_6$	$C_{21}H_{20}O_{11}$
M.W. (g/mol)	679.15	282.46	414.71	334.36	418.44	300.26	330.29	576.85	448.38
Rotatable bonds	23	15	6	7	6	2	3	9	4
H-bond acceptors	2	2	1	6	8	6	7	6	11
H-bond donors	0	1	1	3	2	3	3	4	7
ESOL Class	Insoluble	Moderately soluble	Poorly soluble	Soluble	Soluble	Moderately soluble	Moderately soluble	Poorly soluble	Soluble
TPSA	26.3	37.3	20.23	88.38	95.84	100.13	109.36	99.38	190.28
GI absorption	Low	High	Low	High	High	High	High	Low	Low
BBB permeant	No	No	No	No	No	No	No	No	No
P-gp substrate	Yes	No	No	Yes	Yes	No	No	No	Yes
CYP Inhibitors	None	CYP1A2, CYP2C9	None	CYP2D6, CYP3A4	CYP2D6	CYP1A2, CYP2C9, CYP2D6, CYP3A4	CYP1A2, CYP2C9, CYP2D6, CYP3A4	None	CYP1A2
PAINS alerts	0	0	0	0	0	0	0	0	1
Lipophilicity (Consensus Log$P_{o/w}$)	12.94	5.65	7.24	2.19	2.33	2.19	2.15	5.55	0.15
Bioavailability Score	0.17	0.85	0.55	0.55	0.55	0.55	0.55	0.55	0.17
Lipinski violations	2	1	1	0	0	0	0	1	2

References

[1] K. Farabi, D. Harneti, N. Nurlelasari, R. Maharani, A. Hidayat, U. Supratman, K. Awang and Y. Shiono (2017). Cytotoxic steroids from the bark of *Aglaia argentea* (Meliaceae), *Chiang Mai Univ. J. Nat. Sci.* **16**, 293-306.

[2] M. E. Di Pietro, A. Mannu and A. Mele (2020). NMR determination of free fatty acids in vegetable oils, *Processes* **8**(**4**), 410.

[3] M. E. El-Beeh, A. A. El-Badawi, S. H. Qari, M. F. Ramadan and W. M. Filfilan (2022). Protective and health-promoting impact of *Washingtonia filifera* oil on the kidney of STZ-induced diabetic mice, *Appl. Biol. Chem.* **65**(**1**), 41.

[4] I. A. Nehdi (2011). Characteristics and composition of *Washingtonia filifera* (Linden ex André) H. Wendl. seed and seed oil, *Food Chem.* **126**(**1**), 197-202.

[5] R. A. Gomaa (2019). Physico-chemical Characteristics of *Washingtonia robusta* Fruit Oil. Suez Canal University Journal of Food Sciences. , *Food Sci.; Suez Canal Univ.* **6**(**1**), 19-25.

[6] R. M. Silverstein, F. X. Webster and D. J. Kiemle (2005). spectrometric identification of organic compounds, 7thedition ed.; John Wiley: 2005.

[7] M. Katsuyoshi, O. Yishan and K. Kazuo (1996). Phenolic Constituents of *Irvingia malayana*, *Nat. med.* **50**(**5**), 325-327.

[8] B.-Y. Yang, X. Yin, Y. Liu, Y. Sun, W. Guan, Y.-Y. Zhou and H.-X. Kuang (2018). Terpenes and lignans from the roots of *Solanum melongena* L, *Nat. Prod. Res.* **34**(**3**), 359-368.

[9] P. K. Agrawal and R. S. Thakur (1985). 13C NMR Spectroscopy of lignan and neolignan derivatives, *J. Magn. Reson. Chem.* **23**(**6**), 389-418.

[10] W. Monthong, S. Pitchuanchom, N. Nuntasaen and W. Pompimon (2011). (+)-Syringaresinol lignan from new species *Magnolia thailandica*, *Am. J. Appl. Sci.* **8**(**12**), 1268-1271.

[11] Y. Park, B. H. Moon, H. Yang, Y. Lee, E. Lee and Y. Lim (2007). Complete assignments of NMR data of 13 hydroxymethoxyflavones, *Magn. Reson. Chem.* **45**(**12**), 1072-1075.

[12] X. X. Liu, S. W. Sun, W. J. Yuan, H. Gao, Y. Y. Si, K. Liu, S. Zhang, Y. Liu and W. Wang (2018). Isolation of tricin as a xanthine oxidase inhibitor from sweet white clover (*Melilotus albus*) and its distribution in selected Gramineae species, *Molecules* **23**(**10**), 2719.

[13] C. A. Williams, J. B. Harborne and H. T. Clifford (1973). Negatively charged flavones and tricin as chemosystematic markers in the Palmae, *Phytochemistry* **12**(**10**), 2417-2430.

[14] C. Boudoukha, H. Bouriche, M. Elmastaş, H. Aksit, O. Kayir, N. Genç and A. Senator (2018). Antioxidant activity of polyphenolic leaf extract from *Santolina chamaecyparissus* L. (Asteraceae) and the isolated luteolin-7-*O*-glucoside, *J. Pharm. Res. Int.* **22**, 1-12.

[15] J. Cheung, M. J. Rudolph, F. Burshteyn, M. S. Cassidy, E. N. Gary, J. Love, M. C. Franklin and J. J. Height (2012). Structures of human acetylcholinesterase in complex with pharmacologically important ligands, *J. Med. Chem.* **55**(**22**), 10282-10286.

[16] A. Daina, O. Michielin and V. Zoete (2017). SwissADME: a free web tool to evaluate pharmacokinetics, drug-likeness and medicinal chemistry friendliness of small molecules, *Sci. Rep.* **7**, 42717.

[17] C. A. Lipinski, F. Lombardo, B. W. Dominy and P. J. Feeney (2001). Experimental and computational approaches to estimate solubility and permeability in drug discovery and development settings, *Adv. Drug Deliv. Rev.* **46**(**1-3**), 3-26.

[18] J. B. Baell and G. A. Holloway (2010). New substructure filters for removal of pan assay interference compounds (PAINS) from screening libraries and for their exclusion in bioassays, *J. Med. Chem.* **53**(**7**), 2719-2740.